Università degli studi di Pisa

Thermal analytical techniques applied to the study of Cultural Heritage

Alessio Spepi

PhD in Chemical Sciences CHIM/02

XVII cycle (2011-2013)

Supervisor:

Prof. Maria Rosaria Tinè

Dr. Celia Duce

External supervisor

Prof. Stefana Milioto

Chapter 1 Introduction and aim of the thesis

Chapter 2 Materials and methods

Chapter 3 Pigments and fillers in paints

1 Abstract

Chemical composition of an art paint is influenced by several factors: the painting technique used by the artist, the decay processes affecting the painting materials over time due to environmental factors, and the different materials possibly used for the protection and conservation of the object.

Improved knowledge on the material composition of paint layers on heritage items will allow a better understanding of the painting technique used by the authors, will contribute to the characterization assignment and authentication of artworks, and sustainable conservation of the heritage objects.

This thesis presents a research related to the characterization and physical chemical properties of organic materials used in paint layers both from natural and synthetic origin. Organic materials can be used in painted surfaces for different purposes: as adhesives, when joining together two surfaces; as binging media, if applied in order to assure cohesion in a paint layer; as consolidant if used to return the lost coherence a paint layer; as varnish or protective layer or coatings of the painted surfaces.

In this thesis we focus our attention on proteinaceous materials used as binders in tempera paint layers, their interaction with coloured pigments and their ageing behavior, and on alkyd resins used in modern and contemporary art; in particular synthetic resin produced by the Winsor & Newton, *Series Griffin – fast drying oil colour* were considered. Two formulations of siloxanes produced by *Caparol (Disboxan 450) and Phase Restauro (Hydrophase)* to be used as protective coatings were studied as well.

Analysis were performed by using several techniques with a particular focus on thermoanalytical ones. Differential scanning calorimetry (DSC), thermogravimetric analysis (TGA), thermogravimetric and evolved gas analysis coupled with Fourier infrared spectroscopy (TG-EGA-FTIR), and Fourier infrared spectroscopy (FTIR) on the solid samples enabled the characterization of the chemical physical behavior of the paint layer components.

The first chapter of the thesis introduces the different organic materials studied, natural and synthetic, in particular proteins, proteinaceous materials and alkyd resins.

The second chapter presents the technical aspects of sampling giving an overview of the methods used for binding media and resins analysis (TGA, TG-FTIR, FTIR and DSC) revealing advantages and limits for each of them.

Beginning from the third chapter the thesis presents the analysis of the material studied. The pure pigments (natural or synthetic) used in proteinaceous and alkyd binders, and filler are characterized by TGA and FTIR.

The fourth chapter studies the proteinaceous binder (ovalbumin, casein and rabbit glue), their interaction with five different inorganic pigments (azurite, red ochre, calcium carbonate, cinnabar and minium) and the effect of artificial UV-ageing.

The fifth chapter studies the alkyd resins produced by the *Winsor & Newton- series Griffin-Fast drying oil colour* and their interaction with ten different pigments, organic (arylamide yellow, phthalocyanine, naphtol carbamide) and inorganic (cadmium-zinc sulphide, chromium oxide and

sulphoselenide, aluminium-silicate of sodium, titanium dioxide and bone black), the effect of natural ageing of 8 months and of artificial ageing with acetic acid.

The sixth chapter studies the silane/siloxane coatings, in particular alkyl silane and alkyl-alkoxy siloxane, their characterization, their ageing after two years of natural outdoor ageing and their interactions with acrylic colour. These two formulations of coatings are produced by *Caparol (Disboxan 450) and Phase Restauro (Hydrophase)* and the selected product will be applied on the wall painting "*Tuttomond*o" of Keith Haring on the Church of Sant' Antonio in Pisa.

1 Introduction and aim of the thesis

1.1 What is a painting?

Paint artworks can be considered as a complex multi-layers heterogeneous system where four different layers can be identified: a support, a preparation layer, a paint layer and a coating layer. The term "support" refers to any material onto which the paint is applied. Canvas, wood, and paper are the most common painting supports, but the types of supports used for artwork are very extensive. Cave walls and animal skins were among the first supports used. Plaster frescos and wooden panels later became prominent, which eventually gave way to linen and cotton canvases. The search for the ideal support is perhaps a never-ending quest, and is very much influenced by the types of materials available at the time. It is easy to predict that modern supports such as polyester canvases, AcrylaWeave® and Syntra® panels will most likely succumb to other advancing technology. Today's most common supports include acid-free papers, illustration board, cotton canvas, linen, polyester canvas, masonite, aluminum, and various wood panels.[1]

The support surface, generally, needs to be prepared with a ground layer in order to realize a perfectly smooth and waterproof surface on which to apply the pigments.

The paint layer is a dispersion of pigments (organic or inorganic) in a fluid binder, which enables the pigment to be dispersed and to adhere to the preparation layer.

Sometimes, it is necessary to apply a protective coating on the work surface. Particularly in the case of outdoor applications, e.g. stone facades of churches and ancient buildings, where the synergic effect of sunlight, temperature, moisture and pollution agents is maximum, a coating layer ensures protection against environmental agents and, at the same time, produces saturated deep-toned colours. Coatings are generally synthetic polymers (silicones, acrylate, polyurethanes).

The study of these multi-layers structures is of the utmost importance in order to understand the chemical physical features of a painted artwork and to provide it with the best conservation conditions. However, this procedure is complicated due to the difficulties involved in physically separating the different layers because of their thickness (1-200 μm). Numerous interactions occur between the different components of each layer as well as degradation and ageing phenomena. Moreover, each layer is often composed of a mixture of various compounds, such as pigments and binding medium in paintings. These are not distributed homogeneously and interactions can also occur between the components of individual layers.

In this research we focus on the study of the paint layers and on the reactions that can take place between the organic and inorganic components present in them during drying and ageing phenomena; reactions which strongly influence the painting’s final appearance.

Artist's paints are made up of two components: pigments and binders. In order to produce paints, pigments and binders are ground into a stiff paste which must have three requirements: it must be dispersed with a brush, adhere permanently to the support's surface and not alter significantly in time.

Pigments consist of finely divided insoluble solids, of a natural or synthetic origin, which provide the paint with colour and opacity.

The binders contribute immensly to the aspect of the painting, and the painting techniques can be distinguished depending on the binder used. Oil paints use siccative oil as binders (mainly linseed oil, but also sunflower, soya, sufflower, poppy). Encaustic technique employs waxes as their binding medium. Tempera painting is based on various emulsions, which contain a high level of proteinaceous components (egg, gelatin, animal glue, casein, or mixture of these). It may also contain lipid additives such as siccative oils, and sometimes saccharide materials (arabic gum, fruit tree gums), resins or other additives such as plasticizer (honey) or emulsifier (ox gall). If high levels of lipid additives are present, the technique is called "tempera grassa". Vegetable gum is the only binding medium used in watercolour painting. Modern paintings are realized using different kinds of synthetic resins (acrylic, alkyd, polyvinyl acetate, epoxy resins).

Chemically, the natural organic materials of a paint layer belong to three major chemical classes: lipids, proteins and sugars; they can be used alone, but mainly in mixtures.

Lipid materials can be found in many binders. Drying oils, binders of oil paints, are mixtures of mono-, di- and triglycerides, with high contents of unsaturated fatty acids (>50%). Among the drying oils used as binders, linseed oil is the most common, with an excellent performance in terms of pigments dispersion , drying time, optical transparency, and stability of film produced [2-4]. Waxes, the binders of encaustics, are mainly represented by beeswax (a mixture which, beside hydrocarbons, contains different esters, free fatty acids and free alcohols) or by paraffin and other microcrystalline waxes [5]. Cholesterol, which can be found in tempera paints, is the sterol present in egg yolk together with egg glycerolipids; it acts as an emulsifier for the binder emulsions, as well as the sterols from ox gall. Terpens and terpenoids are major components of resins produced by a variety of plants. They are complex natural mixtures with components built up of isoprene units. Mono – and sesquiterpenoids occur in volatile oils such as turpentine or lavender oil, diterpenoids are extruded by Pinaceae and Caesalpiniaceae species and are represented by colofonium, sandarac or copal resins. They are mainly used as protective layers in varnishes [6].

Among naturally occurring polysaccharides, starches and dextrines, arabic gum, tragacanth, and fruit tree gums (cherry, plum, peach, and others) are used in watercolours. They are natural polymers made up of different simple sugars and uronic acids [7].

Proteinaceous materials can be classified as animal proteins, such as egg proteins (yolk and/or white), gelatin, animal glue or casein, and vegetal proteins such as protein in garlic. The former are used in tempera artworks, while the latter is used as an adhesive for gold foils.

Organic materials in paint undergo several deterioration processes occurring over time resulting from both free radical reactions (mainly auto-oxidations and cross-linking reactions) and hydrolytic processes [8-10]. These processes need to be studied in order to understand the ageing processes occurring over time. It is also important to study and understand the interaction between the binding medium and the pigments, because the latter can promote or prevent the formation of radicals and therefore influence the rate of oxidation. Biodeterioration by enzymatic processes is also a significant decay factor. Understanding the mechanism of decay processes and identifying the resulting degradation products is essential for evaluating the changes and ageing over time, and finding methods to prevent, stop or slow down these processes in order to assure the long term preservation of cultural heritage [11,12].

In this research we have dealt mainly with the study of the chemical-physical properties of proteinaceous materials used as binders in tempera paints and of the ageing processes they undergo. Furthermore, we have studied alkyd resins used in modern and contemporary art paints paying particular attention to fast drying oil colours. Finally, we have investigated the characterisation and ageing of silane/siloxane , in particular alkyl-silane and alkyl-alkoxy siloxanes, and their potential applications as protective coatings. This study was aimed at identifying the best protective product to be applied during the restoration of the mural painting "*Tuttomondo*", by Keith Haring, on the wall of St. Antonio Church in Pisa.

1.2 Proteinaceous binders : Tempera painting

Tempera painting is one of the world's oldest painting techniques. The term "*tempera*" derives from "tempering" meaning diluting colours in a water medium. However, in general term, it refers to a mixture obtained by joining the coloured pigment with adhesive substances (binders) such as egg, fig milk, glue or other water-soluble substances. After the mid 1400's, this technique slowly began to include oily components, inching closer to the technique that would later be called oil painting.

The "Zingarelli" dictionary definition of the word "tèmpera or tèmpra " is: a mixture of colours in the glue or egg white to be painted on wood, plaster, canvas or more precisely, on scenes and theatrical decor". But today, the word "tempera" refers to that technique that uses water to disperse the colours in proteinaceous binders.

In the oldest tempera paintings egg was used as a binder, taking advantage of its rapid drying and hardening. This technique was well known all over the Mediterranean. It was used in ancient Egypt (from the sixth dynasty) and in Greece since the Mycenean and Cretan civilisations. In Italy tempera decorations are present in Etruscan tombs, and the Romans used the tempera technique with excellent results as shown in the splendid portraits found in the Egyptian Fayum area, dating from the 1st century B.C. to the 3rd A.D. It is a series of about 600 very realistic funerary portraits, painted for the most part on wooden boards. Their importance is given not only by the extraordinary realism, but also because they are among the oldest examples of art from in antiquity.

Figure 1.1 Examples of typical tempera portraits in the Fayum area

Egg tempera was also used in the Byzantine period around the tenth century. A.D.; it was the main technique used for painting on wooden boards. Instead, ancient medieval manuscripts, typically made from sheets of parchment or leather, were illustrated using the tempera emulsion which could easily to adhere to the support because it contained lipids of animal origin.

The use of the tempera technique can be divided into three periods according to how the colour was used and the final appearance of the artwork. The first period is prior to 1200, when raw products (casein and egg) mixed with pure pigments were used, and the colours were applied in successive overlapping layers. The second period runs between 1300 and the 1400, when the intervention of Cimabue and Giotto led to the use of glazes which were obtained by applying a layer of colour on another already dried one, allowing the tone shine below to come through, thus creating a wider colour range and a more realistic visual effect. The last period is after 1400 and led to an evolution of the technique. In fact vegetable oils, essences or varnishes were added to the original preparation in order to create a better visual effect. A famous example is Sandro Botticelli's "The Birth of Venus" painted in 1485, on a wooden board, and now housed in the Uffizi Gallery in Florence.

The addition of lipid additives to proteinaceous binders resulted in the development of the oil technique. Tempera, characteristic of the first paintings in the Italian Renaissance, was slowly replaced by oil technique. Many paintings of the late '400, classified by art critics as oils, are actually based on egg emulsions containing oils and finished with oil-based varnishes. A significant example of this fact can be found in the National Gallery of Ancient Art of Rome in Bernini Palace, where two works by the same artist of the '400 were cataloged differently: the first as a tempera painting and the second as an oil painting. In actual fact, they are both egg-based emulsion cases, to which oleo-resinous colours or oil glazes were added on tempera layers.

In the centuries following the Italian Renaissance, the tempera technique was often used as a base for oil paints. For example the Italian painter Antonio Fontanesi (1818 -1882) would sketch his paintings with tempera paints based on egg yolk and arabic gum, and then complete them using oil paints. Other famous artists also adopted the same procedure, such as Carlo Carrà, Arnold Bocklin, Giorgio De Chirico, Pietro Annigoni and many others.

1.3 Synthetic resins in modern and contemporary art

At the beginning of the 20th century synthetic polymers started to be mass-produced and widely used in many areas. One such area was house paints based on synthetic polymers, as these had desirable properties not achievable with the traditional linseed oil based paints of the time. Artists also began to be interested in these new paintings because the house paints allowed them to express themselves in new ways not previously explored. In the 1930s artists started to use synthetic resin based house paints in their painting, thus spawning many new artistic movements. An important part of these new movements, as in the emergence of any new movement, was the use of new and interesting media to create a feel not yet encountered. The muralist David Alfaro Siqueiros had set up a painting workshop in New York to encourage artists to explore paints other than traditional oils, he declared: "I am the first artist to lay claim to the use of painting materials with a synthetic resin base. And already at this moment there are at least some fifty American or

American based painters who are following my example. What will happen when all the painters in the world grasp the convenience of using these modern materials?"

As the decades, commercial oil based paint started to fade out and be replaced by synthetic paints, and many more artists started to embrace these new media. These includes Roy Lichtestein, Jackson Pollock, Franck Stella and one of the most discussed painters of that period, Pablo Picasso.

Consultation with famous living artists by art historians and restorers has enabled direct questioning into why synthetic resins were used and what new effects could be achieved, which were previously impossible with the more traditional linseed oil-based paints. The main reason given for turning to synthetic resins, was their more desirable physical properties such as drying speed , colour, finish, their hard-wearing property and fluidity, a particularly important trait for Jackson Pollock. Furthermore, common house paint materials were cheap and freely available, again making them popular.

Nowadays, synthetic resins are the binding media, or binders used in the vast majority of paints, although oil still remains an important medium in the specialized field of artists' paints. Acrylic resin, alkyd resin and polyvinyl acetate (PVA) resin are the three most important classes of synthetic resin binders used, although other, less common resins used as binders are cellulose nitrate, chlorinated rubber, polyurethane, epoxy resin and silicone. This now widespread use of synthetic resin materials has important implications for the conservation, preservation, and treatment of twentieth - and twenty-first-century works of art. It is likely that each of these different types of paint will display a unique set of physical and chemical properties, as well as responses to ageing, environmental conditions, and conservation treatments.[13]

1.3.1 Conservation of synthetic resin paints

The major concern of the modern conservator concerning synthetic resins is the unknown aspect of their ageing. Before their use as a common paint medium, the use of linseed oil based paint had been prevalent for the least 400 years. During this time many paintings were produced using this medium, affording the modern restorer many opportunities to experiment on oil paintings and an opportunity to build on previous knowledge. Consequently, the established conservation treatments, were mainly designed for old master paintings, and are not suitable for artwork created with these new materials.

One of the most common problems is the high sensitivity of films of many modern paintings to the organic solvents that are commonly used for the cleaning of traditional paintings. In traditional oil paintings the pigmented layer is protected from the external environment by a layer of varnish. This enables the restorer to remove the varnish layer, along with all the dirt accumulated over the years, with gentle solvent cleaning. For many synthetic resins the use of any solvent is dangerous for the painted surface and usually result in the swelling and partial solution of the paint.

In addition, most of the works of modern art are not varnished and dirt builds up on the original pigment layer over time. This implies that preventing dirt from reaching the possibly sensitive surface becomes highly important. The use of a separate protective layer, such as a sheet of glass, is often used although this can impair viewing. Even more important than the accumulation of dirt, is the resin's direct exposure to light, heat, humidity and other possibly damaging substances. All these factors must be taken in the consideration concerning the changes in the properties of the surface and thus the integrity of the art works.

Knowledge of the physical chemical features of a paint's binding medium is invaluable to restorers and art historian for understanding, preserving, and treating works of art. Indeed, a detailed chemical identification of all paint and varnish layers present in a work of art is often a prerequisite for any conservation treatment. This knowledge is also essential for the design and testing of suitable conservation treatments and for a more thorough understanding of the most appropriate environments for the exhibition, transportation, and storage of modern and contemporary works of art. Here, an understanding of the ageing response of each of these new paint types to environmental conditions, in particular, changes in relative humidity, temperature, and exposure to light, is important. Different kinds of paints can be expected to react differently to these conditions [11,12,15-19].

The gaining of knowledge about the ageing of synthetic resins is not the only reason why it is important to study them. It is just as important to be able to characterise them and identify them to provide provenance, and understanding of the working methods of the artists.

Furthermore, contrary to traditional oil paints, a modern paint is a complex mixture composed of a binder (30%), solvent (25%), filler (10%), additives (3%) and pigments (22%). In some formulations of acrylic emulsion paints, water is also present (10%) (table 1.1.) [16].

Component	Mass %
binder	30
solvent	25
water	10
pigments	22
filler	10
additives	3

Table 1.1 Percentage composition of colour used in modern paints

Over the past thirty years, a number of techniques have been developed to identify the various materials used as traditional binding media, and many of the world's major art museums now have the facilities to carry out these analyses routinely. Techniques that work particularly well

for traditional paint analysis are Fourier Transform Infrared Spectroscopy (FTIR), Gas Chromatography (GC), Gas Chromatography-Mass Spectroscopy (GC-MS) and thermal analytical techniques, such as Differential Scanning Calorimetry (DSC) or Thermogravimetry (TGA).

1.4 Thermal analysis and FTIR techniques applied to the study of cultural heritage

In the last decades the role played by thermal analysis and calorimetry in the field of the preservation of cultural heritage has continuously increased [20] and the full range of the most advanced thermo-analytical techniques (thermal analysis, TA, differential scanning calorimetry, DSC, thermogravimetry, TG, thermo-mechanical analysis, TMA, dynamic mechanical analysis, DMA, microthermal analysis, μ-TA) have been widely and successfully used in the context of the characterization of artworks and archaeological objects. When combined with other analytical (size exclusion chromatography, high-performance liquid chromatography, gas chromatography, mass spectrometry), and spectroscopic (Fourier Transform Infrared Spectroscopy, UV-Vis, Raman) techniques, they offer a powerful tool for the long term preservation of artistic objects and to assess the best conservation and display conditions, providing an example of multidisciplinary approach to the chemistry of cultural heritage. Thermoanalytical and calorimetric techniques offer a powerful method for problem solving whenever it is necessary to grasp information on the composition and behavior of materials used in art or to have an understanding on how damage to cultural heritage occurs and how damage processes can be retarded.

Thermal analysis and calorimetry, compared to other techniques, show several advantages: they are micro-destructive techniques, needing only small amounts of sample (usually less than 50 mg); sample requires a minimal preparation; the modern instrumentation is widely automated so that short times are required for each measurement; they provide quantitative results and an easy correlation with end-use properties.

Several papers have been published in the literature that illustrate the interdisciplinary and complementary character of thermal analysis and calorimetry and their potential in the analysis of painting media [21,22], archaeological waterlogged woods [23,24], parchments [25] and historic tapestries [26], mortars employed in historic buildings [27], terracotta sculptures [28], firing temperatures of ceramics [29] and coating materials [30].

In art conservation and diagnostic laboratories, infrared (IR) spectroscopy is the most widely applied spectroscopic method for the investigation of cultural heritage materials as many of their inorganic and organic constituents show characteristic absorption bands in the range (4000-600 cm^{-1}). From the early beginning of IR spectroscopy, its use has been mentioned for the examination of paintings and artifacts [31]. In the 1970s, the transition from dispersive IR to Fourier Transform Infrared (FTIR) instruments has really improved both resolution and detection limits of this techinque, and the possibilities offered by FTIR have been largely exploited for resolving conservation issues [32]. At the beginning of the 1980s, the introduction of micro-sampling accessories for FTIR spectroscopy and, in particular, the development of FTIR microscopy, offered an essential tool in the micro-destructive analysis of small samples [32].

Several papers have been reported on the application of the FTIR microscopy to the field of conservation and the analysis of cultural heritage materials such as pigments [33], binding media [1-8,21,22,34], varnishes [6,35], dyes [36], protective treatments [30,37] and degradation products [8,11,12,38].

References

[1] Amadesi S, Gori F, Grella R. *Holografic methods for painting diagnostics.* Appl Optics (1974) 9, 2009-2013;

[2] Lazzari M, Chiantore O. *Drying and oxidative degradation of linseed oil.* Pol Degrad Stab(1999) 65, 303-313;

[3] Bonaduce I, Carlyle L, Duce C, Ferrari C, Tiné MR, Colombini MP. *A Multi-analytical approach to studying binding media in oil paintings.Characterisation of differently pre-treated linseed oil by DE-MS, TG and GC-MS.* J Therm Anal Calorim (2012) 107, 1055-1066;

[4] Spyros A, Anglos D. *Study of ageing in oil paintings by 1D and 2D NMR spectroscopy.* Anal Chem (2004) 76, 4929-4936;

[5] Mattera J. *The art of encaustic.*(2001) Book Watson-Gaptill Ed.;

[6] Horn BA, Qiu J, Feist WC. *FTIR studies of weathering effects in western Redcedar and southern Pine .* Appl Spectr (1994) 48, 662-668;

[7] Butler G, Poullis N, Sluga C. *Contemporary watercolours. Medium, tools and techniques for contemporary artists.*(2012) Book , Walter Foster Ed,Irvine, CA;

[8] Karpowicz A. *Ageing and deterioration of proteinaceous media.* Stud Conserv (1981) 26, 153-160;

[9] Leo G, Bonaduce I, Andreotti A, Marino G, Pucci P, Colombini MP. *Deamidation at asparagine and glutamine as a ,ajor modification upon deterioration/aging of proteinaceous binders in mural paintings.* Anal Chem (2011) 83, 2056-2064;

[10] Kukcova S, Hynek R, Kodicek M. *MALDI-MS applied to the analysis of protein paint binders.* Organic mass spectrometry in art and archaeology. (2009) Wiley, London;

[11] Odlyha M, Cohen NS, Foster GM. *Dosimetry of paintings: determination of the degree of chemical change in museum exposed test paintings (smalt tempera) by thermal analysis.*Therm Acta (2000) 365, 35-44;

[12] Odlyha M, Cohen NS, Foster GM, West RH. *Dosimetry of paintings: determination of the degree of chemical change in museum exposed test paintings (azurite tempera) by thermal and spectroscopic analysis.* Therm Acta (2000) 365, 53-63;

[13] Spizzotin P. *I secoli d'oro nell'arte* . (1988) Book, Del Drago Ed, Milano;

[14] Chiantore O, Ploeger R, Scalarone D. *Thermal analytical study of the oxidative stability of artists' alkyd paints.* Pol Degrad Stab (2008) 94, 2036-2141;

[15] Cohen NS, Odlyha M, Campana R, Foster GM. *Dosimetry of paintings: determination of the degree of chemical change in museum exposed test paintings (lead white tempera) by Thermal analysis and IR spectroscopy.* Therm Acta (2000) 365, 45-52;

[16] Bieleman JH. *Additives for coatings.* Wiley-VCH. Weinheim(2000) ;

[17]Perrin FX, Irigoyen M. *Artificial aging of alkyd paints: a micro-ATR spectroscopic study.* Pol Degrad Stab (2000) 70, 469-475;

[18] Domenech-Carbò T, Bitossi G, silva MF. *Study of ageing of ketone resins used as picture varnishes by FTIR spectroscopy, UV-Vis spectrometry, ATM and scanning electron microscopy X-Ray microanalysis.* Anal Bioanal Chem (2008) 391, 1351-1359;

[19] Marengo E, Liparota MC, Robotti E. *Monitorin of paintings under exposure to UV light by ATR-FTIR spectroscopy and multivariate control charts.* Vibrat Spectr (2006) 40, 225-234;

[20] Pires J, Cruz JA. *Techniques of thermal analysis applied to the study of cultural heritage.* J Therm Anal Calorim (2007) 87, 411-415;

[21] Odlyha M. *Investigation of the binding media of paintings by thermoanalytical and FTIR techniques.* Thermochim Acta (1995) 269, 705-727;

[22] Odlyha M, Burmester A. *Preliminary investigations of the binding media of paintings by differential thermal analysis.* J Therm Anal (1988) 33, 1041-1052;

[23] Donato DI, Lazzara G, Milioto S. *Thermogravimetric analysis. A tool to evaluate the ability of mixtures in consolidating waterlogged archaeological woods.* J Therm Anal Calorim (2009) 101, 1085-1091;

[24] Cavallaro G, Donato DI, Lazzara G, Milioto S. *A comparative thermogravimetric study of waterlogged archaeological and sound woods.* J Therm Anal Calorim(2010) 104, 451-457;

[25] Odlyha M, Cohen NS, Foster GM. *ICOM ommittee for Conservation 13th Triennial Meeting, Rio de Janeiro 22-27 sept 2002.* James & James Ltd. 615;

[26] Odlyha M, Wang Q, Foster GM, Horton H. *Thermal analysis of model and historic tapestries.* J Therm Anal Cal (2005) 85, 157-165;

[27] Alvarez JJ, Navarro I . *Thermal and chimica studies of the mortars used in the Cathedral of Pamplona (Spain).* Thermochim Acta (2000) 365, 177-186;

[28] Tomasetti M, Campanella L, Urbano S. *Thermal analysis of fictile votive statues of 3rd century BC.* Thermochim Acta (1997) 291, 117-130;

[29] Andres AM, Munoz I. *Materials issues in art and archaeology III.* Symp Proc (1992) 267, 627-636;

[30] Tsakalof A, Manoudis P, Panayiotou C. *Assessment of synthetic polymeric coatings for the protection and preservation of stone monuments.* J Cult Herit (2007) 8, 69-72;

[31] Krevinghaus AB.*Infrared reflectance of paints.* Applied Optics (1961) 8, 807-812;

[32] Shearer JC, Peters DC. *FTIR in the service of art conservations.* Anal Approach (1983) 55, 123-142;

[33] Learner TJS. *Analysis of modern paint.* Book, (2004) Getty conservation Institute Ed.;

[34] Duce C, Bramanti E, Ghezzi L, Bernazzani L, Spepi A, Tinè MR. *Interactions between inorganic pigments and proteinaceous binders in reference paint reconstructions.* Dalton Trans (2012) 212, 160-176;

[35] La Rie D, Rene E. *New synthetic resins for pictures varnishes.* Book, Mills, John S.;(1990) Smith, Perry Ed. London

[36] Gillard SD, Hardman SR. *the detention of dyes by FTIR microscopy.* Stud Conserv (1994) 39, 187-196;

[37] Kaharaman MV, Kugu M, Gungor A, Menceloglu Y, . *The novel use of organo alkoxy silane for the synthesis of organic-inorganic hybrid coatings.* J of Non-Cryst Sol (2006) 352, 2143-2151;

[38] Meilunas RJ, Benstein J, James G. *Analysis of aged paint binders by FTIR spectroscopy. S*Stud Conserv (1990) 35, 33-51;

2 Materials and methods

2.1 Materials

2.1.1 Proteinaceous binders

Paint reconstructions were prepared using Casein (53171), OVA (51541) and Rabbit glue (53921) purchased from Bresciani srl (Milan-Italy) with azurite ($Cu_3(CO_3)_2(OH)_2$), calcium carbonate ($CaCO_3$), hematite (Fe_2O_3), red lead (Pb_3O_4) and cinnabar (HgS) purchased from Zecchi Colour Firenze. Casein was obtained by an acid precipitation of milk and is a mixture of four components (α_{s1} (38%); α_{s2} (10%); β (36%) and κ (13%) casein) with molecular mass in the range of 19-26 kDa [1]. Casein was left to expand in water, and then an ammonia solution (30% w/w) was added one drop at the time until a clear solution was obtained.

OVA was dissolved in water. The pigment was mixed with the fluid binder in proportions that produced a paintable paste. The paint was then applied with a brush on glass microscope slides. A set made up of each typology of pigment/protein replica was artificially aged in the solarbox (see section 2.2.4) and then stored at room temperature in the laboratory.

Rabbit glue was dissolved in water and heated in a bain-marie until a clear/fluid solution was obtained. The pigment was mixed with the fluid binder in proportions that produced a paintable paste.

2.1.2 Alkyd resins

Ten commercially available artists' alkyd samples by Winsor & Newton (Griffin series, fast drying oil colour) were investigated, and namely Cadmium yellow light, Winsor lemon, Phtalo green, Viridian green, Cadmium red medium, Winsor red, French ultramarine, Phtalo blue, Titanium white and Ivory black. The paint samples were applied on glass microscope slides in order to obtain approximately 0.5-1.0 mm thick layer. The paint replicas were naturally aged in our laboratory, without any specific enviromental control. Naturally aged samples were tested after 0 h, 2h, 5h, 10h and 24 h to evaluate the physical drying and then tested after 48h, 120h, 192h, 264h, 384h, 720h, 1050h, 1770h, 3300h and 5600h to evaluate all chages due to ageing process. The paint replicas were artifical aged with acetic acid in our laboratory (see 2.2.5). Artificial aged samples were tested after 6 months to evaluate all changes due to ageing process.

Also pure pigments were studied, produced by Abralux colouri Berghè (Cadmium Yellow light-PY35, Viridian green-PG18, Cadmium red-PR108, Winsor lemon-PY3, French ultramarine-PB29 and Titanium white-PW6) and Zecchi colouri Firenze (Ivory black-PBK9).

The two phthalocyanine pigments (Phthalo blue-PB15 and Phthalo green-PG7) has been synthetized in our laboratory as reported in literature by Achar et. Al [2]

Urea, phthalic anhydride, tetrachloro-phtalic anhydride, ammonium heptamolybdate and copper (II) chloride were A.C.S. reagents from Aldrich Chemical Co., USA. All other chemical reagents were of analytical grade. Dolomite filler was purchased from Kremer Pigmente GmbH & Co. KG, Hauptstr. Aichstetten DE.

- *Synthesis of copper(II) Phthalocyanine blue:*

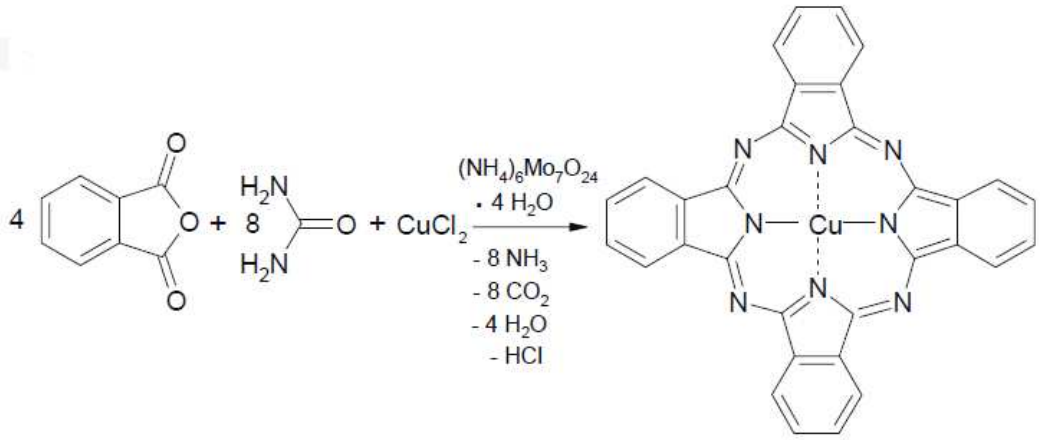

Scheme 2.1 Synthesis of blue pigment Cu(II) phthalocyanine complex

A mixture of 5.53 g (92.0 mmol) urea, 2.67 (18.0 mmol) phtalic anhydride, 500 mg (5.00 mmol) copper (II) chloride and 75 mg (0.061 mmol) ammonium heptamolybdate were finely ground and placed in a 500 cm^3 three-necked flask containing 25 cm^3 of nitrobenzene. The temperature of the stirred reaction mixture was slowly increased to 185°C and maintained at 185 ± 5°C for 4.5 h. The solid product was finely ground and washed with ethanol until to free from nitrobenzene. The product was added to 500 cm^3 of 1.0 N hydrochloric acid saturated with sodium chloride, boiled for about 5 min, cooled to room temperature and filtered. The resulting solid was treated with 500 cm^3 1.0 N sodium hydroxide containing 200 g sodium chloride and heated at 90°C until the evolution of ammonia ceased. The solid product after filtration was treated with 1.0 N hydrochloric acid and separated by centrifugation. Alternate treatment with hydrochloric acid and sodium hydroxide was repeated twice. The copper (II) phthalocyanine was washed with water until chloride-free. The blue complex was dried at 110°C.

The final product, 2.40 g (4.17 mmol, 93%) is blue, fine-crystalline substance, insoluble in organic solvents.

The melting performance of the substance can serve as a criterion for purity: a pure product is given, if until temperatures of above 200°C no melting or decomposition can be noticed. The here isolated substance was stable until 360°C. The side product diyhdrophtalocyanine melts under decomposition at 195-197°C.

The results of elemental analysis and H^1-NMR agreed with the calculated values and were consistent with structures of scheme 2.1.

- *Sinthesis of copper(II) Phthalocyanine green*

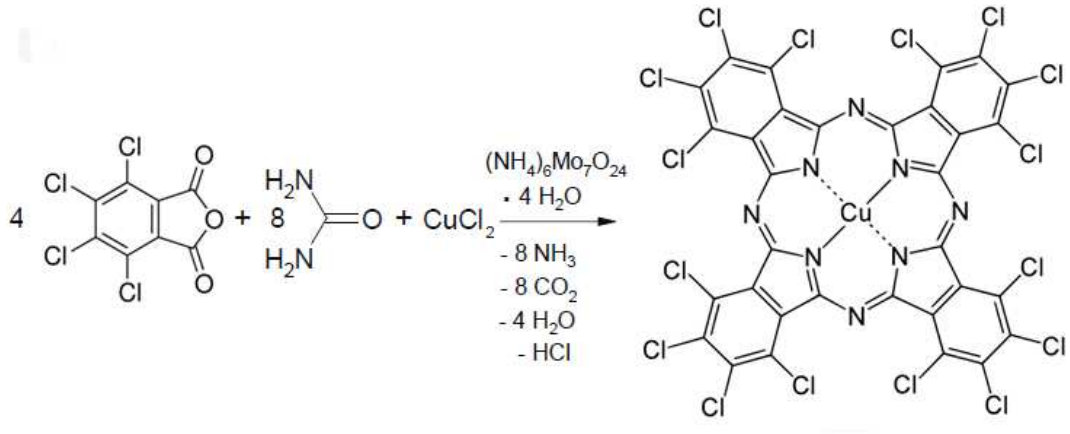

Scheme 2.2 Synthesis of green pigment Cu(II) phthalocyanine complex

A mixture of 10.82 g (180.0 mmol) urea, 5.15 (18.0 mmol) tetrachloro-phtalic anhydride, 500 mg (5.00 mmol) copper (II) chloride and 75 mg (0.061 mmol) ammonium heptamolybdate were finely ground and placed in a 500 cm^3 three-necked flask containing 25 cm^3 of nitrobenzene. The temperature of the stirred reaction mixture was slowly increased to 180°C and maintained at 180 ± 5°C for 6 h. The solid product was finely ground and washed with ethanol until to free from nitrobenzene. The product was added to 500 cm^3 of 1.0 N hydrochloric acid saturated with sodium chloride, boiled for about 30 min, cooled to room temperature and filtered. The resulting solid was treated with 500 cm^3 1.0 N sodium hydroxide containing 200 g sodium chloride and heated at 90°C until the evolution of ammonia ceased. The solid product after filtration was treated with 1.0 N hydrochloric acid and separated by centrifugation. Alternate treatment with hydrochloric acid and sodium hydroxide was repeated twice. The copper (II) phthalocyanine was washed with water until chloride-free. The green complex was dried at 110°C.

The final product, 5.13 g (4.51 mmol, 92% yield) is green, fine-crystalline substance, insoluble in organic solvents.

The melting performance of the substance can serve as a criterion for purity: a pure product is given. The results of elemental analysis agreed with the calculated values and were consistent with structures of scheme 2.2.

2.1.3 Silicone resins

In this work we studied two hydrophobic silicone coatings , Hydrophase® (Phase Restauro-Milan-Italy) and Disboxan 450® (Caparol Pisa-Italy) used as protective of the wall painting “Tuttomondo” by Keith Haring in S. Antonio Church in Pisa.

The first the Hydrophase® is an impregnating ready to use, with no film forming properties and molecular size comparable with water size (5-10 Å), that allows it to penetrate deeply in the wall substrate, preventing water absorption, the effect of water-ice forming and the corrosion by pollutants and rain.

The Hydrophase is composed by monomeric alkyl-siloxanes and is different from the traditional oligomeric siloxane products, for the high penetration deep down in the substrate and consequently they are not disponible to UV light, show high resistance to alkaline characteristics of common support (cement, lime) and high resistance to placer mining. The alkyl-siloxanes are never film-forming polymers also when used in high concentration.

Disboxan has a different formulation from Hydrophase because it is composed by micro-emulsion of oligomeric alkoxy-siloxanes , that show the same characteristic of the monomeric species but having higher molecular size the oligomeric species are enable to penetrate deep down in the support and the interaction with the substrate is mainly in the surface .

Each silicone coatings has been applied on sample reproduction of acrylic colour on glass microscope slides by the microspray technique. The Hydrophase as pure product, while Disboxan has been diluited 1:10 with water and then applied.

2.2 Apparatus and methods

2.2.1 Thermogravimetry (TGA)

Thermogravimetric analysis (TGA) is the most widely used thermal methods. It is based on the measurement of mass loss of materials as a function of temperature. In thermogravimetry a continuous graph of mass change against temperature is obtained when a substance is heated at a uniform rate or kept at constant temperature. A plot of mass change versus temperature (T) is referred to as the thermogravimetric curve (TG curve). Often we also record derivative thermogravimetric (DTG) curves. A DTG curves presents the rate of mass change (dm/dT) as a function of temperature, or time (t) against the temperature (T) when substance is heated at uniform rate as shown in Fig. 2.1.

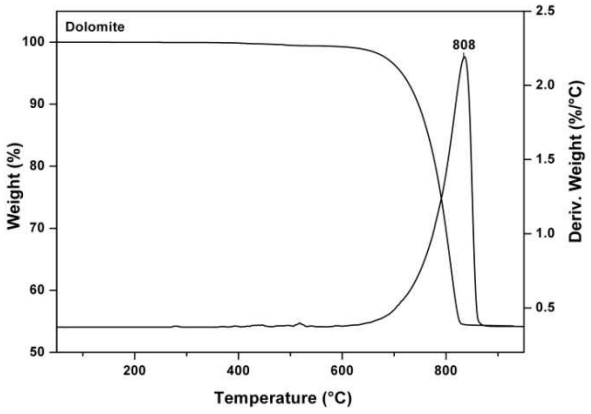

Figure 2.1 Typical TG and DTG curves. Note the plateau of constant mass, the mass loss portion and the final plateau of constant mass.

The instrument used in thermogravimetry (TG) is called a thermobalance. It consist of several basic components in order to provide the flexibility necessary for the production of useful analytical data in the form of TGA curves . Basic components of a tipical thermobalance are listed below:

1. Balance
2. Furnace: heating device
3. Unit for temperature measurement and control (Programmer)
4. Recorder: automatic recording unit for the mass and temperature changes.

These components may be represented by simple block diagrams as in Fig. 2.2.

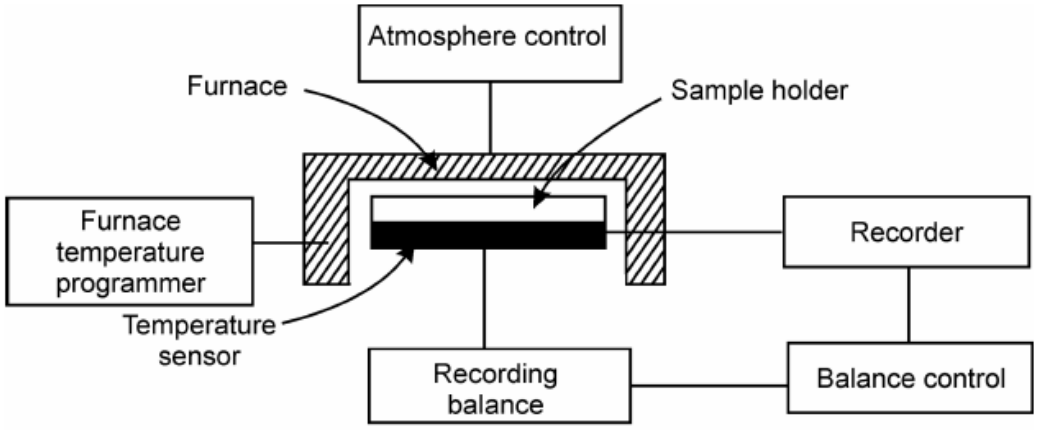

Figure 2.2 Block diagram of a thermobalance

The basic requirement of an automatic recording balance are includes accuracy, sensitivity, reproducibility and capacity. Recording balances are of two types, null point and deflection type. The null type balance, which is more widely used, incorporates a sensing element which detects a deviation of the balance beam from its null position, a sensor detects the deviation and triggers the restoring force to bring the balance beam to back to the null position. The restoring force is directly proportional to the mass change. Deflection balance of the beam type involve the conversion of the balance beam deflection about the fulcrum into a suitable mass change trace by (a) photographic recording i.e change in path of a reflected beam of light available of photographic recording , (b) recording electrical signals generated by an appropriate displacement measurement transducer, and (c) using an electrochemical device. The different balances used in TG instruments are having measuring range from 0.0001 mg to a 1 g depending on a sample containers used.

The furnace and control system must be designed to produce linear heating at over the whole working temperature range of the furnace and provision must be made to maintain any fixed temperature. A wide temperature range generally -150°C to 2000°C of furnaces is used in different instruments depending on the models.

Temperature measurement are commonly done using thermocouples, chromal-alumel thermocouple are often used for temperature up to 1100°C whereas Pt/Pt-10%Rh is employed for

temperature up to 1750°C. Temperature may be controlled or varied using a program controller with two thermocouple arrangements, the signal from one actuates the control system whilst the second is used to record the temperature.

Fig. 2.3 shows a schematic diagram of the specific balance and furnace assembly as a whole to better understand the working of thermobalance. In this diagram we can clearly see that the whole of the balance system is housed in a glass to protect it from dust and provide inert atmosphere. There is a control mechanism to regulate the flow of inert gas (generally nitrogen) to provide inert atmosphere. The temperature sensor of furnace is linked to the program to control heating rates, etc.

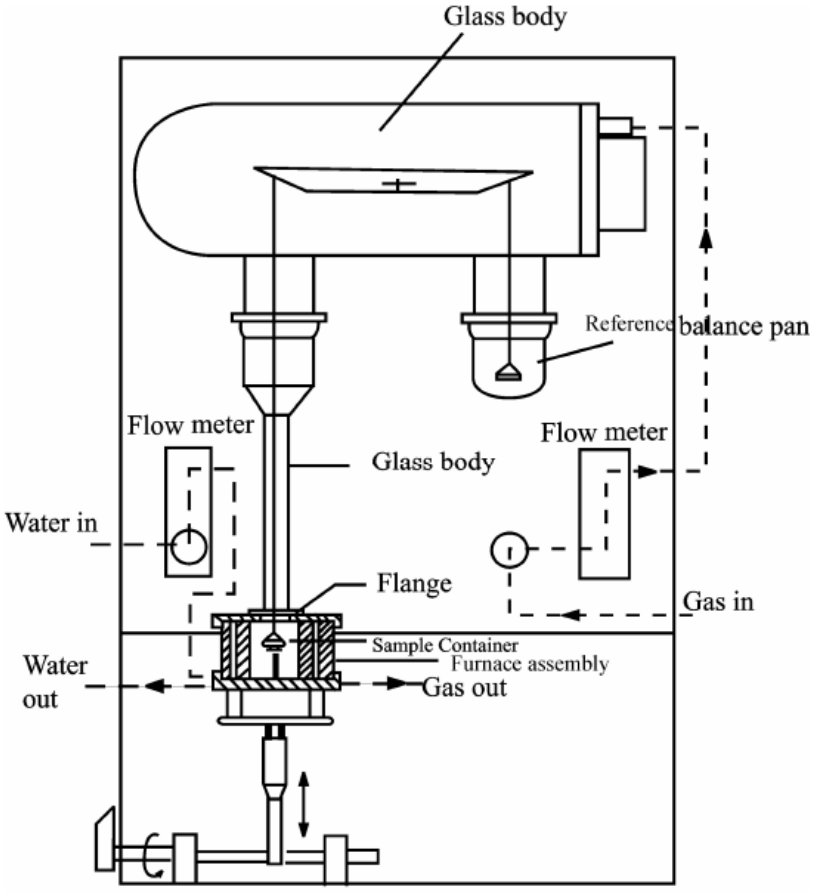

Figure 2.3 Schematic diagram of a typical balance and furnace assembly

A TA Instruments Thermobalance model Q5000IR was used. Measurements were performed at a rate of 10°C/min, from 30 °C to 900°C under air and N_2 flow (25 ml/min). The amount of samples in each TGA measurement varied between 2 and 4 mg. For each samples n= 3 replicates were performed.

The TG system was coupled with an FTIR spectrophotometer (Agilent Technologies, Cary 600 series) for online monitoring of evolved gas. The measurements were performed at 20°C/min scan rate, from 50°C to 800°C using a nitrogen flow of 70 ml/min as the purging gas. The sample mass ranged from 12 to 15 mg. The infrared spectra were recorded with a resolution of 4 cm^{-1} in the spectral range 4000-600 cm^{-1}. Data were collected using Agilent Resolution Pro version 5.2.0 software.

2.2.2 Differential Scanning Calorimetry (DSC)

Differential scanning calorimetry (DSC) monitors heat effects associated with phase transitions and chemical reactions as a function of temperature. In a DSC the difference in heat flow to the sample and a reference at the same temperature, is recorded as a function of temperature. The reference is an inert material such as alumina, or just an empty pan. The temperature of both the sample and reference are increased at a constant rate. Since the DSC is at constant pressure, heat flow is equivalent to enthalpy changes:

$$\left(\frac{dy}{dx}\right)_p = \frac{dH}{dt}$$

Here dH/dt is the heat flow measured in mW sec^{-1} and the heat flow difference between the sample and the reference is :

$$\Delta\frac{dH}{dt} = \left(\frac{dH}{dt}\right)_{\text{sample}} - \left(\frac{dH}{dt}\right)_{\text{reference}}$$

and can be either positive or negative. In an endothermic process, such as most phase transitions, heat is absorbed and, therefore, heat flow to the sample is higher that that to reference. Hence ΔdH/dt is positive. Other endothermic processes include helix-coil transitions in DNA, protein denaturation, dehydratations, reduction reactions and some decomposition reactions. In an exothermic process, such as crystallization, some cross-linking processes, oxidation reactions and some decomposition reactions, the opposite is true and Δ ΔdH/dt is negative.

The calorimeter consists of a sample holder and a reference holder as shown in Fig. 2.4. Both are constructed of platinum to allow high temperature operation.

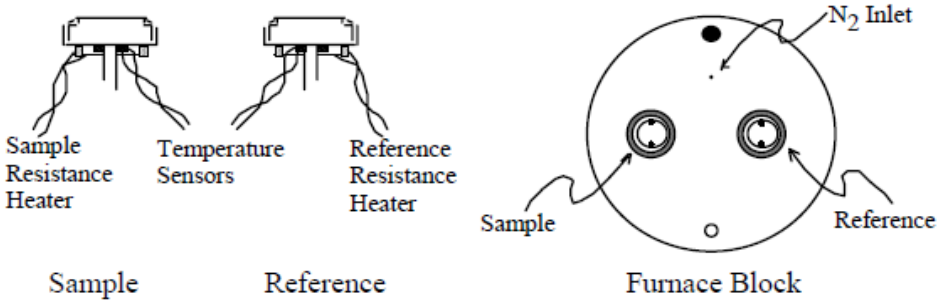

Figure 2.4 Differential scanning calorimeter sample and reference holder

Under each holder is a resistance heater and a temperature sensor. Currents are applied to the two heaters to increase the temperature at the selected rate. The difference in the power to

the two holders, necessary to maintain them at the same temperature, is used to calculate ΔdH/dt. A schematic diagram of a DSC is shown in Fig. 2.5. A flow of gas (nitrogen or air) is dehydrated before to arrive over the samples, with a drier cartridge, to create a reproducible and dry atmosphere. The sample is sealed into a small aluminum pan and the reference is usually an empty pan and cover.

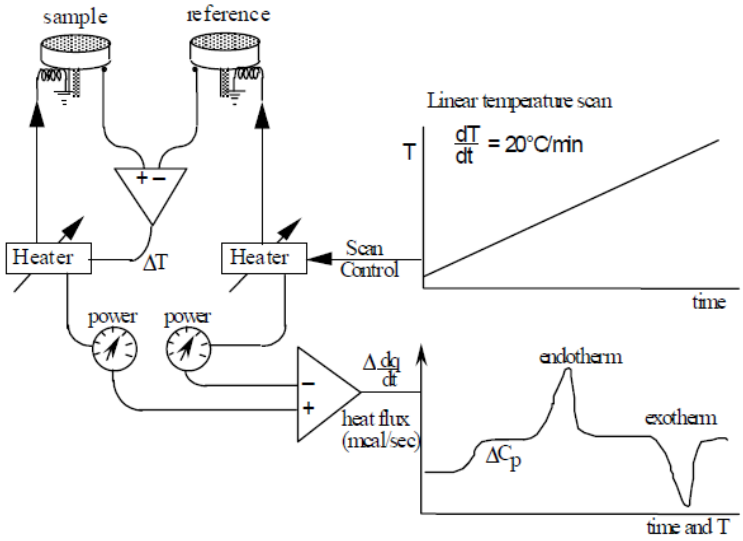

Figure 2.5 Schematic of a DSC, the sample heat power is adjusted to keep the sample and reference at the same temperature during the scan

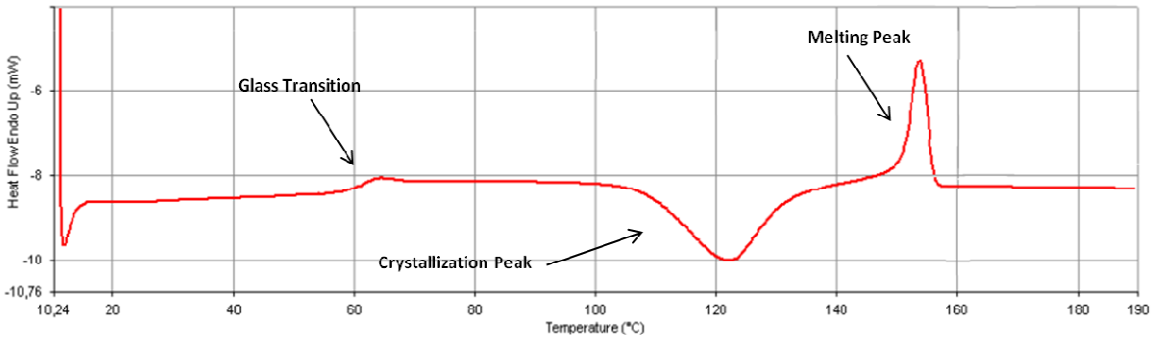

Figure 2.6 Typical DSC scan

As shown in Fig. 2.6 glass transition cause a baseline shift due to the different heat capacity of the sample, in fact is the temperature at which amorphous (noncrystalline) polymers are converted from a brittle, glasslike form to a rubbery, flexible form. This is not a true phase transition but one that involves a change in the local degrees of freedom. Crystallization is a typical exothermic process and melting a typical endothermic process, ΔH_{tr} is calculated from the area under the peaks.

The integral under the DSC peak, above the baseline, gives the total enthalpy change for the process:

$\int \left(\frac{dH}{dt}\right)_{sample} dt = \Delta H_{sample}$

Assuming that the heat capacity of the reference is constant over the temperature range covered by the peak, $\Delta H_{reference}$ will cancel out because the integral above the baseline is taken.

Heat capacities and changes in heat capacity can be determinate from the shift in the baseline of the thermogram. The heat capacity is defined as:

$$C_p = \left(\frac{dq}{dT}\right)_p = \left(\frac{dH}{dT}\right)_p$$

The temperature scan rate is:

$$\text{Scan rate} = \frac{dT}{dt}$$

Using the chain rule:

$$C_p = \left(\frac{dH}{dT}\right)_p = \frac{dH}{dt}\,\frac{dt}{dT}$$

Where dH/dt is the shift in the baseline of the thermogram and the last derivative is just the inverse of the scan rate. For differential measurements, we determine the difference in the heat capacity of the sample and the reference:

$$\Delta C_p = C_{p\,(sample)} - C_{p\,(reference)}$$

$$\Delta C_p = \Delta\left(\frac{dH}{dT}\right) = \Delta\,\frac{dH}{dt}\,\frac{dt}{dT}$$

A Perkin Elmer Pyris Diamond Differential Scanning Calorimeter was used. The measurements were performed in the temperature range 30 - 300°C at 10°C/min, under nitrogen as purging gas. The sample masss ranged from 7 to 8 mg and were prepared in aluminium pans.
In order to determine the glass transition temperature, T_g, the sample was first heated up to 200 °C at 20°C/min (first run), then quickly cooled to -20°C at 40°C/min, and finally heated again to 200°C at 20°C/min (second run). The T_g was evaluated by graphical construction over the second run curve as abscissa of the flex point. The presence of a glass transition was confirmed by experiments with the second run recorded at doubled scan rate.
Each experiments were performed three times.

2.2.3 Fourier Transform Infrared Spectroscopy (FTIR)

The total internal energy of a molecule in a first approximation can be resolved into the sum of rotational, vibrational and electronic energy levels. Infrared spectroscopy is the study of interactions between matter and electromagnetic fields in the IR region. In this spectral region, the EM waves mainly couple with the molecular vibrations. In other words, a molecule can be excited to a higher vibrational state by absorbing IR radiation. The probability of a particular IR frequency being absorbed depends on the actual interaction between this frequency and the molecule. A frequency will be strongly absorbed if its photon energy coincides with vibrational energy levels of the molecule. IR spectroscopy is therefore a very powerful technique, which provides fingerprint information on the chemical composition of the sample.

In spectroscopy, it is essential to know which frequencies are absorbed and which are not. This requires that the radiation source covers a broad spectral range and the individual frequencies of the radiation are analyzed. In the conventional dispersive-type spectrometer, a grating or a prism is used to disperse light into individual frequencies, and a slit placed in front of the detector to determine which frequency to reach the detector.

However the FTIR spectrometer operates on a different principle called Fourier Transform. The mathematical expression of Fourier transform can be expressed as

$$F(\omega) = \int_{-\infty}^{+\infty} f(x) e^{i\omega x} \, dx$$

And the reverse Fourier transform is:

$$F(x) = \int_{-\infty}^{+\infty} f(\omega) e^{-i\omega x} \, d\omega$$

Where ω is angular frequency and x is the optical path difference in our case. F(ω) is the spectrum and f(x) is called the interferogram that is determined experimentally by using the Michelson interferometer and the spectrum F(ω) can be obtained by using Fourier transform.

The basic Michelson interferometer consists of :

- A broad-band light source which emits light covering the mid-IR range,
- A beamsplitter made of KBr or CsI,
- Two front surface coated mirrors, one moving and one fixed, and
- A detector.

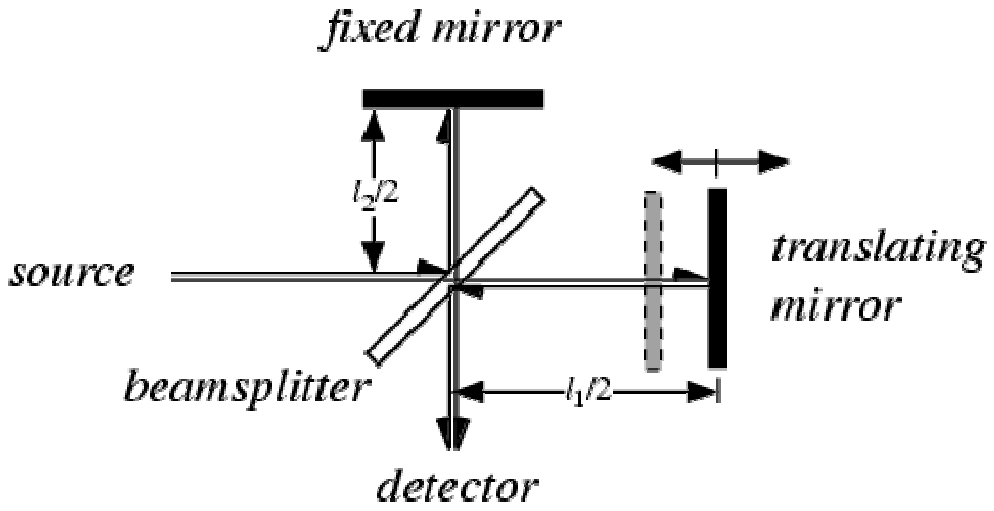

Figure 2.7 Schematic diagram of a Michelson Interferometer

The light from the light source is directed to the beamsplitter, half of the light is reflected and half is transmitted. The reflected light goes to the fixed mirror where it is reflected back to the beamsplitter. The transmitted light is sent to the moving mirror and is also reflected back towards the mirror. At the beamsplitter, each of the two beams (from the fixed and moving mirrors) are split into two: one goes back to the source (and "lost" since it does not reach the detector) and the other goes towards the detector. Hence the detector sees two beams: one from the moving mirror and the other from the fixed mirror. The two beams reaching the detector come from the same source and have an optical path difference determined by the positions of the two mirrors, i.e. they have a fixed phase difference. Therefore the two beams interfere. The two beams may be made to interfere constructively or destructively for a particular frequency by positioning the moving mirror. If the moving mirror is scanned over a range (corresponding to (x) in the function seen before), a sinusoidal signal will be detected for that frequency, with its maximum corresponding to constructive interference and the minimum corresponding to destructive interference. This sinusoidal signal is called interferogram-detector signal (intensity) against optical path difference. Assume a light which emits only two frequencies, each frequency will produce its own sinusoidal interferogram. Both interferograms will have maximum at optical path difference δ equals to zero (corresponding to the pint that the two mirrors are equidistance from the beamsplitter). But the other maxima will not coincide, since their positions are determined by the equation

$$\delta = 2\Delta x = 2n\lambda_i \ , \lambda_i = \lambda_1 \ , \lambda_2$$

where Δx is the difference in the distances between the beamsplitter an the two mirrors.

Because the source emits a range of frequencies, the detector output is the sum of all the interferograms, the resulting interferogram will have a maximum at Δx = 0 (centreburst) and tails off rapidly away from the centreburst.

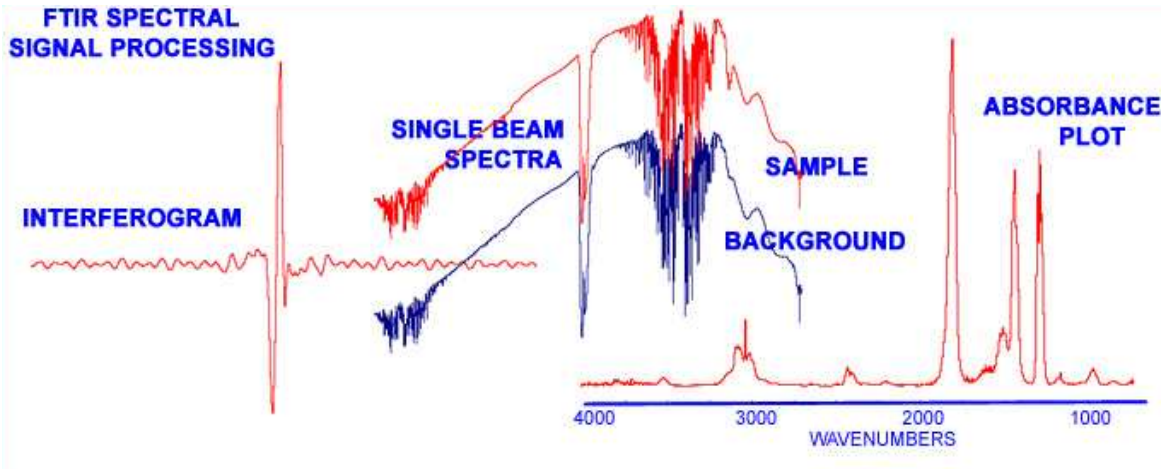

Figure 2.8 Relationship between spectrum and interferogram (detector signal)

As has explained earlier, interferogram is determined experimentally in FTIR spectroscopy, and the corresponding spectrum- frequency against intensity plot, is computed using Fourier transform. This transformation is carried out automatically and the spectrum is displayed.

FTIR spectrometer is inherently a single beam instrument. It is imperative to record a relevant background spectrum for each sample examined. The empty beam background (no sample in the light path) is recorded first. This spectrum shows the instrument energy profile, which is affected by the characteristics of the source, the beamsplitter, the absorption by the air (mainly due to CO2 and water vapour) in the beam path, and the sensitivity of the detector at different wavelengths. After the sample is placed in the combined beam and the sample spectrum is the ratio of the spectrum containing sample against that of the background.

Under certain conditions, infrared radiation passing through a prism made of a high refractive index infrared transmitting material (ATR crystal) will be totally reflected. When total internal reflection occurs, there exists an evanescent wave extends beyond the surface of the crystal. Hence when a sample is brought in contact with the totally reflecting surface of the ATR crystal, the evanescent wave will interact with sample. It will be attenuated in spectral regions where the sample absorbs energy and hence a spectrum can be obtained. The IR light undergoes several reflections inside the crystal to increase the interaction with the sample. ATR produces a very short pathlenght of the IR light in the sample, this makes this technique ideal for highly absorbing materials such as aqueous solutions, rubber or polymers.

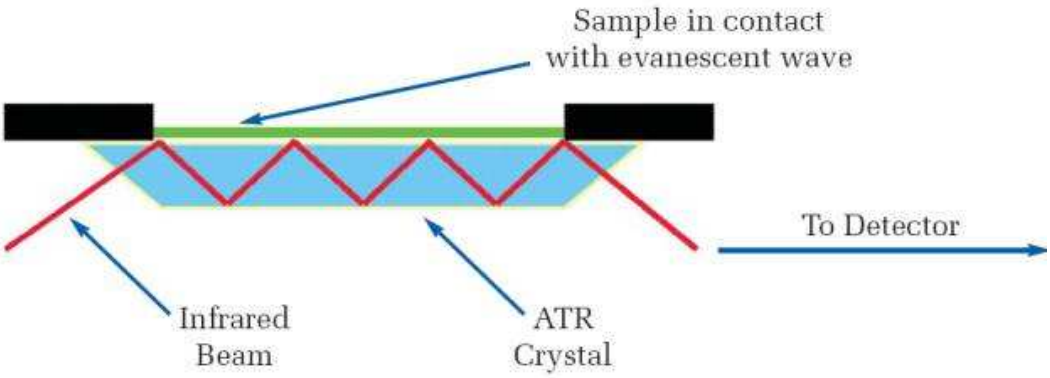

Figure 2.9 Principle of FTIR-ATR

The depth of penetration into sample is given by the equation:

$$dp = \lambda / 2n_p\pi (\sin 2\theta - n_{sp})^{1/2}$$

where λ = wavelength in air
n_p = refractive index of crystal
n_s = refractive index of sample
$n_{sp} = n_s/n_p$
θ = angle of incidence

Infrared spectra were recorded using a Perkin Elmer Spectrum One FTIR Spectrophotometer, equipped with a universal attenuated total reflectance accessory (ATRU) and a TGS detector. Few micrograms of powder scratched from each paint reconstruction were used. For each sample, 128 interferograms were recorded in order to obtain a suitable S/N ratio, averaged and Fourier-transformed to produce a spectrum with a nominal resolution of 4 cm^{-1}. Spectrum software and a written-in-house LabView program for peak fitting were employed to run and process the spectra respectively.

2.2.4 Solarbox

The solarbox (1500e RH), purchased from Erichsen (Germany), was used for artificially ageing the paint replicas with proteinaceous binder. The exposure conditions were 720 h at 25°C, 50% relative humidity (RH). A soda-lime glass UV filter was used to simulate the indoor exposure. A parabolic reflector chamber guaranteed irradiation uniformity with a xenon lamp in the focus.

2.2.5 Ageing with CH_3COOH of Winsor & Newton alkyd paint colour

The alkyd paint sample replicas were placed in closed glass case at 25°C for 6 months and atmosphere saturated with glacial acetic acid.

2.2.6 Patrizia Zara's paints

Small portions of samples (3-4 mg) from the back side of the works (scratching with a stainless steel knife) was taken. In particular we chose two points where the artist used pure colour (to avoid analysing colour mixtures) in each painting : orange and green for "Salto di qualità" and grey and blue for "Senza nome" respectively.

References

[1] Holt C. Adv. Prot Chem (1992) 43, 63-151;

[2] Achar BN, Fohlen GM, Parker JA. *Synthesis and structural studied of metal (II) 4,19,16,23-phthalocyanine tetraamines.* Polhyedron (1987) 6, 1463-1467;

3 Pigments and fillers in paints

3.1 Introduction

3.1.1 Pigments

Pigments provide colour and opacity to paint and usually consist of finely divided insoluble solids with particle size from about 0.2 to 20 μg diameter. They may be inorganic or organic in nature. The nomenclature of all pigments is now fully standardized and listed in the *Colour Index (C.I.)*, published by the Society of Dyers and Colourists (1971). Each pigments is given a C.I. name, for example, PW6 (for White Titanium) is the Pigment White n° 6 and this makes it possible to look up the pigment's chemical composition. With many of the inorganic pigments, however, their more conventional names – White Titanium, in the example cited here – are still widely used.

The inorganic pigments used in the tempera paint replicas are shown in the table 3.1 with their classical name and chemical composition.

Name pigment	Chemical composition	Chemical formula
Red Ochre	Iron (III) oxide	$Fe_2O_3 \cdot nH_2O$
Azurite	Basic Cu(II) carbonate	$Cu_3(CO_3)_2(OH)_2$
Calcium Carbonate	Calcium Carbonate	$CaCO_3$
Minium	Pb(II) + Pb(IV) oxides	$2PbO \cdot PbO_2$
Cinnabar	Mercury (II) sulphur	HgS

Table 3.1 Inorganic pigments studied in the tempera's paint replicas

The inorganic pigments are complemented by a vast range of organic pigments, often comprising dozens of variations of a particular chemical class like azo pigments, quinacridone pigments or phtalocyanine pigments.

The pigments based on the azo compounds can be produced in many different colours, most important are reds, oranges, and yellows. Some of the more frequently used red azo pigments are PR5, PR7, PR9, PR112 and PR170, all of which are based on the structure shown in Fig 3.1.

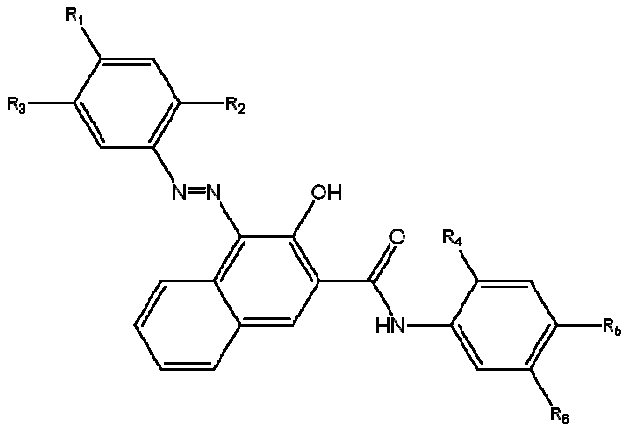

Figure 3.1 Chemical structure of five red azo pigments: PR5, PR7, PR9, PR112, PR170

Where R1-R6 are the following:

	R1	R2	R3	R4	R5	R6
PR5	H	OCH_3	$SO_2N(C_2H_5)_2$	OCH_3	OCH_3	Cl
PR7	Cl	CH_3	H	CH_3	Cl	H
PR9	H	Cl	Cl	OCH_3	H	H
PR112	Cl	Cl	Cl	CH_3	H	H
PR170	NH_2CO	H	H	C_2H_5	H	H

Yellow azo pigments are also a significant group of organic pigments. Important examples are PY1, PY3, PY73, PY74 AND PY97, whose structure are shown in Fig. 3.2.

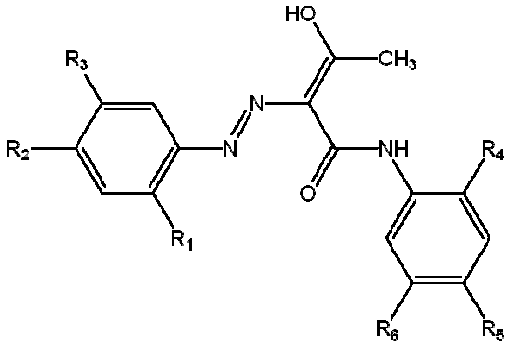

Figure 3.2 Chemical Structure of six yellow azo pigments : PY1, PY3, PY73, PY74 and PY97

Where R1-R6 are the following:

	R1	R2	R3	R4	R5	R6
PY1	NO_2	CH_3	H	H	H	H
PY3	NO_2	CH_3	H	Cl	H	H
PY73	NO_2	Cl	H	OCH_3	H	H
PY74	Cl	NO_2	H	OCH_3	H	H
PY97	OCH_3	$SO_2NHC_6H_5$	OCH_3	OCH_3	Cl	OCH_3

Quinacridone pigments are based on the structure shown in fig. 20. The molecule shown is a violet shade, pigment PV19(quinacridone violet) but many other pigments of different colours and shades (from deep reds to golden oranges) are produced by the substitution of various on the two and benzene rings. For example, I two commonly used quinacridone reds, PR122 and PR209,substitution occurs at the position shown in Fig. 3.3 (a,b).

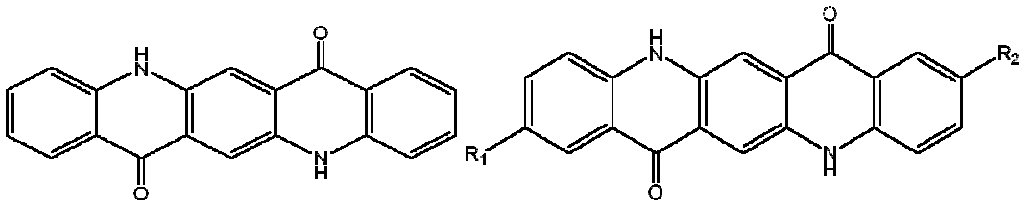

Figure 3.3 Chemical structure of three quinacridone pigments: a) PV19 and b) PR122 and PR209

The last important category of organic pigments is the phthalocyanine pigments, which the principal pigments are blue (PB15) and two greens (PG7, PG36), all of which are based on the structure shown in Fig. 3.4 that represent the phthalocyanine blue pigment (PB15). The colour can be altered to shades of green, however, by the substitution of chlorine and/or bromine atoms on the four outer benzene rings. PG7 is substituted with chlorine only, while PG36 with bromine and chlorine. PG7 usually contains 15 chlorine atoms, although some manufacturing processes produce higher quantities of the molecule substituted with 14 or 16 chlorine atoms. The proportion of bromo- to chloro-substitution in PG36 determines the precise hue of the pigment, with the shade becoming more yellow with the increase in bromine content.

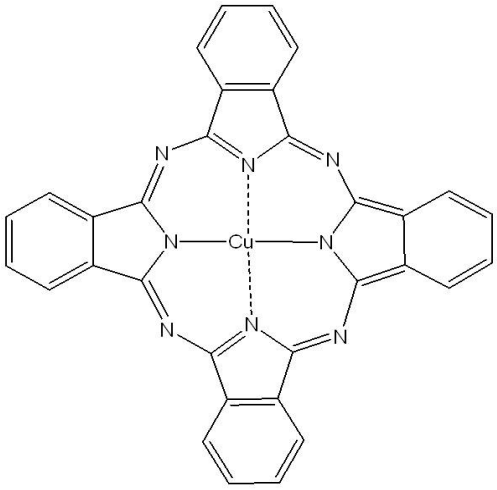

Figure 3.4 Chemical structure of phthalocyanine pigments

All the pigments of the alkyd resin produced by the Winsor & Newton studied in this work (organic and inorganic) are reported in the table 6 with their names, chemical structures and C.I. names and numbers.

Colour Name	*Index Colour*	*Pigment Name*	*Pigment Chemical Structures*
Cadmium Yellow	PY35	Cadmium/Zinc Sulphide	$(Cd,Zn)S_2$
Phthalo Green	PG7	Chlorinated copper phtalocyanine	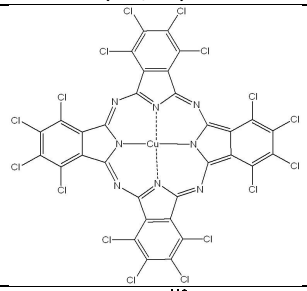
Winsor Lemon	PY3	Arylamide yellow	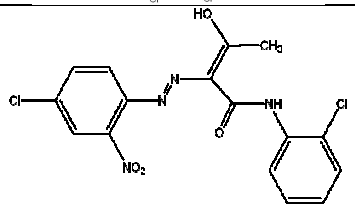
Viridian Green	PG18	Hydrated Cr (III) oxide	$Cr_2O_3 \cdot 2\ H_2O$
Cadmium Red	PR108	Cd (II) sulphoselenide	CdSSe
Winsor Red	PR170 + PR188	Naphtol carbamides	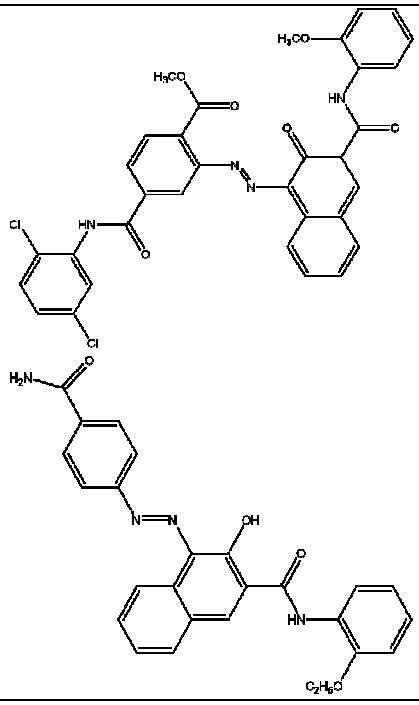
French Ultramarine	PB29	Complex sodium alumino-silicate containing sulphur	$Na_6Al_6Si_6O_{24}S_4$
Phthalo Blue	PB15	Copper Phtalocyanine	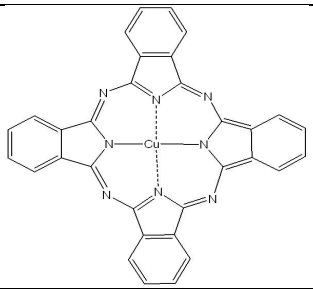
Titanium White	PW6	Titanium white	TiO_2
Ivory Black	PBK9	Ivory black	$Ca_3(PO_4)_2 + C + CaCO_3$

Table 3.2 Name colour and chemical composition of the alkyd colour studied in this work

3.1.2 Fillers

Fillers (or extenders) are inert inorganic solids that usually are white and have refractive indices in the range of 1.4 to 1.7, so that they are practically transparent in synthetic binding media. The most common used in the preparation of the final colour are:

- Calcium carbonate PW18 (also known as chalk or whiting)
  also: magnesium carbonate, PW18 (magnesite)
  also: double carbonate of calcium and magnesium, PW18 (dolomite)
- Hydrated aluminum silicate, PW19 (kaoline or chine clay)
- Barium sulphate, PW21 [synthetic] or PW22 [natural
- Hydtrated calcium sulphate, PW25 (gypsum or terra alba)
- Hydrated magnesium silicate, PW26 (talc or asbestine)
- Silicon dioxide, PW27 (silica or quartz)

Filler are used to add bulk to paint, to achieve a desired surface texture or appropriate rheological properties, and to reduce the cost of the formulation. If used above their critical pigment volume concentration (CPVC), fillers can also add opacity to a paint, as their refractive indexes are higher than that of the air in the voids that characterize such a film.

The addition of filler is particularly necessary with certain modern pigments, notably the phthalocyanine colours, to reduce their tinting strengths to those of the other pigments. Some synthetic fillers, for example, blanc fixe, are known to have an optical brightening effect.

3.2 Results and discussion

The easiest way of classification of the pigment is in organic or synthetic and inorganic pigments.

The spectra and TG curves from many of the inorganic pigments are rather simple and sometimes completely featureless. The spectra of minium and red ochre, for example, have just o very broad absorption at the low wavenumber end of the spectrum (between 500 and 700 cm^{-1}), like shown in Fig. 3.5

In stark contrast to the results displayed by the inorganic pigments, the FTIR spectra of organic pigments are characteristic and usually contain a multitude of absorptions in all the wavenumber of the spectrum (4000-600 cm^{-1}) and the TG curve are typical and characteristic for each pigment analyzed.

Table 3.4 and 3.6 reports the characteristic vibrational modes of the inorganic pigments in paint temperas and alkyd colour respectively.

Table 3.3 and 3.5 report the experimental temperatures and the percentage mass losses of the corresponding degradation steps in air of inorganic pigment in paint temperas and alkyd colour respectively. Table 3.7 reports the experimental temperatures and the percentage mass losses of the corresponding degradation steps in air of organic pigment in alkyd colour and the table 3.8 the characteristic vibrational modes of the organic pigments .

3.2.1 Inorganic pigments

3.2.1.1 Inorganic pigments in tempera paints

The pigments used in tempera colours are of inorganic origin (Table 3.1) so the FTIR spectra and the thermogravimetric analysis are very simple (Table 3.3-3.4)

The spectra are characterize from a broad absorption at the low wavenumber end of the spectrum (between 600 and 900 cm^{-1}) and generally the spectrum after 1000 cm^{-1} is empty. (Fig. 3.5, Table 3.4)

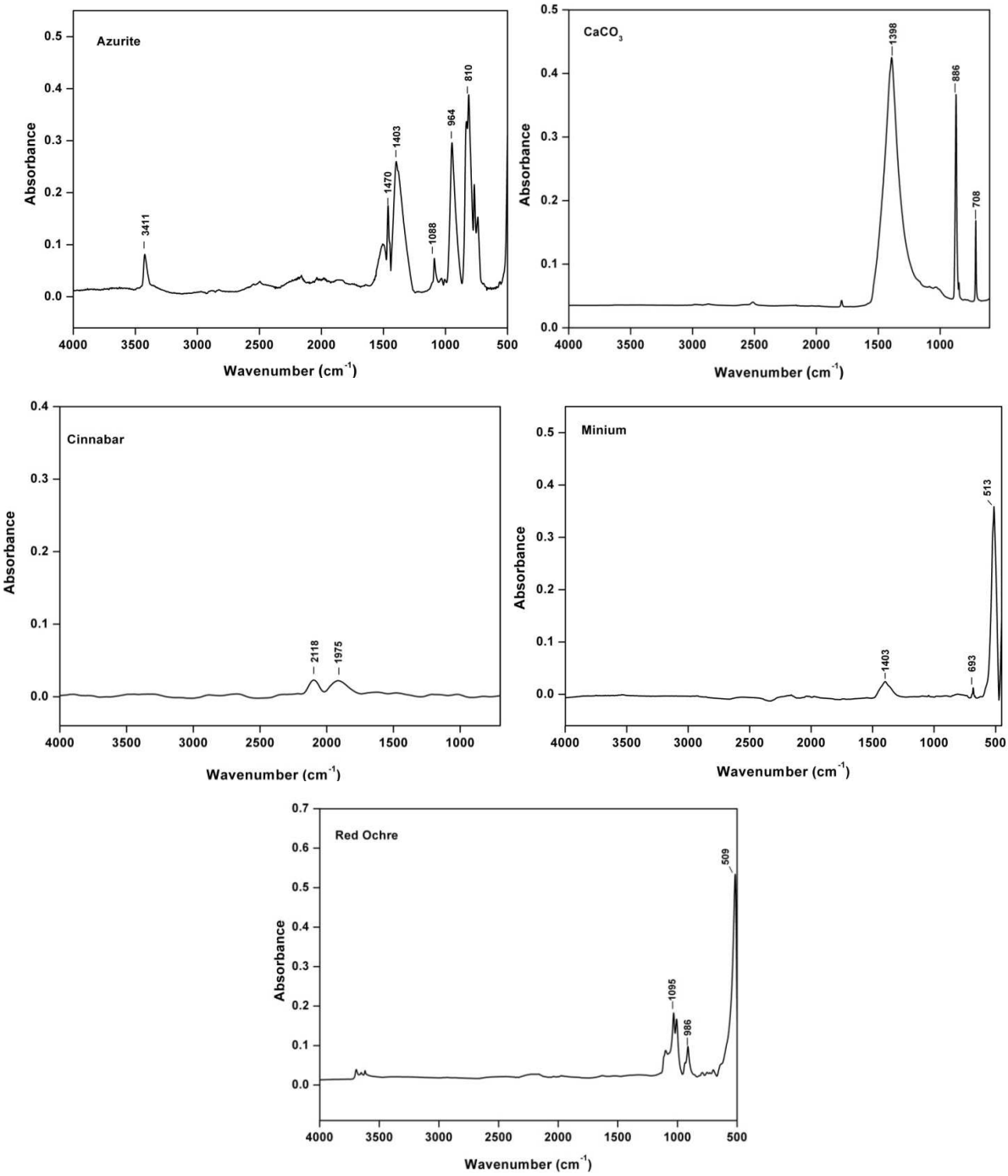

Figure 3.5 FTIR spectrum in the range 4000-600 cm^{-1} of pigments in paint temperas

In TG in air is possible to observe for each pigment one degradation step, (Fig 3.6, table 3.3), with the exception of red ochre that is stable in the range of temperature analyzed and no degradation step are visible.

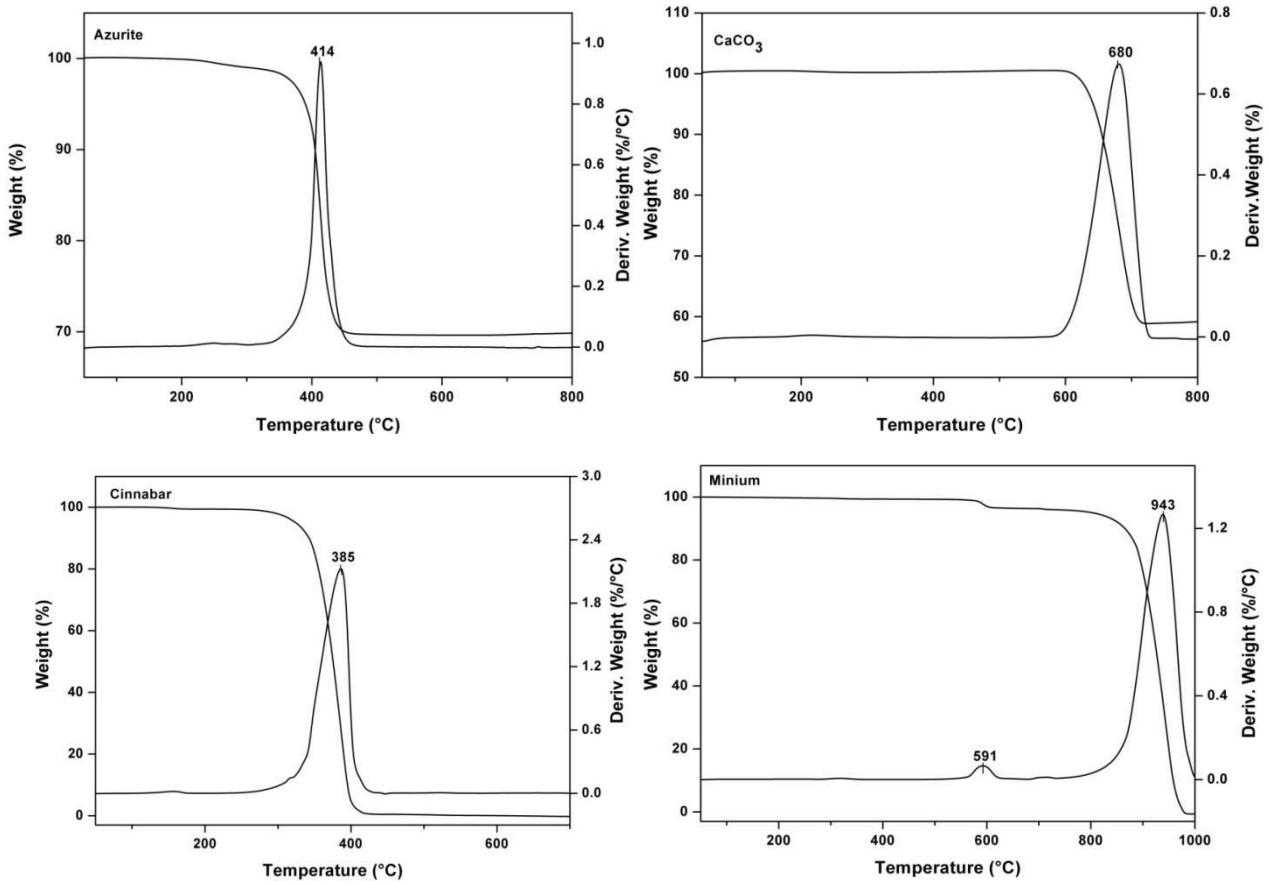

Figure 3.6 TG curve and its derivative of inorganic pigment (cinnabar ,minium, azurite and $CaCO_3$) performed under air flow at 10°C/min heating rate (right)

Pigment	Peak 1	Peak 2	Residual mass
Azurite	414 °C (30.2%)	-	69.8%
$CaCO_3$	680 °C (42.0%)	-	58.0%
Cinnabar	385.1 °C (100%)	-	0.0%
Minium	591 °C (3.2%)	943°C (96.8%)	0.0%
Red ochre	-	-	99.9%

Table 3.3 Experimental temperatures and the percentage mass losses of the corresponding degradation steps in air of inorganic pigments in tempera colour

Frequency (cm^{-1})	Assignment	Ref.
Azurite ($Cu_3(CO_3)_2(OH)_2$)		
3411	ν O-H	[9]
1470	ν CO_3^{2-}	[9]
1403	ν CO_3^{2-}	[9]
1095	ν CO_3^{2-}	[9]
810	ν CO_3^{2-}	[9]
Calcium Carbonate ($CaCO_3$)		
1398	ν CO_3^{2-}	[7]
886	ν CO_3^{2-}	[7]
708	ν CO_3^{2-}	[7]
Cinnabar (HgS)		
(130-250)	Not observed	[10]
Minium (Pb_3O_4)		
513	ν Pb-O	[11]
Red ochre (Fe_2O_3)		
509	ν Fe-O	[11]

Table 3.4 Characteristic vibrational modes and their assignment of inorganic pigments in tempera paints

3.2.1.2 Inorganic pigments in alkyd colours

In agreement with the results for the inorganic pigments used in tempera paints the FTIR and TG curve of inorganic pigments used in alkyd colours are very simple. The spectra of Titanium white (PW6) and Viridian green (PG18), for example, have just one very broad absorption at the low wavenumber end of the spectrum (between 500 and 700 cm^{-1}), like shown in Fig 3.7. In TG none mass loss is observed and this indicates that these two pigment are very stable up to 800°C .

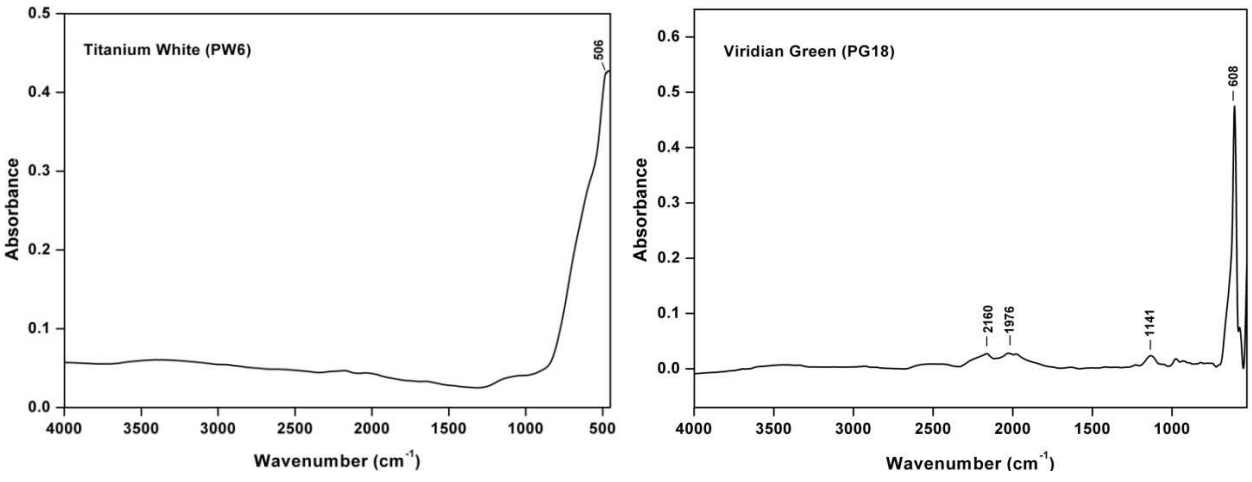

Figure 3.7 FTIR spectrum in the range 4000-600 cm^{-1} of titanium white PW6 (left) and viridian green PG18 (right)

French blue ultramarine (PB29) a polysulphide of sodium aluminosilicate, however, displays a strong and very broad absorption at 970 cm^{-1}, with another slightly weaker area of absorption with two peaks at 665 and 680 cm^{-1} (Fig 3.8 left), all likely to correspond to Si-O bond vibrations.

The TG curve shows a little total mass loss (2.4 %) split in three different degradation steps. (Fig. 3.8 right)

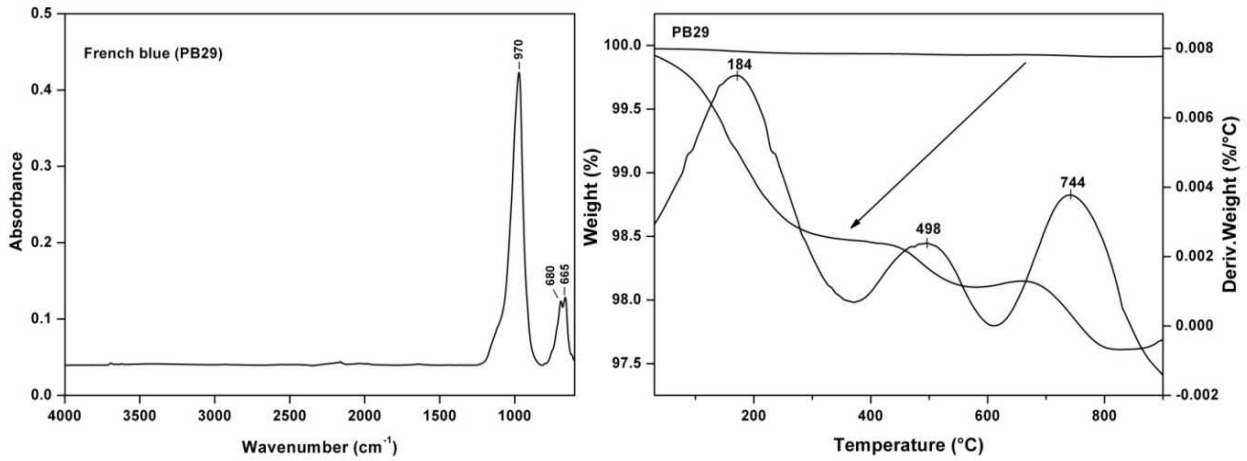

Figure 3.8 FTIR spectrum in the range 4000-600 cm^{-1} (left) and TG curve and its derivative of French blue (PB29) performed under air flow at 10°C/min heating rate (right)

Particular are the results of the two cadmium colours, PY35 (cadmium zinc sulphide) and PR108 (cadmium sulphoselenide). The cadmium colours are completely transparent to IR (absorption below 250 cm^{-1}) [10], but in both FTIR spectra we can observe many strong signal (Fig. 3.9) in the region between 700 and 1400 cm^{-1} and weak between 1700 and 2600 cm^{-1} . These signal in the spectrum of PR108 are characteristic of a particular kind of filler, the dolomite ($MgCaCO_3$), as we can see in the next paragraph. The spectrum of yellow cadmium is more complex, in fact we can identify two different kind of filler, calcium carbonate (peak at 3345, 1420 and 874 cm^{-1}) and barium sulphate (strong peak at 1096 cm^{-1} , 942 and 609 cm^{-1}).

So in these formulation small amount of different type of filler is added at the pure pigment, because they have high tinting strengths, and the filler reduce it to nearer that of the other pigments.

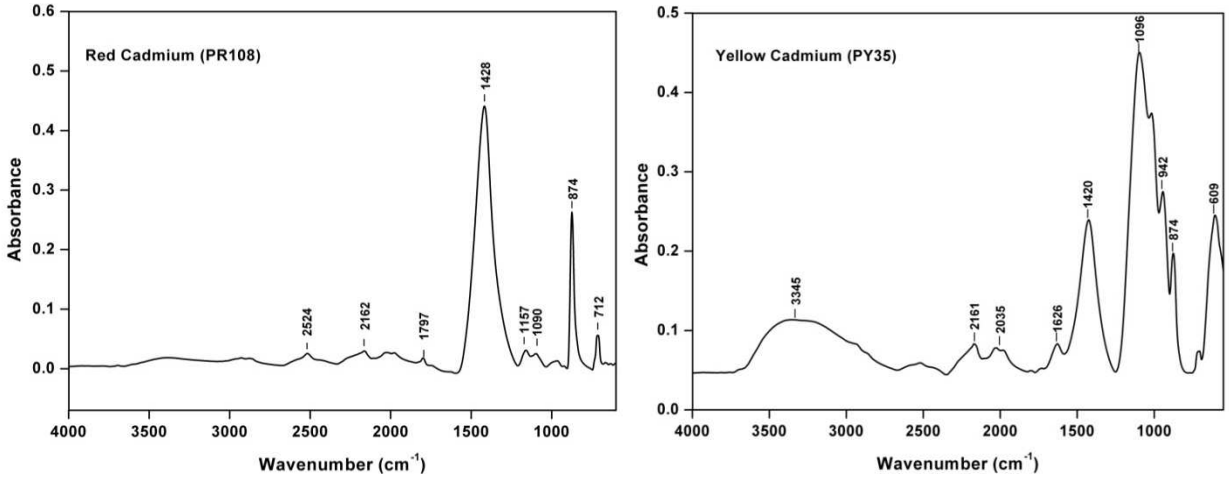

Figure 3.9 FTIR spectrum in the range 4000-600 cm^{-1} of Red cadmium (PR108) (left) and Yellow cadmium (PY35) (right)

The TG results for the cadmium pigments are particular (Fig. 3.10). The TG in air flow exhibit an increase in mass about 6 % after 600 °C (634°C for PR108 and 665 °C for PY35), due at the formation of $CdSO_4$, confirmed by the FTIR spectrum of residual at 650°C and 670°C respectively (single broad absorption in the sulphate region 1050 - 1200 cm^{-1}). After 700°C we observe the degradation of $CdSO_4$ formed and of the residual cadmium sulphur pigment.

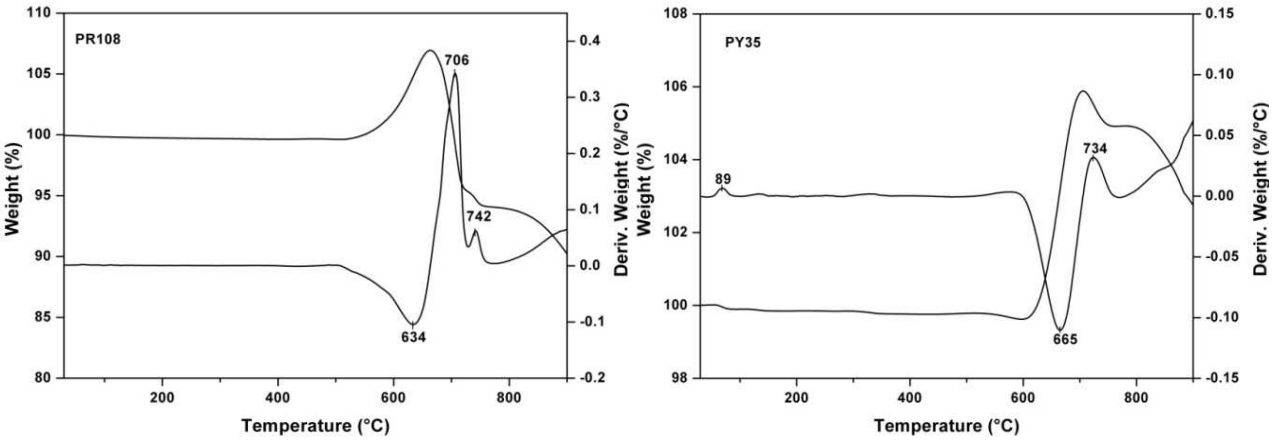

Figure 3.10 TG curve and its derivative Red cadmium (PR108) (left) and Yellow cadmium (PY35) (right) performed under air flow at 10°C/min heating rate

The pigment Ivory black, by contrast, has a characteristic spectrum (Fig. 3.11 left). Ivory black, in fact, is a mixture of Carbon, $Ca_3(PO_4)_2$ and traces of $CaCO_3$. In the spectrum is possible to observe the signal of P-O at low wavenumber (570 and 1015 cm^{-1}).

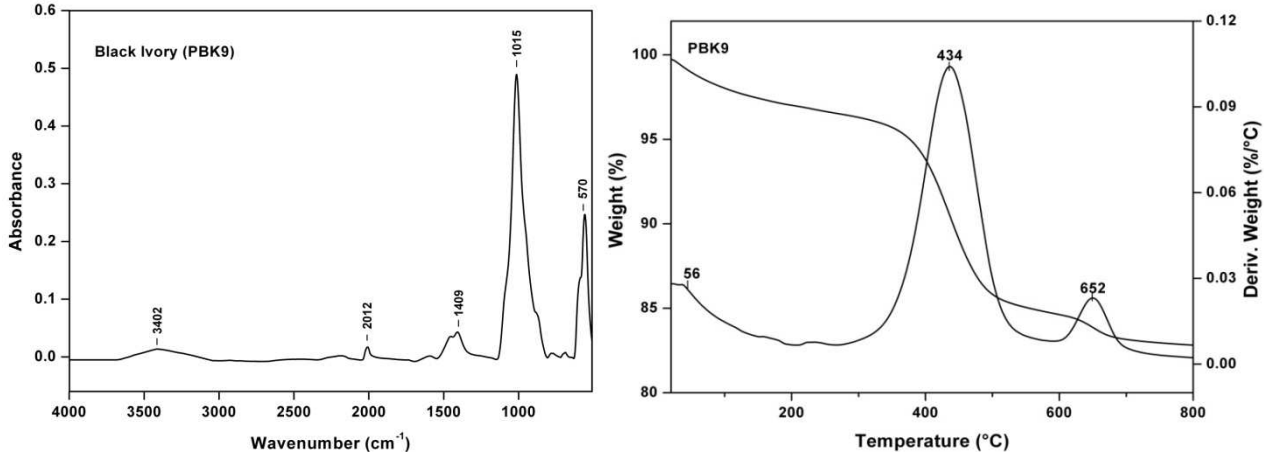

Figure 3.11 FTIR spectrum in the range 4000-600 cm^{-1} (left) and TG curve and its derivative of Black ivory (PBK9) performed under air flow at 10°C/min heating rate (right)

TG in air (Fig. 3.11 right) show three different mass loss, the first at 56°C (2.8%) is the loss of water adsorbed , the main mass loss at 434 °C (12.3%) is the oxidation of carbon at carbon dioxide and the last at 652 °C is due to the degradation of $CaCO_3$. (1.8%).

Pigment	Peak 1	Peak 2	Peak 3	Residual mass
White titanium (PW6)	-	-	-	98.8%
Viridian green (PG18)	-	-	-	99.98%
French blue (PB29)	184°C (1.5%)	498°C (0.35%)	744°C (0.55%)	97.6%
Yellow cadmium (PY35)	665°C (+6.01%)	734°C (1.2%)	-	104.8%
Red cadmium (PR108)	634°C (+6.8%)	706.4°C (11.8%)	741.6°C (1.6%)	90.2%
Black ivory (PBK9)	56.0°C (2.85%)	433.7°C (12.3%)	652°C (1.8%)	83.05 %

Table 3.5 Experimental temperatures and the percentage mass losses of the corresponding degradation steps in air of inorganic pigments in alkyd colour

Frequency (cm^{-1})	Assignment	Ref.
Titanium White (PW6)		
506	ν Ti-O	[3]
Viridian green (PG7)		
608	ν Cr-O	[4]
French Blue (PB29)		
970	ν Si-O	[5]
660-680	ν Al-O	[5]
Red Cadmium (PR108)		
2524	ν CO_3^{2-}(dolomite filler)	[6]
1797	ν CO_3^{2-} (dolomite filler)	[6]
1428	ν CO_3^{2-} (dolomite filler)	[6]
874	ν CO_3^{2-} (dolomite filler)	[6]
712	ν CO_3^{2-} (dolomite filler)	[6]
Yellow Cadmium (PY35)		
1420	ν CO_3^{2-} ($CaCO_3$filler)	[7]
874	ν CO_3^{2-} ($CaCO_3$filler)	[7]
1096	ν SO_4^{2-} ($BaSO_4$ filler)	[6]
942	ν SO_4^{2-} ($BaSO_4$ filler)	[6]
609	ν SO_4^{2-} ($BaSO_4$filler)	[6]
Black Ivory (PBK9)		
1409-2012	Impurities	
1015	ν P-O (PO_4^{3-})	[8]
570	ν O-P=O (PO_4^{3-})	[8]

Table 3.6 Characteristic vibrational modes and their assignment of inorganic pigments in alkyd colour

3.2.2 Organic pigments

All organic pigments give very characteristic FTIR spectra, usually containing a multitude of sharp and strong absorptions in the fingerprint region, as well as a fairly distinctive area of absorption between 2900 and 3300 cm^{-1} from C-H, O-H and N-H bond stretching.

Also the TGA signals are not simple, because, being organic species, we can observe many degradation step, typical of each pigment.

In the following discussion are shown the FTIR spectra and TGA signals for the organic samples studied: the arylamide yellow (PY3) and two phthalocyanine pigments ,blue (PB15) and green (PG7).

3.2.2.1 Yellow azo pigment Arylamide Yellow (PY3)

Fig. 3.12 (left) shows the FTIR spectrum of yellow organic pigment PY3, the region between 1400 and 1600 cm^{-1} is the most highly absorption.

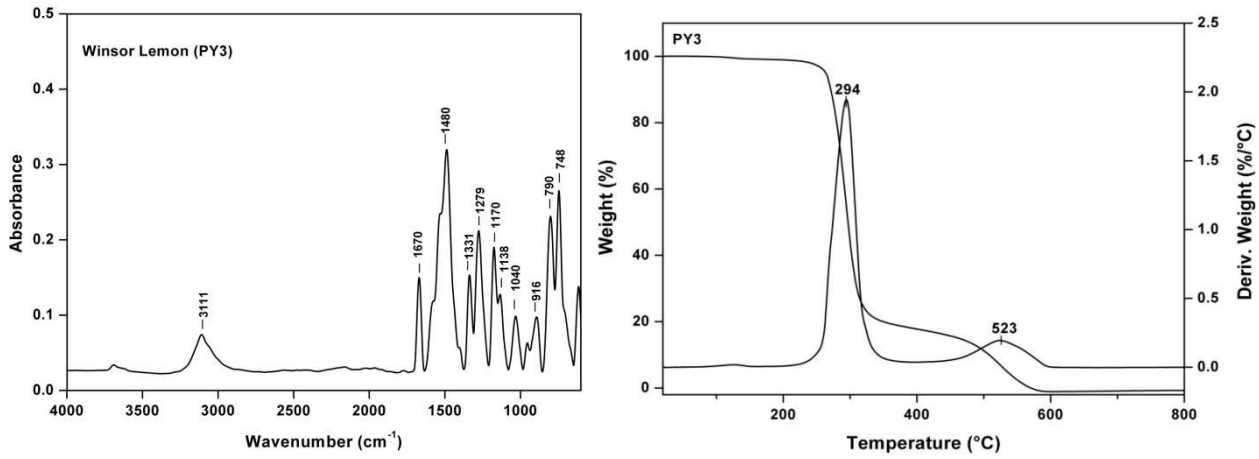

Figure 3.12 FTIR spectrum in the 4000-600 cm^{-1} range (left) and TG curve and its derivative of arylamide yellow PY3 performed under air flow at 10°C/min heating rate (right)

Fig. 3.12 (right) shows the TG and DTG curves in air flow of the pigment PY3. The residual mass is zero, in agree with the behavior of organic species in air flow.

3.2.2.2 Phthalocyanine pigments : Blue (PB15) and Green (PG7)

The FTIR of the two common phthalocyanine pigments, blue (PB15) and green (PG7) are shown in Fig. 3.13 (left and right respectively).

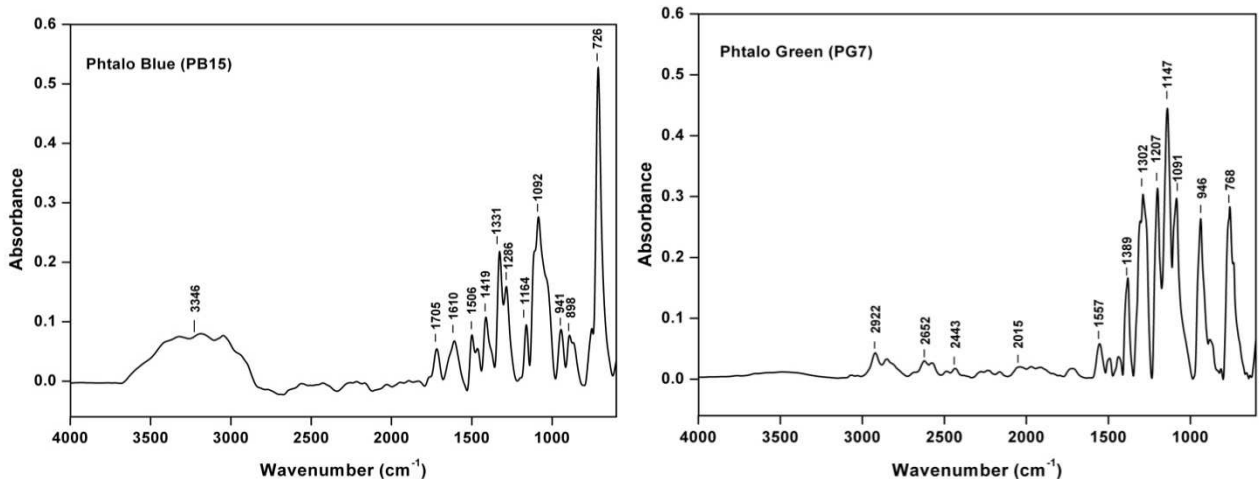

Figure 3.13 FTIR spectrum in the 4000-600 cm^{-1} range of phthalocyanine blue pigment PB15 (left) and green pigment PG7 (right)

The spectra of these two organic pigments are very different from those of the yellow azo pigments. The most notable difference is the lack of a area absorption between 1600 and 1700 cm^{-1} . In both spectra are present impurities, due to residual solvent in laboratory synthesis.

The TG curves for the phthalocyanine pigments in air flow are shown in Fig. 3.14. The two curves are very similar, with one small mass loss at lower temperature and main degradation step around to 400°C. The first peak at 35°C (3.5%) for the PB15 is probably due at the loss of ethanol used as washing solvent in the synthesis of the pigment.

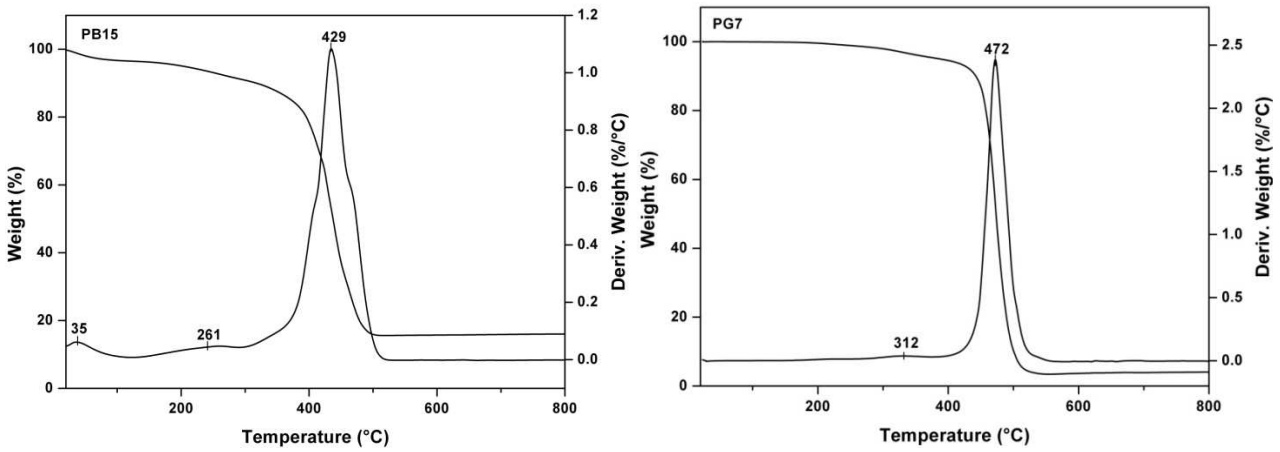

Figure 3.14 TG curve and its derivative of phthalocyanine blue PB15 (left) and phthalocyanine green PG7 (right) performed under air flow at 10°C/min heating rate

Pigment	Peak 1	Peak 2	Peak 3	Residual mass
Winsor lemon (PY3)	294.5°C (81.3%)	523.5°C (18.6%)	-	0.1%
Phthalo green (PG7)	312.0°C (2.0%)	472.2°C (95.8%)	-	2.2%
Phthalo blue (PB15)	35.3°C (3.5%)	261°C (5.3%)	428.8°C (75.4%)	15.8%

Table 3.7 Experimental temperatures and the percentage mass losses of the corresponding degradation steps in air of organic pigments in alkyd colour

Frequency (cm^{-1})	Assignment	Ref.
Winsor lemon (PY3)		
3111	ν NH- (amide)	[1,2]
1670	ν C=O (Amide I)	[1,2]
1480	ν C=C (aromatic)	[1,2]
1331	δ C-N	[1,2]
1279	ν C-O	[1,2]
1170	ν C-N	[1,2]
1138	νC-O-C	[1,2]
1040	ν =C-H (aromatic)	[1,2]
916	ν -C=C-C=O (skeletal)	[1,2]
748-790	δ C-H (aromatic)	[1,2]
Phthalo green (PG7)		
2000-2900	impurities	
1510-1557	ν C=N	[1,2]
1389	ν C=C (aromatic)	[1,2]
1302-1207	ν N-C-N	[1,2]
1147	ν_s Ar-Cl	[1,2]
946	δ =C-H (H arom. isolated)	[1,2]
768	ν_{as} Ar-Cl	[1,2]
Phthalo blue (PB15)		
3346	EtOH impurities	[1,2]
1705	ν N-C=N	[1,2]
1506-1610	ν C=N	[1,2]
1419	ν C=C (aromatic)	[1,2]
1331-1286	ν N-C-N	[1,2]
1092	ν C=N	[1,2]
726	δ =C-H	[1,2]

Table 3.8 Characteristic vibrational modes and their assignment of the organic pigments in alkyd colour

3.2.3 Filler

Fig. 3.15 (left) shows the FTIR of the filler used in alkyd paint colours, the strong and broad absorption observed between 1350 and 1550 cm^{-1} is attributed to the presence of a carbonate species. The positions of the other diagnostic peaks at 2538, 1820, 880 and 730 cm^{-1} indicate that it is dolomite, the double carbonate of calcium and magnesium, ($CaCO_3 \cdot MgCO_3$).[6]

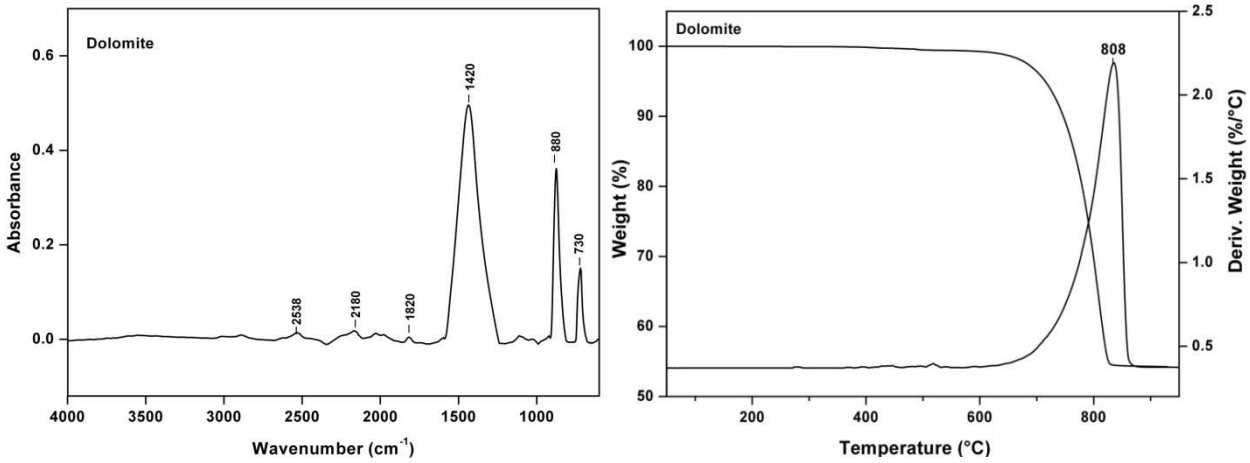

Figure 3.15 FTIR spectrum in the range 4000-600 cm^{-1} (left) and TG curve and its derivative of filler used in alkyd colour performed under air flow at 10°C/min heating rate (right)

Also the TGA in air , shows the typical profile of the degradation of dolomite, with one degradation step at 808°C (46.2%) like shown in Fig. 3.15 (right). [12]

References

[1] Silverstein RM, Bassler W. *Spectrometric identification of organic compounds.*(1991). Book , John Wiley &Sons Ed, New York;

[2] www.science-and-fun.de

[3] Nolan NT, Seery MK, Pillai SC. *Spectroscopic investigation of the anatase-to-rutile transformation of sol-gel synthesized TiO_2 photocatalysts.* J Phys Chem(2009) 20, 65-73;

[4] Marengo S, Tittarelli P, Morelli G. *Spectroscopic study of the structure of chromium , molybdenum and tungsten oxospecies anchored on aluminium oxide.* J Chem Soc. Faraday Trans (1984) 1, 2209-2223;

[5] Markovic S, Dondur V, Dimitrievic R. *FTIR spectroscopy of aluminosilicate structures.* J Molec Struc (2003) 654, 223-234;

[6] Learner TJS. *Exthenders in modern paints, analysis by FTIR and pyrolysis GC-MS spectrometry.* (2004) Research in conservation, Getty publications.

[7] Shaw S, Benning LG. *The kinetics and mechanism of amourphous calcium carbonate to calcite.* Nanostruc (2011) 1, 233-245;

[8] Arai Y, Sparks DL. *ATR-FTIR investigation on phopsphate adsorption at the ferrihydrite-water interface.* J Colloid Interf Sc (2001) 241, 317-326;

[9] Manzano E, Pastor-Romero J, Navas N, Cardell C. *A study of the interaction between rabbit glue binder and blue copper pigment under UV radiation : a spectroscopic and PCA approach.* Vib Spectr (2010) 53, 260-268;

[10] Qutub N, Sabir S. *Characterization of cadmium sulphide nanoparticles synthesized by chemical precipitation method.* Adv science. Engineer and Medicine (2013) 5, 852-857;

[11] Kharlamov AA, Almeida RM. *Vibrational spectra and structure of heavy metal oxide .* J Non-Crystal Sol (1996) 202, 233-240.

[12] Kok MV, Smykatz-Kloss W. *Thermal characterization of dolomites.* J Therm anal Calorim (2001) 64, 1271-1275.

4 Characterization of protein-pigment interactions in tempera paint replicas

4.1 Introduction

Kind and relative percentage composition of amino acids resulting from the hydrolysis of a protein depends on the nature of the protein. Table 4.1 presents the main proteins used as binder in tempera paints with the corresponding relative percentage amino acids composition of each of them. [1]

	Ala	**Gly**	**Val**	**Leu**	**Ile**	**Ser**	**Pro**	**Phe**	**Asp**	**Glu**	**Hyp**
casein	5.0	3.0	7.6	13.9	6.6	5.8	11.5	5.9	7.5	22.2	0.0
egg	7.7	4.8	7.7	10.0	6.7	10.3	5.7	6.4	12.6	15.0	0.0
animal glue	12.3	29.4	3.9	4.7	2.5	3.8	12.4	2.8	6.6	9.9	7.7

Table 4.1 Average relative percentage composition of amino acids fractions of the main proteinaceous binders

Each binder is characterized by a specific set of amino acid percentages and ratio values, which can be used as a "fingerprint", in particular the following remarks can be made:

- Egg based binders:
  - the highest percentages of *asp* and *ser*, and lowest percentages of *pro*;
  - the highest values of *ser/ile* and *ala/gly* ratios and the lowest ones of *pro/leu;*
  - five ratio values (*glu/asp*, *leu/ala, val/ala, ala/phe and ala/gly*) close to1-3.
- Milk or casein binders :
  - the highest percentages of glu and leu;
  - the highest values of *glu/asp, leu/ala, val/ala* and *ala/gly* ratios and the lowest one of *ala/phe and gly/ile.*
- Animal glue binders:
  - presence of *hyp*;
  - the highest percentage of *gly*;
  - the highest values of *gly/ile, ale/phe, pro/le*u and *hyp/leu* ratios and the lowest ones of *leu/ala , val/ala* and *ala/gly*.

Hystorically proteinaceous materials, such as egg, casein and animal glue, have commonly been used as paint binders, in the "tempera" painting technique. It has been widely documented that organic paint constituents undergo physical-chemical modifications that are referred to as "ageing", as a result of the interactions with light and oxygen[1,2]. Most research on proteinaceous paint media has focused on identifying these constituents in paint samples [1-3].

The degradation phenomena undergone by proteins in the course of ageing are still far fro being completely understood. Proteins used as paint media lose water upon application, and the tertiary and quaternary structures change through a rearrangement of the internal bonds between functional groups [4]. Oxidative changes in amino acids as a function of artificial ageing has been investigated by both Raman and fluorescence spectroscopy [5] a recent study based on proteomic techniques revealed that aminomalonic acid is present in the casein-aged films as a product of the oxidation of Ser and Phe [6]. In addition, it has also been observed that the deamidation of Gln and Asn is an extensive deterioration process in casein.

During ageing, further chemical changes occur: oxidation and cross-linking of the organic media, reaction between the paint binder and the pigments, as well as reactions of the pigments with the atmosphere and with each other [1,7-9]

However, to our knowledge, very little has been published on the nature and the effects of the interactions between the inorganic and proteinaceous matter in paint layers. As far as the interactions between proteinaceous matter and pigments are concerned, some cations, such as Hg(II), Fe(III), Cu(II), Pb(II), Cd(II) and Ca(II), are believed to give rise to strong complexes with proteins, as can be inferred by the analytical interferences observed in the GC-MS analysis of pigmented paint samples [10,11,17,18]. In paint reconstructions, TG is used for characterizing the thermal stability of binders and pigments, their interactions and their modifications due to ageing [12-16].

To date, thermal analytical studies on proteinaceous binder have included whole egg, egg yolk and egg white [11-18]. In particular, DSC and DMTA were used together with FTIR, SEM, XPS to evaluate the effects of natural and artificial ageing on samples of smalt tempera used as museum-exposed test paintings. Differences between controls and natural/artificial aged sample are discussed in terms of enhanced light levels, temperatire, exposure to pollutants, pigments and medium concentrations. Odlyha and co-workers evaluated the effects of natural and artificial ageing on samples of smalt tempera [14], lead white tempera [13] and azurite tempera [15]. Some results highlighted interactions between pigments and binding medium: the formation of oxidation products of cholesterol and glycerolipids together with the hydrolysis of glycerol esters and the enhanced formation of free fatty acids and dicarboxylic acids due to light ageing, the formation of network structures of cobalt ions with lecithins composed of cross-linked aggregates, and finally the catalysis of autoxidation on pigmented temperature control sample by azurite pigment [13-15].

In previous studies, liquid chromatography (LC) coupled to an AF detector were successfully applied to investigate proteins [19,20], low molecular weight thiols [21,22], mercaptans [23] and nitrosothiols [24]. Many studies have been reported on the interactions of inorganic and organic mercury with thiols and proteins [19], although only one paper studied the interactions of HgS with proteins [32]. It has been reported that HgS nanoparticles interact with bovine serum albumin (BSA), thus affecting its secondary structure because of the interactions with –OH and –NH groups [32].

The effect of crosslinking agents on thermal stability of rat collagen fibre has been studied by DSC and the results showed a marked increase in the peak temperature and enthalpy due to a net

increase in the number of intermolecular crosslinks and alterations in the secondary structure of collagen [25].

Romero-Pastor and co worker studied the binder (animal glue)-pigment interaction under UV ageing by MALDI-TOF-MS , and the results suggested different ageing behavior based on the pigment present, indicating diverse interactions between pigment and collagen. [26]

Cucos and co-workers studied the type I collagen by DSC and DTA and demonstrated that thermal analysis method were applicable to the characterization of leathers from some historical and cultural objects [27].

Odlyha et.al. studied the binding media of paintings by DTA and DSC, in particular interaction of animal glue with lead white and zinc oxide demonstrated that the results are sensitive to the age of sample and kind of white pigment, in particular lead white promoted an accelerated ageing of paints [28].

Manzano et.al. studied the interactions between rabbit glue binder and blue copper pigment and the modifications of paint replicas after artificial UV ageing. It revealed that the azurite FTIR spectral variability decreased in the presence of glue [29].

FTIR is commonly employed to study proteins [30-32]. The amide group of proteins and polypeptides presents characteristic vibrational modes (amide modes) that are sensitive to the protein conformation [31].

In this work I studied the interactions of ovalbumin, casein and rabbit glue with five inorganic compounds that are commonly employed in paintings as pigments: red lead (or minium) (PB_3O_4), red ochre (hematite, $Fe_2O_3 \cdot n\ H_2O$), calcium carbonate ($CaCO_3$), azurite ($Cu_3(CO_3)_2(OH)_2$) and cinnabar (HgS). The paints films were studied by a multi-analytical approach which includes TGA, TG-FTIR, DSC and FTIR before and after artificial ageing in a Solarbox.

This allowed us to characterize the molecular modifications undergone by proteins as an effect of light ageing, and depending on the pigment present, in terms of amino acid side chain oxidations, cross-linking, hydrolysis and the formation of stable complexes.

4.2 Results and discussion

4.2.1 Thermoanalysis

A comparison between the thermo-oxidative degradation curves and the corresponding derivative curves recorded under air flow for the unaged and aged proteinaceous media is reported in Fig. 4.1 and table 4.2, shows the experimental temperatures and the percentage mass loss of the thermal degradation steps.

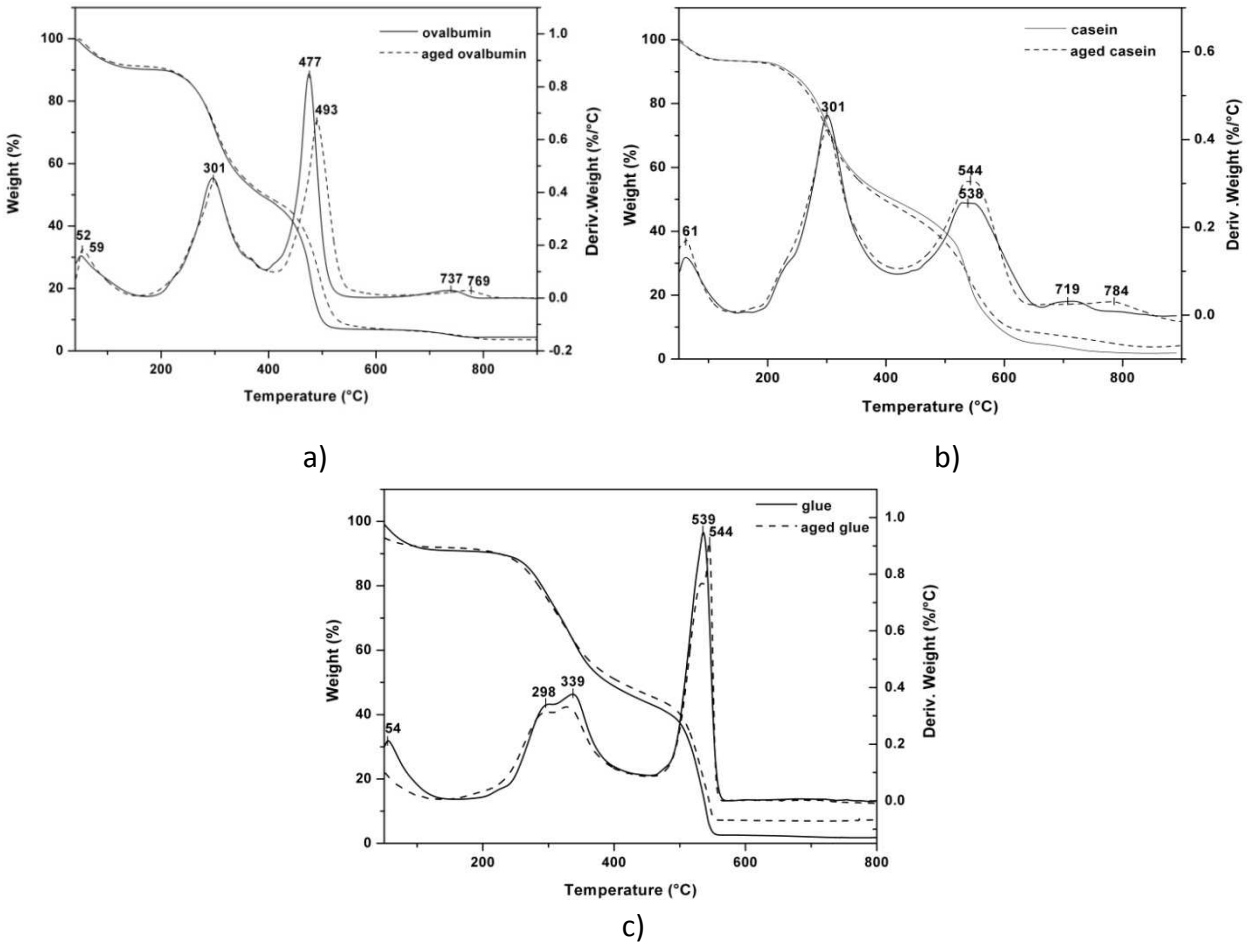

Figure 4.1 Thermogravimetric curve and its derivative of unaged and aged ovalbumin (a) , casein (b) and rabbit glue (C) performed under air flow at 10°C/min heating rate .

The TG curves of OVA, casein and rabbit glue under air flow show four different degradation steps [33-35]. The first mass loss of about 10% occurring at around 55°C in both proteins is due to the evaporation of moisture, in accordance with the literature data [33].

This step in fact disappeared when the samples were maintained 10 hours at 100°C under nitrogen flow before registering the TG curve. A shoulder at 225°C and a step at 300°C are found in the TG curves under nitrogen and air of both proteins. The same mass losses at exactly the same temperatures have also been observed in a broad variety of other proteins [34-35]. This would seem to suggest that they are typical of the polypeptide chain thermal decomposition. The shoulder at 225°C in ovalbumin disappeared after ageing in the curves recorded both under

oxygen and nitrogen, most likely because of the cross-linking taking place as a consequence of the OVA –SH group oxidation [4,36]. This interpretation is confirmed by the fact that this phenomenon was less evident in casein and glue characterized by a much lower number of –SH groups (no –SH are present in rabbit glue, only one –SH is present in k-casein, no –SH groups in α- and β- casein, three to four –SH in OVA).

OVA showed two additional typical steps at 477°C and 737°C, which are shifted at a higher temperature in the aged OVA, which indicates the presence of species of a higher molecular mass due to the protein cross linking. Casein shows characteristic steps at 538°C and 719°C, which in the literature have been attributed to the carbonizing and ashing of the hard residues of casein [34] . These steps were shifted at a higher temperature in the TG curve of aged casein (544 and 784°C, respectively), thus indicating the presence of a species of a higher molecular mass due to the protein cross-linking. Rabbit glue shows two overlapping peak at 298 and 339 °C due to polypeptide chain thermal decomposition which in glue occur in two steps. An additional peak at 539°C is shown which is shifted to higher temperature (544°C) in the aged glue, as already observed for OVA and casein the maximum of the complete combustion DTG peak is shifted to higher temperature after artificial ageing though this effect is quite small. The same conclusions can be drawn from the measurements recorded under nitrogen flow.

The oxygen uptake of both OVA, casein and rabbit glue was monitored by following the mass changes in the thermobalance of the samples exposed to a constant temperature of 80°C under air flow. It is interesting to note that neither material showed any mass increase due to oxygen uptake after 48 h. This suggest that if oxidation was taking place, it was a minor event.

N° of step	Temperature of the step and (wt. loss)					
	OVA	Aged OVA	casein	Aged casein	Rabbit glue	Aged Rabbit glue
1	52° (19.4 %)	59°C (8.6 %)	61°C (6 %)	61°C (6%)	54°C (10%)	58°C (8%)
2 (shoulder)	225°C	-	225°C	225°C	225°C	-
3	300°C (41.1%)	300°C (42.7%)	301°C (44%)	301°C (45%)	298+345°C (45%)	298+328°C (45%)
4	477°C (41.6%)	493°C (41.5%)	536°C (45%)	544°C (39%)	539°C (42%)	545°C (40%)
5	737°C (2.3%)	769°C (2.4%)	719°C (2.5%)	784°C (4%)	-	-

Table 4.2 Experimental temperature and mass loss percent of thermal degradation steps of aged/unaged OVA and casein

The paint replicas, the interaction protein/pigment and the effect of the artificial ageing of each sample were also studied. In the Tables 4.3 – 4.7 we can observe the thermal degradation of aged pure OVA, casein and glue and pigmented binders.

All the TG results show that pigments shift the main peak due to protein combustion to lower temperatures. This indicates that the metals, either in the form of salts ($CaCO_3$ or HgS) or oxides (Pb_3O_4 or Fe_2O_3), interact with proteins by decreasing their thermal stability. The only exception is the OVA/Fe_2O_3 unaged paint replicas in air flow, which shows a reproducible shift (TGA and DSC) of the combustion peak to a higher temperature. The artificial ageing shows little shift to lower temperature in TG of aged samples.

Moreover in the thermograms of $CaCO_3$ and cinnabar with OVA, we can observe two additional steps at 362 and 381°C for HgS and 336 and 439°C for $CaCO_3$, which may due to chemical interactions between OVA and metal ions. These interactions seem to lead to two structures with different thermal stabilities, most likely due to their different molecular mass.

With ageing the percentage mass loss of the interaction species of $CaCO_3$ with OVA decreases so they are less stable after artificial ageing. Whereas the TG of OVA with HgS show that the percentage mass loss of two steps at 362°C and 384 °C (aged) decreased from 60% to 46% and 547 (unaged) and 543 °C (aged), increased from 6% to 13%. This highlights that the relative amount of free HgS, responsible for the peak at about 380°C, decreases, and further interacts with the protein. It is possible that the high MW aggregates OVA/HgS, responsible for the signal at about 545°C, are more stable, and that their relative amount increases with ageing. On the other hand, the high MW aggregates OVA/HgS, responsible for the signal at about 362°C are less stable, and their relative amount decreases with ageing.

Also the thermograms of $CaCO_3$ and HgS with casein in air shows the formation of new interactions species at 355°C for $CaCO_3$ and 360°C for HgS. The thermograms of the fresh and aged paint reconstructions are very similar, suggesting that the casein/HgS and casein/$CaCO_3$ interactions are quite stable and not sensitive to artificial ageing.

The thermograms of Fe_2O_3 with rabbit glue shoes the formation of new interaction species at 464°C and as well as casein the thermograms of fresh and aged paint reconstructions are very similar and it suggest that glue/Fe_2O_3 interactions species are stable and not sensible to artificial ageing.

Similarly, the TG in nitrogen flow shows an increasing in thermal stability of the protein with a shift of pyrolysis to lower temperatures of pigmented samples. The ageing doesn't show any significant change in pyrolysis temperature of each sample.

Temperature of the step (wt. loss) in Air (OVA)												
N° step	**OVA**	**Aged OVA**	**OVA/ $Cu_3(CO_3)_2(OH)_2$**	**Aged OVA/ $Cu_3(CO_3)_2(OH)_2$**	**OVA/ $CaCO_3$**	**Aged OVA/ $CaCO_3$**	**OVA/ Fe_2O_3**	**Aged OVA/ Fe_2O_3**	**OVA/ Pb_3O_4**	**Aged OVA/ Pb_3O_4**	**OVA/ HgS**	**Aged OVA/ HgS**
1	52°C (9 %)	59°C (9 %)	55°C (7 %)	57°C (7%)	58°C (2%)	57°C (1%)	51°C (4%)	55°C (5%)	54°C (3 %)	55°C (5%)	53°C (3.5)	52°C (4%)
2	301°C (41 %)	301°C (43 %)	298°C (38 %)[b]	306°C (37 %)[b]	291°C (15%)[b]	291°C (14%)[b]	291°C (21%)	296°C (25%)	281°C (20 %)[b]	287°C (22 %)[b]	300°C (16%)	300°C (22%)
3	-	-	352°C (38%)[b]	345°C (37 %)[b]	336°C (15%)[b]	338°C (14%)[b]	-	-	329°C (20%)[b]	334°C (22 %)[b]	362°C (60%)[b]	362°C (46%)[b]
4	-	-	-	-	439 °C (22%)[c]	418°C (18%)[c]	-	-	-	-	381°C (60%)[b]	384°C (46%)[b]
5	477°C (42%)	493°C (42%)	503°C (31 %)	504°C (23 %)	465°C (22%)[c]	451°C (18%)[c]	506 °C (28%)	514°C (35 %)	469°C (19 %)	466°C (24 %)	474°C (9%)	474°C (7%)
6[a]	-	-	-	-	676°C (32%)	666°C (34%)	-	-	707 °C (0.6 %)	709 °C (1 %)	547°C (6%)	543°C (13%)

Table 4.3 Experimental temperatures and mass loss percent of thermal degradation steps in air of unaged and aged pure OVA and pigmented OVA.
[a]Degradation step due to unreacted pigment; [b] Total mass loss in the range 200-400°C; [c] Total mass loss in the range 400-500°C

Temperature of the step (wt. loss) in Air (Casein)												
N° step	**cas**	**Aged cas**	**cas/ $Cu_3(CO_3)_2(OH)_2$**	**Aged cas/ $Cu_3(CO_3)_2(OH)_2$**	**cas/ $CaCO_3$**	**Aged cas/ $CaCO_3$**	**cas/ Fe_2O_3**	**Aged cas/ Fe_2O_3**	**cas/ Pb_3O_4**	**Aged cas/ Pb_3O_4**	**cas/ HgS**	**Aged cas/ HgS**
1	61°C (6 %)	61°C (6 %)	54°C (2%)	52°C (2%)	55°C (3%)	58°C (3%)	54°C (4%)	56°C (3%)	54°C (2 %)	55°C (1.4%)	57°C (3.4%)	55°C (3.6%)
2	301°C (44 %)	301°C (45 %)	200-600°C (50%)[b]	200-600°C (47%)[b]	311°C (32%)[a]	311°C (28%)[a]	301°C (27%)	301°C (27%)	313°C (15 %)	305°C (13 %)	301°C (13.4%)	301°C (15.4%)
3	-	-	-	-	355°C (32%)[a]	351°C (28%)[a]	-	-	-	-	360°C (65%)	364°C (60%)
4	538°C (45%)	544°C (39%)	-	-	514 °C (19%)	513°C (19%)	483 °C (28%)	489°C (28 %)	470°C (14 %)	463°C (8 %)	538°C (15.4%)	538 °C (19%)
5[**]	-	-	-	-	685°C (18%)	684°C (19%)	-	-	-	711°C (1%)	-	-

[**] Degradation step due to unreacted pigment; [a] Total mass loss in the range 200-400°C; [b] Total mass loss in the range 200-600°C

Table 4.4 Experimental temperatures and mass loss percent of thermal degradation steps of unaged and aged pure casein and pigmented casein.

Temperature of the step (wt. loss) in Nitrogen (OVA)												
N° step	**OVA**	**Aged OVA**	**OVA/ $Cu_3(CO_3)_2(OH)_2$**	**Aged OVA/ $Cu_3(CO_3)_2(OH)_2$**	**OVA/ $CaCO_3$**	**Aged OVA/ $CaCO_3$**	**OVA/ Fe_2O_3**	**Aged OVA/ Fe_2O_3**	**OVA/ Pb_3O_4**	**Aged OVA/ Pb_3O_4**	**OVA/ HgS**	**Aged OVA/ HgS**
1	65°C (9 %)	65°C (9 %)	59°C (6 %)	57°C (5%)	66°C (2%)	57°C (2%)	54°C (8%)	55°C (7%)	55°C (3 %)	57°C (5%)	53°C (3%)	52°C (4%)
2	304°C (61 %)	304°C (62 %)	302°C (56 %)	303°C (54 %)	300°C (15%)	304°C (16%)	292°C (47%)	296°C (48%)	284°C (23 %)	287°C (24 %)	300°C (16%)	300°C (20%)
3[a]	-	-	-	-	695°C (40%)	687°C (40%)	-	-	400-600°C (16%)[b]	400-600°C (15 %)[b]	394°C (54%)	395°C (53%)

Table 4.5 Experimental temperatures and mass loss percent of thermal degradation steps in nitrogen of unaged and aged pure OVA and pigmented OVA.

Temperature of the step (wt. loss) in Nitrogen (Casein)												
N° step	**cas**	**Aged cas**	**cas/ $Cu_3(CO_3)_2(OH)_2$**	**Aged cas/ $Cu_3(CO_3)_2(OH)_2$**	**cas/ $CaCO_3$**	**Aged cas/ $CaCO_3$**	**cas/ Fe_2O_3**	**Aged cas/ Fe_2O_3**	**cas/ Pb_3O_4**	**Aged cas/ Pb_3O_4**	**cas/ HgS**	**Aged cas/ HgS**
1	62°C (6%)	62°C (6%)	53°C (2%)	51°C (2%)	59°C (5%)	58°C (4%)	53°C (4%)	58°C (5%)	54°C (2 %)	55°C (1.4%)	57°C (3%)	55°C (3%)
2	328°C (62%)	328°C (62%)	324°C (49%)	326°C (48%)	328°C (38%)	328°C (37%)	325°C (37%)	323°C (35%)	321°C (18%)	324°C (19%)	326°C (13%)	325°C (15%)
3[a]	-	-	-	-	692°C (28%)	692°C (30%)	-	-	400-600°C (11%)[b]	400-600°C (10%)[b]	392°C (58%)	394°C (56%)

[a] Degradation step due to unreacted pigment; [b] Total mass loss in the range 400-600°C

Table 4.6 Experimental temperatures and mass loss percent of thermal degradation steps in nitrogen of unaged and aged pure casein and pigmented casein.

Temperature of the step (wt. loss) in Air (Rabbit glue)										
N° step	**glue**	**Aged glue**	**glue/ $Cu_3(CO_3)_2(OH)_2$**	**Aged glue/ $Cu_3(CO_3)_2(OH)_2$**	**glue/ $CaCO_3$**	**Aged glue/ $CaCO_3$**	**glue/ Fe_2O_3**	**Aged glue/ Fe_2O_3**	**glue/ Pb_3O_4**	**Aged glue/ Pb_3O_4**
1	298°C (45 %)[a]	298°C (45 %)[a]	296°C (38%)[a]	-	299°C (31 %)	305°C (33 %)[a]	320°C (19 %)	284°C (18 %)[a]	281°C (29 %)[a]	296°C (31 %)[a]
2	339°C (45 %)[a]	337°C (45 %)[a]	326°C (38 %)[a]	335°C (39 %)[a]	-	323°C (33 %)[a]	-	324°C (18 %)[a]	309°C (29 %)[a]	334°C (31 %)[a]
3	539°C (42 %)	545°C (40 %)	494°C (27%)[b]	494°C (27 %)	485°C (27 %)	505°C (28 %)	429-464 °C (20 %)	427-470°C (19 %)	475°C (30 %)	490°C (30 %)
4	-	-	509°C (27 %)[b]	-	-	-	-	-	-	-
5[**]	-	-	-	-	632°C (12 %)	635°C (11 %)	-	-	708°C (1 %)	709°C (2 %)

[**] Degradation step due to unreacted pigment; [a] Total mass loss in the range 200-400°C;[b] Total mass loss in the range 400-600°C

Table 4.7 Experimental temperatures and mass loss percent of thermal degradation steps in air of unaged and aged pure rabbit glue and pigmented rabbit glue.

The DSC of proteinaceous materials pure or present in paint replicas in air showed two exothermic processes, which correlate with the main TG decomposition steps.

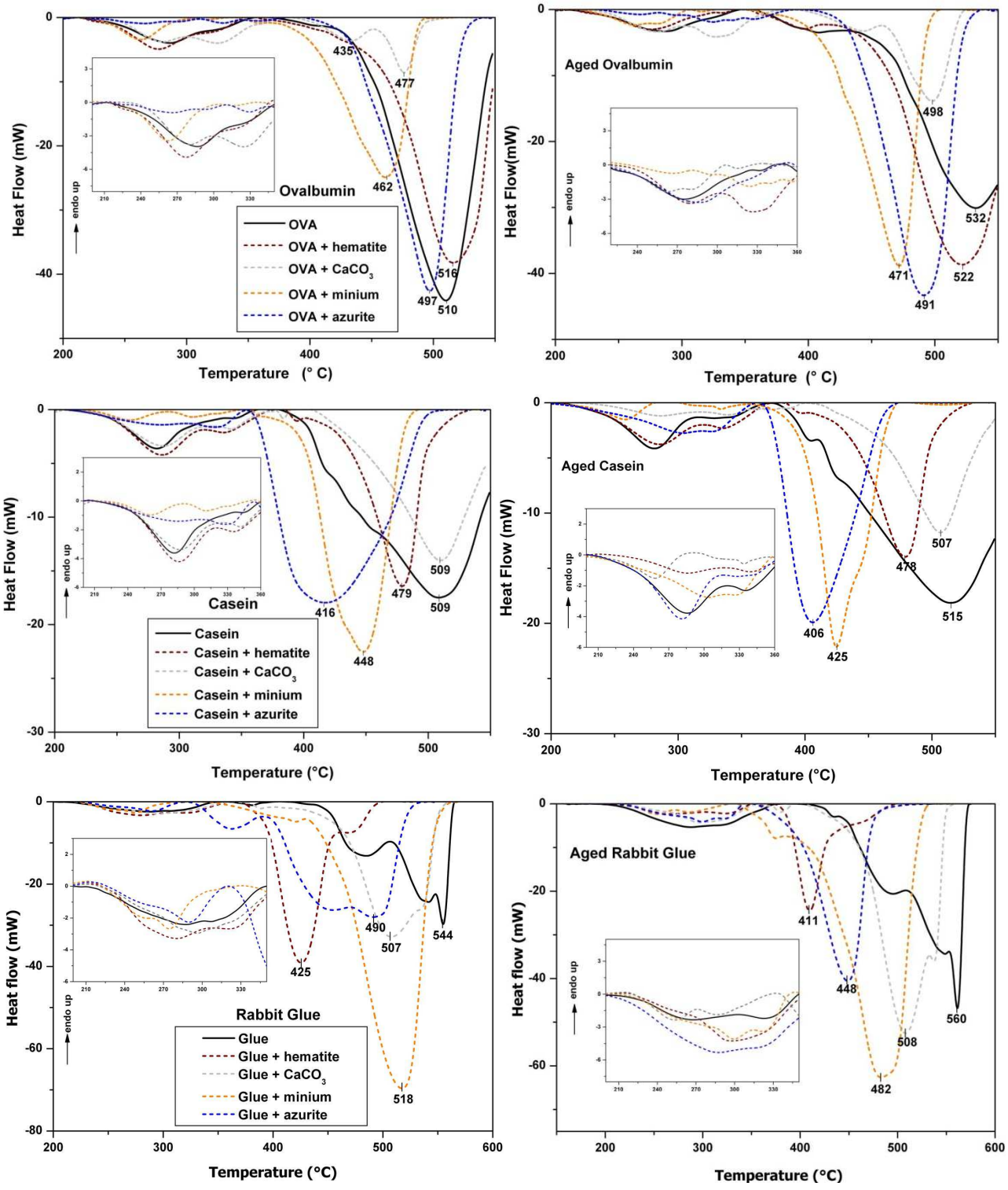

Figure 4.2 DSC curve under air flow of unaged and aged Ovalbumin (OVA), Casein and Rabbit glue

The first was around 300°C, which is typical of the thermal oxidative degradation of the polypeptide chain, and the second step was around 500°C, which is due to the complete combustion process.

The second degradation step was a combustion, which is strongly exothermic, whereas the first most likely peak involves a non-oxidative degradation (pyrolytic process). It is reasonable to assume that around 300°C the combustion is only a minor event, although strongly exothermic, and the endothermic pyrolytic degradation is the prevailing process. The exothermic peak observed at 300°C most likely arises from overlapping of an endothermic and exothermic process, wherein the exothermic signal was prevailing.

Concerning the first exothermic peak, the inserts of Fig. 4.2 show essentially a two step degradation process. In the case of pure OVA a peak at 290°C and a shoulder at 330°C are visible. However, the presence of each pigment generally indices a shift of these signals to lower temperature. Moreover a shoulder/peak around 360°C appears in all the pigmented samples. This seems to suggest that it is typical of a non specific protein-pigment interaction.

As it can be noticed, the case of azurite containing samples is peculiar showing a much lower signal within the range 200-350°C with respect to other paint replicas though maintaining an analogous signal structure. This could be attributed to some degree of cooperation between the pyrolisis/oxidation of the protein and the degradation of the bonded azurite which should undergo loss of H_2O and/or CO_2 molecules, through and endothermic process, in a much lower temperature range respect to free azurite. This hypothesis could find support in TG experiments (see table 4.3) where the OVA/azurite samples undergo a mass loss of 38 % in the range 200-400°c against 31 % around 500°C, whereas OVA samples showed practically the same mass loss in both degradation step (41 % and 42 % respectively).

In the case of casein the first peak (280°C) shift to higher temperature in pigmented samples with the only exception of minium paint replica (260°C), whereas the shoulder (345°C) shifts to lower temperatures in all cases. New small signals appear in the range 365-395°C in paint reconstructions containing red ochre, $CaCO_3$ and minium, whereas no such signal is observed in the case of azurite containing sample due to the overlapping of the main combustion peak.

On the other hand, in rabbit glue, the first exothermic band (200-350°C) shows a two step degradation process (inserts Fig 4.2). In the case of unaged pure glue two signals at 280°C and 306 °C, respectively are visible. Generally, the presence of pigment induces a modification of the band profile. This modification is limited in hematite and calcium carbonate samples, whereas a significant shift of the signals to lower temperature is observed in glue/minium and glue/azurite paint replicas. In all aged samples the whole exothermic band is slightly shifted to higher temperature with respect to unaged ones though maintaining similar shape. The only evident shape modification concerns the azurite paint replica whose evaluation is biased by the partial overlapping, in the unaged sample, with the signal at 362°C which probably pertains to the main thermo-oxidation pathway of the protein.

The combustion peak shifts to higher temperatures after artificial ageing in each proteins, although this phenomenon is more evident in the case of OVA. The mass losses associated with the two steps observed by TG were similar and the thermal effect observed by DSC related to the second peak was much greater than the first one.

The DSC curves of pure pigments, recorded in the same temperature range, did not show any significant calorimetric signals, except for azurite which exhibits a single sharp endothermic peak at 401°C assigned in the literature to the loss of both H_2O and CO_2. In the azurite/protein samples, the weak endothermic heat characteristic of pure azurite is overwhelmed by the

exothermic heat of the combustion of proteins and is likely to be responsible only for a slight modification to the shape of the combustion peak.

As concerns the first exothermic band, the general behaviour of unaged and aged samples is quite similar. In particular the temperature of the first peak of aged samples matches almost exactly the temperature of unaged ones. The only exception is represented by the azurite-casein aged paint reconstruction whose first peak falls at significantly higher temperature compared to unaged one. This behavior could appear to conflict with the above observations about the decreasing of thermal stability as inferred by the combustion peak temperature. However, the strengthening of the Cu-protein bonds could both stabilize the protein respect to pyrolisis and decrease the thermal stability respect to combustion by catalyzing the hydrolysis.

As a general remark the degradation band of aged pigmented samples shows a more complex structure of the signal compared to unaged ones. This probably reflects the presence of many structures which form through multiple degradative pathways involving the pigment during the ageing of proteinaceous binders.

In the case of OVA samples the main combustion peak shifted to higher temperatures during ageing showing that artificial ageing increases the thermostability of both pure protein and pigmented paint replicas with the exception of OVA/ azurite samples.

In the case of unaged and aged casein samples, an increase in protein thermostability due to artificial ageing was observed in pure casein, a decrease in its thermostability occurred in casein/red lead and casein/azurite paint replicas, whereas casein/hematite and casein/calcium carbonate did not show any significant modification in combustion temperature.

In the case of unaged and aged pure rabbit glue, the thermal behavior of aged samples is quite similar to that of unaged ones except for a slight shift of the combustion peak to lower temperatures not exceeding 20°C. This shift suggests that artificial ageing slightly decreases the thermostability of pigmented paint replicas accelerating the degradation process. This behavior is quite similar to that of casein based paint replicas.

The observed shift in the combustion DSC peaks to a higher temperature in aged pure proteins indicates the formation of more thermostable species during ageing. We can hypothesize the presence of higher molecular mass compounds due to protein cross-linking aggregation. The more pronounced peak shift observed in OVA compared to casein could be explained by cross-linking in OVA involving the formation of disulfide bridges and dityrosines [37-39], whereas a simple aggregation is expected to occur in casein which is poorer in SH groups and tyrosines.[40,41].

In both OVA and casein paint replicas, red lead (minium) and azurite showed the highest decrease in thermostability with respect to pure proteins, which becomes even more evident in aged casein-based samples. This suggest a stronger interaction between these pigments and the proteinaceous binders, probably due to the ability of the metallic centres to be involved in metal-protein coordination. In the case of azurite this could be explained by the coordination of Cu(II) with nitrogen atoms of several amino acid side chain such as Lys and Arg, whereas the lead metal centre in red lead probably interacts with oxygen atoms. The stronger effect observed in aged casein based samples could be explained by a gradual strengthening of the metal- protein bonds, which is reflected in a corresponding weakening of the intermolecular protein-protein interactions and/or by favouring hydrolysis phenomena.

It should be highlighted that the combustion peak of calcium carbonate paint replicas appears to be rather less exothermic compared to the other paint replicas, even normalizing the DSC curves for protein quantity. This suggest that an interaction between the protein and the pigment takes place, leading to the formation of complexes whose enthalpy associated with degradation/combustion is much lower than that of the protein alone. In addition, in the case of the OVA-$CaCO_3$ samples, the signal showed two resolved peaks in the range 400-500°C temperature range, matching the results of the corresponding TGA experiments (table 11-15) . In this regard it has been previously shown that calcium ions on the $CaCO_3$ crystalline surface strongly bind the OVA carboxylate groups [42]. The first observed peak (450°C) could thus be due to a shift to higher temperature of a degradation pathway (which normally occurs in the 250-350°C temperature range) ascribable to this interactions. On the other hand we cannot rule out that the two resolved peaks are ascribable to different combustion processes of the proteinaceous materials.

In the rabbit glue, the DSC results show that pigments shift the peak attributed to protein combustion, to lower temperatures according to TG results. The phenomenon is particularly evident in the case of hematite paint replica, which shows the highest decrease in thermostability with respect to pure binder, which becomes even more evident in aged samples.

This suggests a stronger interaction between hematite and the glue binder, probably due to the ability of iron to be involved in metal-protein coordination. In particular the iron metal centre can interact with histidine and with the oxygen atoms of proline and hydroxyproline aminoacids whose content in the collagen is particularly high compared to other proteinaceous binders [24-26]. As observed in the case of minium and azurite with ovalbumin and casein the stronger is the binding of the metal centre with specific aminoacidic residues, the easier is the thermal degradation of the whole protein. Probably two concurrent effects are responsible for this behaviour: the coordinative bond metal-heteroatom i) weakens the closer bonds of the proteic backbone and ii) frozens the protein in a conformation which is easily degraded by thermo-oxidative process.

4.2.2 FTIR

Proteins present characteristic vibrational modes (Amide modes) sensitive to protein conformation. Amide I (1700-1600 cm^{-1} region) is primarily due to the C=O stretching vibration, Amide II (1600-1480 cm^{-1} region) to the coupling of the N-H in-plane bending and C-N stretching modes and Amide III (1350-1190 cm^{-1} region) to the C-N stretching coupled to the in-plane N-H bending mode. Furthermore, vibrations of certain amino acid side chains have absorption bands in the 1480-1350 cm^{-1} and 1190-700 cm^{-1} regions and are affected by the chemical changes in proteins. The FTIR spectra of unaged and aged OVA and casein paint reconstructions showed significant differences (Fig 4.3). The FTIR spectra of aged samples showed a relative increase in the C=O and C-O stretching bands at 1735-1719 and 1070-1040 cm^{-1}, respectively, a shift of amide I band (from 1632 to 1636 cm^{-1} in aged samples) and a relative decrease and a shift of amide II band at 1529 cm^{-1} (1519 cm^{-1} in aged samples). These findings can be interpreted as follows:

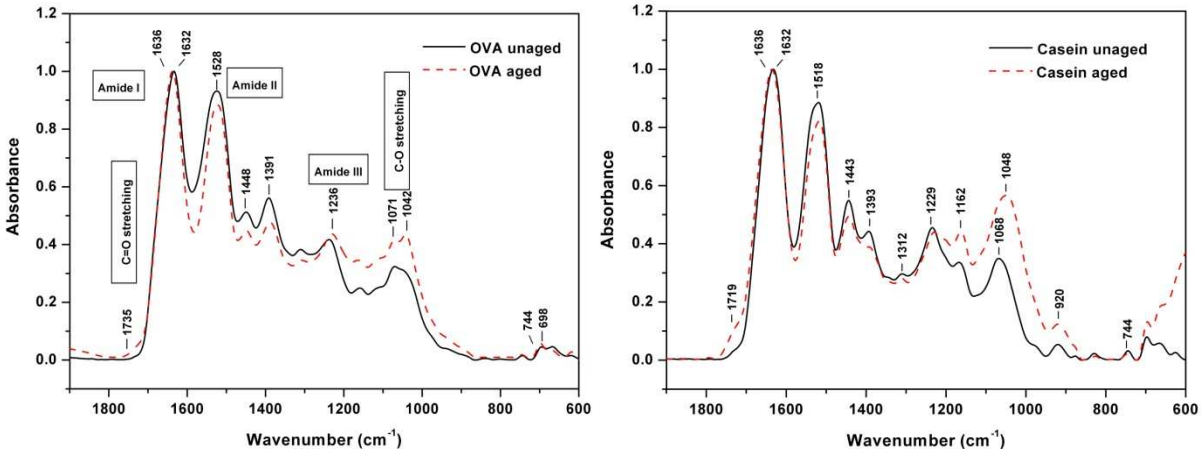

Figure 4.3 Normalized FTIR spectra of aged (dot red line) and unaged (black line) OVA (left) and casein (right) paint reconstructions in the 1900-600 cm^{-1}

- Changes in amides I, II and III bands are correlated with changes in the secondary structure of proteins [43] . In addition changes in the 1620-1690cm^{-1} region could also be associated with C=C oxidation.[43]
- Partial protein unfolding may be responsible for the increae in protein-protein interactions, causing a change in the strength of the bond between C=O and N-H moieties, and consequently the protein solubility. The decrease in amide II with respect to amide I has been correlated with the formation of aggregates of a high molecular mass [30].
- The relative increase in the bands in the 1070-1040 cm^{-1} range suggest the partial oxidation of some aromatic side chains (Phe, Tyr, and other aromatic rings) [44,45].
- The relative increase in the C=O stretching vibration at 1731 cm^{-1} indicates an oxidation of the alcoholic groups of amino acids, such as Tyr and Ser, to aldehydes or ketones.
- The relative increase in the C=O stretching vibration around 1719 cm^{-1} can be ascribed to the hydrolysis of peptide bonds as well as the Asn and Gln residues, with

the consequent formation of carboxylic acids moieties. The formation of imide bonds derived from the oxidation of peptide bonds [31] must also be taken into account.

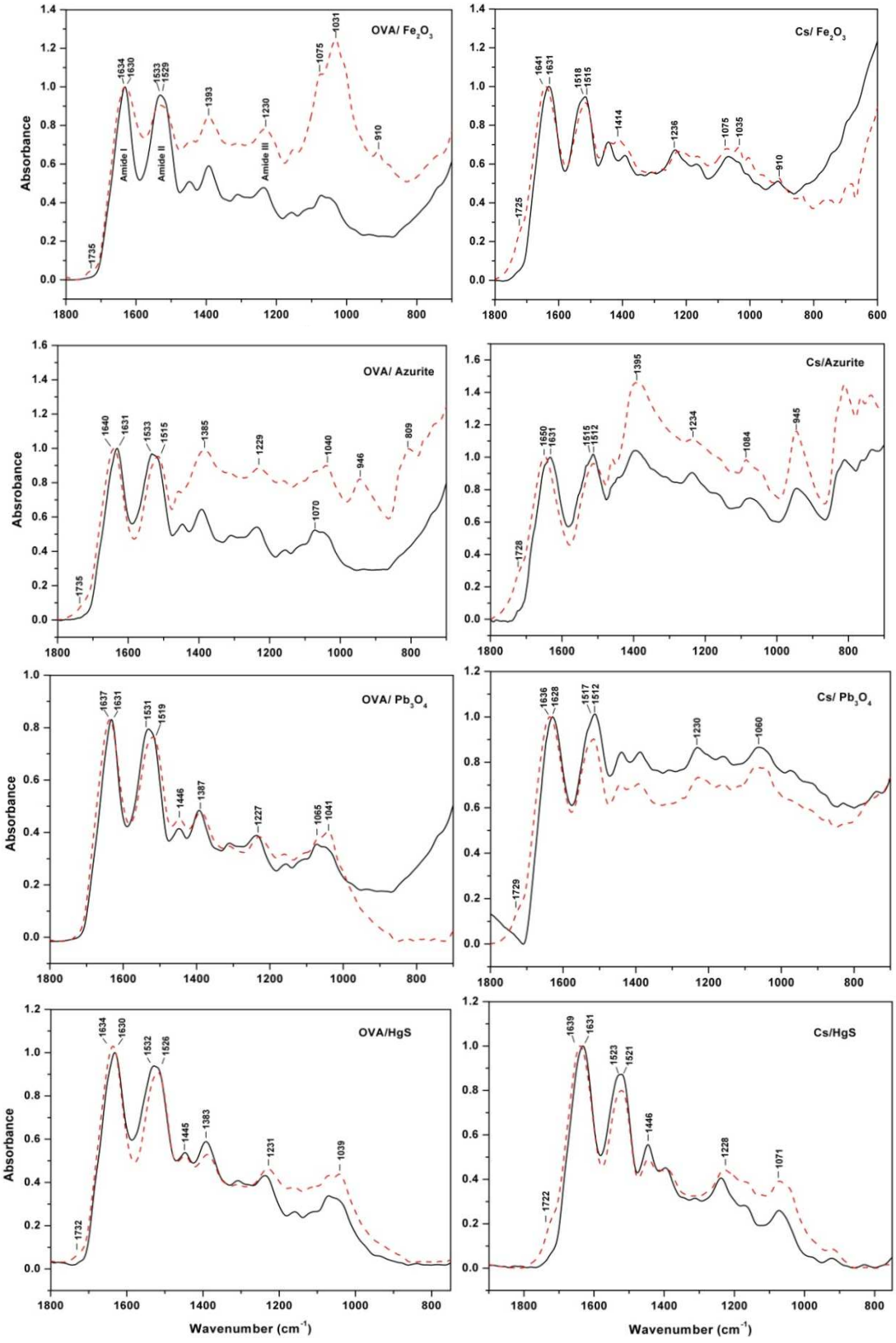

Figure 4.4 ATR-FTIR spectra in the 1800-750 cm^{-1} region unaged (black line) and aged (red dot line) OVA and Casein pigments paint replicas

The FTIR spectra of unaged and aged protein/pigments paint replicas are reported in Fig. 4.4.

The FTIR spectra of protein/$CaCO_3$ paint samples are not reported because of the high absorption carbonate, which covers all protein characteristic absorptions except for Amide I band.

Major changes can be seen in the FTIR spectra of the pigmented aged paint reconstructions, qualitatively analogous to those described for the unpigmented reconstructions. In order to get semi-quantitative information on the significant changes observed in the FTIR spectra, we evaluated the ratio between the optical densities of the amide II and amide I bands (AII/AI ratio) and the bands assigned to aldehyde, ketone and carboxylic acid C=O stretching vibration in the 1750-1700 cm^{-1} region.

A significant relative increase in the band with a maximum at 1070-1040 cm^{-1} was observed only in the case of aged OVA/ hematite and OVA/cinnabar samples. This absorption can be assigned to both C-O and S=O stretching vibrations and could be correlated with the partial oxidation of various aromatic side chains (Phe, Tyr and other aromatic rings) as well as with the formation of methionine sulphoxide from methionine.[37]

A relative increase in the shoulder at 1730 cm^{-1} was more evident in the casein/pigment samples compared to the OVA/pigments samples with ageing, suggesting an oxidation of amino acid side chains to aldehydes or ketones (1730 cm^{-1}). This shoulder was not observed in the OVA/ minium paint replicas.

However, the maximum, identified by second derivative analysis, is at about 1731 cm^{-1} in OVA and about 1720 cm^{-1} in casein. This suggest that aldehydes moieties deriving from the –OH group oxidation contribute more to this band in OVA, while acidic moieties ascribable to hydrolysis reactions are more important in casein. Oxidation of irradiated proteins probably occurs in the presence of photosensitizers, such as aromatic amino acids themselves or dyes used as pigments. Histidine, tryptofane, tyrosine, methionine, cystine and cysteine are the amino acid residues that are most susceptible to photo-oxidation . [4]

During ageing, a blue shift in the amide I band of about 4-10 cm^{-1} was also observed for all the samples examined except for OVA/hematite. In the case of OVA/$CaCO_3$ and casein/$CaCO_3$, the amide I band shifted in both unaged and aged samples by 15 cm^{-1}, indicating that a strong interaction of CaCO3 with C=O of peptide bond is rapidly estabilished.

In the case of the OVA paint replicas, both the protein/pigment interaction and the ageing process gave strong changes in the ratio between the optical densities of the Amide II band compared to Amide I (Fig. 4.5).

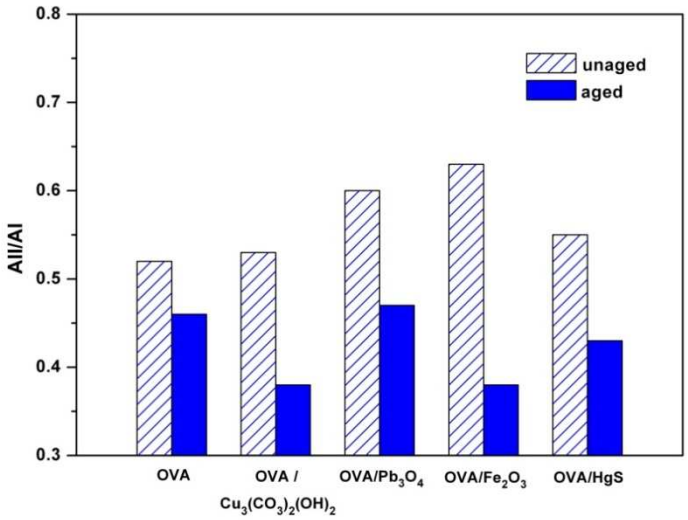

Figure 4.5 Ratio between the optical densities of Amide II and Amide I (AII/AI) of FTIR spectra of aged and unaged OVA/pigment reconstructions

In casein based samples, on the other hand, we observed small changes in the Amide II/Amide I ratio.

The relative decrease in Amide II compared to Amide I has been previously correlated with the formation of intermolecular β sheets. [46] . However, conformational changes due to protein oxidation or protein-metal interaction contributed to variations in the Amide II/Amide I ratio.

In order to gain further insight into protein conformational changes induced by pigment-protein interaction and ageing, the spectral deconvolution of the Amide I band was performed.

The choice of the Amide I band for structural analysis is due to the very low contribution of the amino acids side chain absorptions present in this region, and to its higher intensity compared to other Amide modes. The secondary structure can be obtained from the FTIR spectra on the basis of the infrared assignment of the Amide components, assuming that the extinction coefficient is the same for all the secondary structures. The percentages of different secondary structures were estimated by expressing the amplitude of the bands assigned to each of these configurations as a fraction of the total sum of the amplitudes of the Amide I components. Although the general validity of the above assumption regarding the extinction coefficients remains to be proved. Its use seems justified by the good correlation between the secondary structures results obtained by FTIR and the X-ray crystallography approaches. [47]

A summary of the secondary structure analysis of unaged and aged replicas with OVA and casein is shown in tables 16 and 17.

The assignment of the Amide I components (1700-1600 cm^{-1}) obtained after peak deconvolution enabled us to quantify the different secondary structures in the pure and metal-complexed proteins, both aged and unaged . Antiparallel β-sheets exhibit a strong band in the 1630-1640 cm^{-1} range and a weaker band around 1690-1700 cm^{-1}. The position of these bands is barely affected by the number of Amide groups in the β-sheets strands, but depends on the number of strands. [48] A band in the wide range 1610-1630 cm^{-1} can be characteristic of aggregated intermolecular β-sheets, [47-49] β-hairpin with specific turns that give more rigid

structures [50] or β-structures that are less accessible to the external medium. [51] This band often develops in aggregated proteins and has been attributed to intermolecular contacts of extended chain segments [52-53]

Alpha-helix and random coil structures often give Amide I components overlapping in the range in the range 1646-1657 cm^{-1}. Their position is affected by hydrogen bonds, by the presence of bonded water molecules as well as adjacent amino acids or other species, such as pigments, which may give strong interactions contributing to the distortion of the structures. For this reason, when possible the assignment should take into account knowledge of the protein secondary structures obtained by other methods.

Thus, the component at 1647-1658 cm^{-1} of OVA was attributed to solvated (1648 cm^{-1}) and buried (not solvated) α-helix (1658 cm^{-1}) [54,55]. The main band position shifts down with increasing helix length [54], when the helix is bent in coiled coils [56] and when the helix is solvent exposed [57] . Absorptions at 1660-1663 cm^{-1} are associated with an extended helix or 3_{10}-helix structure. [58] The component at 1649-1655 cm^{-1} of casein was assigned to a random coil, since casein is basically a random coil protein. The component at 1674-1686 cm^{-1} is determined by turns connecting β-strands.

In the case of pure OVA, ageing increased the α-helix structure from 10 % to 23 % suggesting that a more compact structure forms after ageing. This may be due to the formation of disulfide bridges and dityrosines leading to covalent cross-linked structures.[37-39]

The results of deconvolution applied to unaged and aged pure casein show that intermolecular β-sheets increase after ageing from 50 % to 72 %, while the random content decreases from 23 % to 3 %. Casein is in fact a hydrophobic random coiled protein. Hydrophobic interactions may lead to the formation of intermolecular β-sheets and aggregation during ageing. [37] These results are in agreement with the increased thermostability observed for both pure OVA and casein after ageing observed by DSC and TG.

Pure Ova	Aged OVA	Pure Casein	Aged casein	Assignment
1619 (27%)	1610 (21%)	1624 (50%)	1629 (72%)	β-Sheets (intermolecular)
1640 (28%)	1633 (31%)	1636 (2%)	-	β-Sheets (intramolecular)
1654 (10%)	1653 (23%)	1652 (23%)	1652 (3%)	α-Helix
1664 (12%)	1665 (3%)	-	-	Extended Helix
1676 (12%)	1675 (14%)	1674 (20%)	1676 (25%)	β-Turns
1690 (11%)	1692 (7%)	1697 (5%)	-	Antiparallel β-Sheets

Table 4.8 Summary of the secondary structure analysis of unaged and aged pure OVA (up) and pure Casein (down) paint replicas (data frequency (cm^{-1}) and proportion (%))

The addiction of pigments in protein led to the disappearance of intermolecular β-sheets and an increase in intramolecular β-sheets. Also taking into account the decrease in thermostability evidenced by TG and DSC, we can hypothesize that pigments intercalate between protein molecules. This is not the case of azurite with OVA, which maintains intermolecular β-sheets content and switches intramolecular β-sheets to α-helix (form 28 % to 19 % β-sheets, from

10 % to 23 % α-helix). However, during ageing, we observed a formation of new intermolecular β-sheets in OVA/pigments systems. This could be due to ageing-induced aggregation, which matches the increase in thermostability highlighted by TG and DSC analysis. The OVA/azurite sample did not give significant variations in the protein structure during ageing, and a small decrease in the combustion temperature (from 497 °C to 491°C) was observed.

The disappearance of intermolecular β sheets induced by the pigment addition in unaged samples correlates with an increase in the AII/AI ratio, while the increase in intermolecular β sheets during ageing correlates with the AII/AI ratio decrease.

In casein paint replicas, the presence of pigments decreases the intermolecular β-sheets characterizing the pure protein and increases the intramolecular β-sheets content, thus suggesting a partial distruption in protein-protein intermolecular interaction. This results in a pigment-induced labilization, which is in line with the decrease in the thermal stability of the system highlighted by DSC/TG results. This phenomenon continues during ageing. In fact the intermolecular β-sheets completely disappeared and there was a further increase in intramolecular β-sheets and random coil. This result is in agreement with the structural properties of casein, whose aggregation is known to be induced by hydrophobic interactions.

OVA/ $Cu_3(CO_3)_2(OH)_2$	Aged OVA/ $Cu_3(CO_3)_2(OH)_2$	OVA/ $CaCO_3$	Aged OVA/ $CaCO_3$	OVA/ Fe_2O_3	Aged OVA/ Fe_2O_3	OVA/ Pb_3O_4	Aged OVA/ Pb_3O_4	OVA/ HgS	Aged OVA/ HgS	Assignment
1623 (33%)	1625 (37%)	-	1603 (25%)	-	1626 (48%)	-	1613 (24%)	-	1610 (23%)	β-Sheets (intermolecular)
1637 (19%)	1645 (15%)	1639 (43%)	1628 (23%)	1632 (67%)	1642 (11%)	1630 (56%)	1635 (32%)	1640 (42%)	1630 (24%)	β-Sheets (intramolecular)
1652 (24%)	1658 (29%)	1650 (15%)	1652 (19%)	1657 (8%)	1655 (9%)	1655 (20%)	1652 (17%)	1652 (16%)	1654 (18%)	α-Helix
1666 (3%)	-	1665 (29%)	1667 (7%)	-	1666 (21%)	-	1666 (9%)	1667 (5%)	1667 (6%)	Extended Helix
1675 (21%)	1683 (19%)	1686 (13%)	1676 (26%)	1674 (25%)	1686 (12%)	1675 (23%)	1679 (19%)	1678 (28%)	1675 (29%)	β-Turns

Cs/ $Cu_3(CO_3)_2(OH)_2$	Aged Cs/ $Cu_3(CO_3)_2(OH)_2$	Cs/ $CaCO_3$	Aged Cs/ $CaCO_3$	Cs/ Fe_2O_3	Aged Cs/ Fe_2O_3	Cs/ Pb_3O_4	Aged Cs/ Pb_3O_4	Cs/ HgS	Aged Cs/ HgS	Assignment
1614 (16%)	-	1614 (5%)	-	1608 (7%)	-	1607 (30%)	-	1615 (4%)	-	β-Sheets (intermolecular)
1634 (38%)	1639 (65%)	1633 (38%)	1642 (68%)	1621 (39%)	1634 (1%)	1636 (4%)	1640 (82%)	1639 (39%)	1640 (64%)	β-Sheets (intramolecular)
1655 (21%)	1651 (29%)	1655 (28%)	-	1651 (39%)	1650 (90%)	1649 (2%)	-	1654 (20%)	-	α-Helix
1667 (3%)	1662 (1%)	1667 (7%)	1661 (2%)	-	-	1665 (19%)	-	1663 (8%)	1662 (9%)	Extended Helix
1678 (22%)	1680 (5%)	1680 (22%)	1680 (22%)	1683 (15%)	1686 (9%)	1684 (7%)	1686 (17%)	1680 (29%)	1679 (26%)	β-Turns

Table 4.9 Summary of the secondary structure analysis of unaged and aged OVA (up) and Casein (down) paint replicas (data frequency (cm^{-1}) and proportion (%)

4.3 Conclusions

Despite to the extensive work on the analysis and identification of organic materials in painting [14-16], fundamental research aimed at systematically investigating the interaction between inorganic pigments and proteins are lacking in the literature. Only a very few studies discuss, rather than hypothesise, the ageing and degradation of proteins in proteinaceous paint binders, while data are available on the degradation of lipids in egg tempera paint reconstructions. [34].

In this thesis, we investigated the interactions between five inorganic pigments ($Cu(CO3)2(OH)2$, ($Fe2O3$), ($CaCO3$), ($Pb3O4$) and (HgS) and OVA, casein and rabbit glue in paint replicas using the combined approach of TG, DSC and FTIR.

The analysis of proteinaceous binders revealed that the presence of inorganic pigments in tempera paints reconstructions in most cases induces a decrease in thermal stability, as highlighted by TG/DSC results, and a protein network labilization, which causes disruption of the protein-protein intermolecular interaction, as showed by spectral deconvolution of the Amide I band. On the other hand, the study clearly showed that ageing could induce aggregation, oxidation of some amino acid side chains and hydrolysis of the polypeptide chain in both pure and pigmented proteins.

To sum up, pigments may act directly on the stability of the protein structure because of their interaction with amino acid functional groups or indirectly, promoting oxidative stress. In turn, oxidative stress may induce global unfolding rearrangements of the proteins, which decrease their thermal stability . Thermal stability is reported to be inversely correlated also to proteolytic susceptibility [59] A decrease of thermal stability is correlated with the increase of proteolytic susceptibility, which indicates the resistance of protein to enzymatic digestion. Greater oxidative damages lead to aggregated, more thermostable structures characterized by a decrease of their proteolytic susceptibility [59] **.**

Aggregates were found to be both formed by covalent cross-linking (dityrosines, disulphide bridges) and by intermolecular hydrophobic interactions (intramolecular beta-sheets).

Characterizing the physic-chemical composition of paint layers is fundamental to understand how these degrade over years, which is fundamental knowledge to plan an efficient preservation of our painted Cultural Heritage.

References

[1] Andreotti A, Bonaduce I, Colombini MP, Modugno F. *Characterisation of natural organic materials in painting by GC/MS anaytical procedures*. In : Colombini MP, Tassi L (eds) *New trends in analytical, environmental and cultural heritage chemistry.* Transworld Research Network, (2008) 389-424;

[2] Tokarski C, Martin E, Rolando C, Cren-Olive C. *Identification of proteins in Resinassance paintings by proteomics.* Anal. Chem. (2006) 78, 1494-1502;

[3] Kukcova S, Hynek R, Kodicek M.ò *MALDI-MS applied to the analysis of protein paint binders.* Organic mass spectrometry in art and archaeology . (2009) Wiley, London;

[4] Karpowicz A. *Ageing and deterioration of proteinaceous media.* Stud Conserv (1981) 26, 153-160;

[5] Osticioli I, Nevin A, Anglos D, Chater S, Becucci M. *Micro-Raman and fluorescence spectroscopy for the assestment of the effects of the exposure to light on films of egg white and egg yolk.* J Raman Spectrosc (2008) 39, 307-313;

[6] Leo G, Bonaduce I, Andreotti A, Marino G, Pucci P, Colombini MP. *Deamidation at asparagine and glutamine as a ,ajor modification upon deterioration/aging ofproteinaceous binders in mural paintings.* Anal Chem (2011) 83, 2056-2064;

[7] Bonaduce I, Carlyle L, Colombini MP, Duce C, Ribechini E, Selleri P, Tinè MR. J Therm Anal Calorim (2012) 107, 1055-1066;

[8] Duce C, Ghezzi L, Onor M, Bonaduce I, Colombini MP, Tinè MR. Anal Bioanal Chem. (2012) 402, 2183-2193;

[9] Bonaduce I, Carlyle L, Colombini MP, Duce C, Ferrari C, Tinè MR. PLoS One.(2012) 7, 49333

[10] Colombini MP, Andreotti A, Bonaduce I, Modugno F, Ribechini E. *Analytical strategies for characterizing organic paint media using GC/MS spectrometry.* Accounts Chem (2010) 43, 715-727;

[11] Colombini MP, Gautier G. *GC/MS in the interactions of protein paint binders*. (2009) Wiley, London;

[12] Ciomartan DA, Clark RJH, McDonald LJ, Odlyha M. *Studies on the thermal decomposition of basic lead (II) carbonate by Fourier-transform Raman Spectroscopy, X-ray diffraction and thermal analysis.* J Chem Soc (1996) 3639-3645;

[13]Cohen NS, Odlyha M, Campana R, Foster GM. *Dosimetry of paintings: determination of the degree of chemical change in museum exposed test paintings (lead white tempera) by Thermal analysis and IR spectroscopy.* Therm Acta (2000) 365, 45-52;

[14] Odlyha M, Cohen NS, Foster GM. *Dosimetry of paintings: determination of the degree of chemical change in museum exposed test paintings (smalt tempera) by thermal analysis.*Therm Acta (2000) 365, 35-44;

[15] Odlyha M, Cohen NS, Foster GM, West RH. *Dosimetry of paintings: determination of the degree of chemical change in museum exposed test paintings (azurite tempera) by thermal and spectroscopic analysis.* Therm Acta (2000) 365, 53-63;

[16] Bonaduce I, Carlyle L, Colombini MP, Duce C, Ferrari C, Tinè MR. J Thermal Anal and Calorim (2011) 14, 765-771;

[17] Colombini MP, Fuoco R, Giacomelli A, Muscatello B. Stud. Conserv(1998) 43, 33-41;

[18] Wouters J, Van Bos M, Lamens K. Stud. Conserv (2000) 45, 169-179;

[19] Bramanti E, D'Ulivo A, Lampugnani L, Zamboni R. *Application of mercury cold vapour atomic fluorescence spectrometry to the characterization of mercury-accessible -SH groups in native proteins.* Anal Biochem (1999) 274, 163-173;

[20] Bramanti E, Lomonte C, Galli A, Onor M. *Characterization of denatured metallothioneins by reversed phase coupled with on-line chemical vapour generation and atomic fluorescence spetrometric detention.* J Chromatogr A (2004) 1054, 285-291;

[21] Bramanti E, Cavallaro R, Onor M, Zamboni R. *Determination of thiolic compound sas mercury complexes by cold vapor atomic absorption spectrometry and its application to wines.* Talanta (2010) 74, 936-943;

[22] Angeli A, Chen H, Mester Z, Bramanti E. *Derivatization of GSSG by pHMB in alkaline media .* Talanta (2010) 82, 815-820;nor

[23] Bramanti E, D'Ulivo L, Lomonte C, Onor M, Raspi G. *Determination of hydrogen sulphide and volatile thiols in air samples by mercury probe derivatization coupled with liquid chromatography-atomic fluorescence spectrometry.* Anal Chim Acta (2006) 579, 38-46;

[24] Bramanti E, Angeli V, Mester Z, Pompella A, Paolicchi A. *Determination of S-nitrosoglutathione in plasma: comparison of two methods.* Talanta (2010) 81, 1295-1299;

[25] Usha R, Ramasami T. *Effect of crossilinking agents on the thermal and thermomechanical stability of rat tail tendon collagen fibre.* Therm Acta (2000) 356, 59-66;

[26] Romero-Pasor J, Navas N, Kuckova S, Cardell C. *Collagen-based proteinaceous binder-pigment interaction study under UV ageing conditions by MALDI-TOF-MS and principal component analysis.* J Mass Spectrom (2012) 47, 322-330;

[27] Cucos A, Budrugeac P, Miu L. *The use of thermal analysis meyhods for authentication and conservation state determination of historical and cultural objects manufacted from leather.* J Therm Anal Calorim (2011) 104, 439-450;

[28] Odlyha M, Burmester A. *Preliminary investigations of the binding media of paintings by DTA.* J of Thermal Anal (1988) 33, 1041-1052;

[29] Manzano E, Pastor-Romero J, Navas N, Cardell C. *A study of the interaction between rabbit glue binder and blue copper pigment under UV radiation : a spectroscopic and PCA approach.* Vib Spectr (2010) 53, 260-268;

[30] Bramanti E, Lenci F, Sgarbossa A. *Effects of hypericin on the structure and aggregation properties of beta-amyloid peptides.* Eur Biophys J Biophy (2010) 39, 1493-1501;

[31] Barth A. *Infrared spectroscopy of proteins. BBA-Bioenergetics.*(2007) 1767, 1073-1101;

[32] Qin DZ, Ma XM, Yang L, Zhang L. *Biomimetics synthesis of HgS nanoparticles in the bovine serum albumin solution.* J Nanopart Res (2008) 10, 559-566;

[33] Somanathan N, Subramanian V, Mandal AB. *Thermal stability of modified casein.* Therm Acta (1997) 302, 47-52;

[34] Purevsuren B, Davaajav Y. *Thermal analysis of casein.* J Therm Anal Calorim(2001) 65, 147-152;

[35] Purevsuren B, Davaajav Y. *Investigation on pyrolysis of casein.* J Therm Anal Calorim (2001) 66, 743-748;

[36] Kasarda DD, Black DR. *Thermal degradation of proteins studied by mass spectrometry.* Biopol (1968) 6;

[37] Lasch P, Petras T, Ullrich O, Backmann J, Naumann, Grune T.*Hydrogen peroxide-induced structural alterations of RNase A.* J Biol Chem (2001) 276, 9492-9502;

[38] Giulivi C, Davies KJ. J Biol Chem (1993) 268, 8752-8759;

[39] Karpowicz A. *Ageing and deterioration of proteinaceous media.* Stud Conserv (1981) 26, 153-160;

[40] Wallace GM, Aiyar KR. *Sulphydryl and disulphide groups in casein.* J Dairy Res (1969) 36, 115-123;

[41] Bramanti E, D'Ulivo A, Lampugnani L, Zamboni R, Raspi G. *Application of mercury cold vapor atomic fluorescence spectrometry to the characterization of mercury –accesible –SH grouos in native proteins.* Anal Biochem (1999) 274, 163-173;

[42] Wang X, Kong R, Pan X, Xu H, Shan H, Lu RJ. *Role of ovalbumine in the stabilization of metastable vaterite in calcium carbonate biomineralization.* J Phys Chem (2009) 113, 8975-8982;

[43] Haque H, Bhandari BR, Gidley MJ, Deeth HC, Moller SM. *Protein conformational modifications and kinetics of water-protein interactions in milk protein concentrate powder upon aging: effect on solubility .* J Agric Food Chem (2010) 58, 7748-7755;

[44] Nevin A, Anglos D, Cather S, Burnstock A. *The influence of visible light and inorganic pigments on fluorescences excitation emission spectra of egg-, casein- and collagen-based painting media.* Appl Phys a-Mater (2008) 92, 69-76;

[45] Nevin A, Osticioli I, Anglos D, Cather S, Castellucci E. *The analysis of naturally and articially aged protein-based paint media using Raman spectroscopy combined with principal component analysis.* J Raman Spectrosc (2008) 39, 993-1000;

[46] Bramanti E, Benedetti E. *Determination of the secondary structure of isomeric forms of human serum albumin by a particular frequency decovolution procedure applied to FTIR.* Biopol (1996) 38, 639-653;

[47] Bramanti E, Benedetti E, Sagripanti A, Papineschi F. *Determination of secondary structure of normal fibrine from human peripheral blood.* Biopol (1997) 41, 545-553;

[48] Chirgadze YN, Fedorov OV, Trushina NP. Biopol (1975) 14, 679-694;

[49] Van Stokkum IHM, Linsdell H, Hadden JM, Haris PI, Chapman D. *Temperature-induced changes in protein structures studied by FTIR and global analysis.* Biochem (1995) 34, 10508-10518;

[50] Chenin H, Iloro I, Marcos MJ, Villar E, Arrondo JLR. Biochem(1999) 38, 1525-1530;

[51] Herzik E, Lee DC, Dunn RC, Chapman D. *Determination of protein secondary structure using factor analysis of infrared spectra.* Biochim Biophys Acta, Lipids Lipid Metab(1987) 922, 145-154 ;

[52] Heimburg T, Weber K, Geisler N. *Specific recognition of coiled coils by infrared stectroscopy: analysis of the three structural domains of type III intermediate filament proteins.* Biochem (1996) 35, 1375-1382;

[53] Muga A, Mantsch HH, Surewicz WK. *Determination of protein secondary structure by FTIR: a critical assessment.* Biochem (1991) 30, 7219-7224;

[54] Nevskaya NA, Chirgadze YN. *Infrared spectra and resonance interactions of amide-I and II vibrations of alfa-helix.* Biopol (1976) 15, 637-648;

[55] Torii H, Tasumi M. *Effects of intermolecular hydrogen-bonding interactions on the amide-I mode of N-methylacetamide matrix-isolation infrared studies and ab initio molecular orbital calculations.* J Chem Phys (1992) 96, 3379-3387;

[56] Residorf WC, Krimm S. *Infrared amide-I band of the coiled coil.* Biochem (1996) 35, 1383-1386;

[57] Venyaminov SY, Kalnin NN. *Quantitative IR spectrophotometry of peptyde compounds in water solutions.* Biopol (1990) 30, 1259-1271;

[58] Kennedy DF, Crisma M. *Studies of peptides forming 3-10 and alpha-helixes and beta-dend ribbon structures in organic solutions by FTIR.* Biochem (1991) 30, 6541-6548;

[59] Grune T, Blasig IE, Sitte N, Roloff B, Haseloff R. *Peroxynitrite increases the degradation of aconitase and other cellular proteins by proteasome.* J Biol Chem (1998) 273, 10857-10862.

5 Analysis of alkyd resins

5.1 Introduction

Alkyd paints are polyesters, which are modified by the addition of oil or fatty acids and other additives (Fig. 5.1). The term *alkyd* is derived from the *alc*ohol and ac*id* constituting the monomer used to make the polyester polymer, namely, a polyhydric alcohol (also called polyol) and a polybasic carboxylic acid (or poly acid). For the production of a usable alkyd resin, the poly acid must have at least two acid (-COOH) groups. Instead the polyol must be at least trihydric; that is, it must contain at least three hydroxyl (-OH) groups [1]. The polyester produced from these two components is typically a hard, cross-linked thermosetting resin. Oil modified alkyd resins are prepared by condensation of a polyol, a polybasic acid, and a monobasic fatty acid, thus modifying the polyester backbone and significantly reducing the degree of cross-linking [1]. A drying oil (siccative or semi-siccative oil) is often used as the source of monobasic acids. Oil modified alkyds are used as paint binders [1-3].

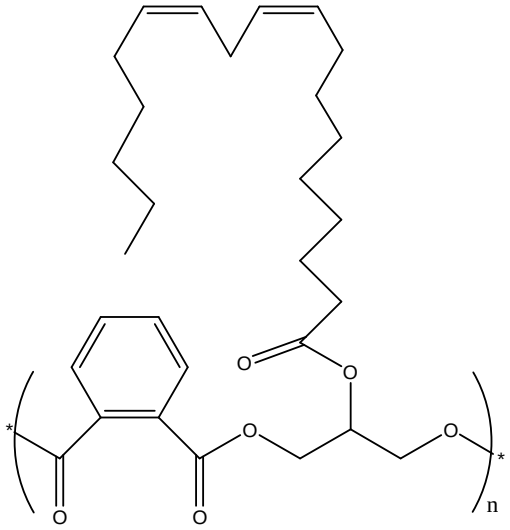

Figure 5.1 Example of an alkyd resin containing phtalic anhydride, glycerol and linoleic acid

5.2 Polyol

The two most widely used polyols in alkyd resins are glycerol (propan-1,2,3-triol) and pentaerythritol (2,2-bis(hydroxymethyl) 1,3-propane-diol), but surbitol (1,2,3,4,5,6- hexanehexol) is also sometimes used [3].(Fig 5.2)

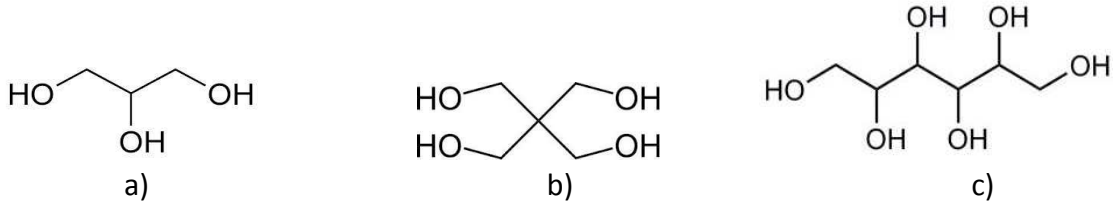

Figure 5.2 Chemical Structure of the three common polyols used in alkyd resin :a) Glycerol; b) pentaerythritol; c) Surbitol.

Before 1960's glycerol was the most commonly used polyol in alkyd paints. Pentaerythrytol was introduced for the first time after that period [3,4]. At present, glycerol is used mainly, but not exclusively, in short and medium oil alkyds but, at these oil lengths, pentaerythritol tends to gel rapidly. Long oil alkyds for use in house paints, are produced mainly from pentaerythritol. In fact, compared with long oil glycerol alkyds, pentaerythritol alkyds tend to dry faster and give more resistant films, are more flexible, slightly more durable, and have a higher water resistance [5].

5.3 Polybasic acid

The most common polybasic acid in alkyd resins is the dibasic acid phthalic anhydride, shown in Fig. 5.3(a) which behaves as *ortho*-phthalic acid (1,2- benzenedicarboxylic acid), shown in Fig. 5.3(b) [2-5].

a) b)

Figure 5.3 Chemical Structure of a) Phthalic anhydride and b) *ortho*-phthalic acid.

Almost all alkyd house paints contain phthalic anhydride in the resin composition. Other dibasic acids are found only in more specialised industrial alkyd paints and include isophthalic (1,3.benzenedicarboxylic), terephthalic (1,4-benzenedicarboxylic), maleic (z-2-butenedioic), fumaric (e-2-butenedioic), adipic (hexanedioic) and sebacic (decanedioic) acids. The linear chain dibasic acids (adipic and sebacic) give more flexible polyesters and are therefore used almost exclusively in plasticizing alkyds [6].

5.4 Drying oil

The nature of the monobasic fatty acid used in the resin's formulation, is fundamental to determining the overall drying characteristics of the final alkyd resin: adding a saturated fatty acid would yield a nondrying or plasticizing product, but adding an unsaturated fatty acid confers true drying properties [4-6].

Linseed and soya (or soybean) oils are the most used vegetable oils (drying oils) in alkyd house paints. The drying properties of linseed oil are superior to those of soya, but the former has a greater yellowing tendency. Linseed oil is the preferred choice for colors in which a small amount of yellowing should not be noticed, while in all white paints and light colors, soya oil is the most suitable. [2,4]. Safflower oil also has good resistance properties to yellowing but it is rarely used in paints because it is more expensive. Industrial alkyd paint formulations use a whole range of oils, including tall, tung, sunflower and dehydrated castor oil [4].

The “oil length” determines the working properties and solubility of the paints. Long oil alkyds, with an oil content greater than 60% by mass, can be applied by brush and thinned in aliphatic mineral spirits. These types of paints are the most commonly used ones in the home. Short oil alkyds (less than 40% oil content) are normally used as industrial paints, since they require aromatic hydrocarbons for thinning and quick-drying. The medium oil alkyds, with an oil content between 40 and 60%, show working properties similar to those of short and long oil alkyds. They are not as commonly used and only in some brands of paint for the home [7].

Alkyd paints are often further modified in order to improve certain properties such as decreasing drying time, increasing film hardness, or water resistance. These modifications include the addition of styrene [8-9], vinyl toluene [9], isocyanates [10], acrylic [9], epoxy [11], or silicone compounds [12].

Furthermore, alkyd resins may be combined with polyamide resins to produce a thixotropic (non drip) coating. Alkyd resins can also be emulsified and modified into water-soluble films by introducing a number of well-distributed free carboxyl and hydroxyl groups into the polymer [13].

As mentioned above, long oil alkyd paints are the most commonly used paints for the household given that their drying process is similar to that of an oil paint whereby the unsaturated fatty acids initiate the oxidation and cross-linking processes which lead to a solid paint film. The relative drying rate of an alkyd resin is determined by the degree of unsaturation in its fatty acid chains (see below). This cross-linking also means that the alkyd resins are often stiff and may therefore be prone to cracking if used on canvas or other flexible supports. [4-6]

Although alkyds are generally faster drying than pure oil paints, they usually contain driers able to accelerate the speed of curing and drying of the final color, especially in the formulations containing semi-dryings oils (like soya oil). [1]

5.5 Drying of alkyd paints

The drying process of alkyd paints can be divided into two stages. The first stage is a physical drying stage in which the solvent evaporates. The second stage is a curing stage (chemical drying or oxidative drying) in which the resin of the formulation reacts and forms a network by the formation of cross-links. These two stages involve different time scales: the evaporation stage takes from minutes up to several hours, whereas the curing process takes place over several hours up to days, or even months or years, depending on the formulation of the paint color. In fact the last stage can continue for many years, which is often called ageing. During this chemical ageing, the painting becomes brittle and cracks appear at the end of this process, a characteristic of many historic oil based paintings on display in museums.[14]

The evaporation stage has been studied extensively. During this stage the solvent evaporates while the resin remains on the surface. The speed of this process is very important in practical terms. The film should dry within reasonable time limits without being too fast. The time characterising this process is often referred to as open time. The open time is the time during which the layer flows enough to remove small irregularities. The evaporation process, together with the deformation of the particles in solvent-borne systems, determines the paint’s gloss and

fluidity, making it an important topic for research. Thermogravimetric analysis has been widely used to follow the physical drying process (solvent loss) [15].

During the curing (chemical drying) stage the double bonds of the fatty acid side chains present in the alkyd molecules react with oxygen, which results in cross-links. The curing of the resin is a complex oxidative process, which will be explained in more detail in the following paragraph. The research on oxidative drying of alkyds can be subdivided in two research topics. The first topic concerns the chemical reactions taking place during oxidation of model systems.

These models are mostly oils or fatty acid esters, which still have low viscosities after oxidation. The second research topic focuses on the curing process inside alkyd coatings films monitored as function of depth. Not much research has been carried out on this topic, because there is a limited number of analytical techniques to probe the film structure as a function of depth. Compared to model systems, the curing of alkyd paint films is more complex, because physical aspects such as diffusion of oxygen or diffusion of radicals, plays a significant role. The fact that oxygen diffusion plays an important role was already mentioned in 1954 [16]. Oxygen diffusion might limit the curing reaction, as it requires oxygen, resulting in an oxygen gradient. Such a limitation of the curing reaction is demonstrated by many examples of inhomogeneous curing, e.g., the formation of a skin-layer at the surface of the films that can cause wrinkling [17]. Until recently little or no research was performed in the diffusion and reaction as a function of depth inside alkyd films. Only recently, the depletion of double bonds inside alkyd coatings was performed using CRM (Confocal Raman Microscopy) and described in terms of a reaction-diffusion model [18,19]. Generally, in all works of alkyd resins no diffusion in function of depth was studied whereby the films were considered as a thin homogeneous layer.

The curing of alkyds is an autoxidation process in which oxygen reacts with unsaturated oils or the unsaturated fatty acid side chain of the resins. This process has been studied in great detail, as it is an important process in food science and biology. The autoxidation mechanism of fatty acids is a complex process in which many intermediate species can be formed [19]. The process is generally divided in 6 stages [16,20-22]:

I. Induction
II. Initiation
III. Hydroperoxide formation
IV. Hydroperoxide decomposition
V. Cross-linking
VI. Side-reactions

5.5.1 Induction

The induction period exists because of the presence of natural anti-oxidants (α–, δ– tocopherols and β–carotene) or added anti-oxidants inside the original paint (2-butanone oxima, hydroxyquinone). These anti-oxidants trap radicals, thereby inhibiting the oxidative reactions. [23] Oxidative reactions are also inhibited via quenching of singlet oxygen to the triplet

state by carotenoids (β–carotene). In fact in this triplet state direct addition of oxygen to the double bonds is spin-forbidden.

5.5.2 Initiation

This step is the least understood step of the autoxidation process. A certain free radical (X •) for initiation of the oxidation reaction is required. After H-atom abstraction from the unsaturated fatty acid (R-H), a radical R• remains. From an energetic point of view, the most favorable position of hydrogen abstraction in the case of unconjugated double bonds, is for one of the two hydrogens to be positioned between the double bonds. [24] These radicals can be inhibited during the induction period. The hydrogen abstraction speeds up when a radical generating species is added.(I)

$$R\text{-}H + X\bullet \rightarrow R\bullet + X\text{-}H \qquad (I)$$

5.5.3 Hydroperoxide formation

The radical R• reacts instantaneously with atmospheric oxygen to form a hydroperoxide radical (II). By abstracting another H-atom from the unsaturated fatty acid it forms a hydroperoxide.(III)

$$R\bullet + O_2 \rightarrow R\text{-}O\text{-}O\bullet \qquad (II)$$

$$R\text{-}O\text{-}O\bullet + R\text{-}H \rightarrow R\bullet + R\text{-}O\text{-}O\text{-}H \qquad (III)$$

5.5.4 Hydroperoxide decomposition

In this stage, the hydroperoxides are decomposed into radical species and/or radical species are formed (IV-V)

$$R\text{-}O\text{-}O\text{-}H \rightarrow R\text{-}O\bullet + \bullet O\text{-}H \qquad (IV)$$

$$2\ R\text{-}O\text{-}O\text{-}H \rightarrow R\text{-}O\bullet + R\text{-}O\text{-}O\bullet + H_2O \qquad (V)$$

The decomposition of peroxides is a very slow process, but can be accelerated by adding metal catalysts (see below). During the decomposition, the amount of radicals rises, thus increasing the chance of hydrogen abstraction and new hydroperoxide formation.(VI-VII)

$$R\text{-}O\bullet + R\text{-}H \rightarrow R\bullet + R\text{-}O\text{-}H \qquad (VI)$$

$$H\text{-}O\bullet + R\text{-}H \rightarrow R\bullet + H_2O \qquad (VII)$$

5.5.5 Cross-linking

Given that there is a rise in the amount of radicals, the probability to form a cross-link by recombination increases. Different kind of bonds are formed; alkoxy (C-O-C), peroxide (C-O-O-C) and carbon-carbon (C-C) bonds.(VIII-XIII)

$$2\ R\bullet \rightarrow R\text{-}R \qquad \text{(VIII)}$$

$$2\ R\text{-}O\bullet \rightarrow R\text{-}O\text{-}O\text{-}R \qquad \text{(IX)}$$

$$2\ R\text{-}O\text{-}O\bullet \rightarrow R\text{-}O\text{-}O\text{-}R + O_2 \qquad \text{(X)}$$

$$R\bullet + R\text{-}O\bullet \rightarrow R\text{-}O\text{-}R \qquad \text{(XI)}$$

$$R\bullet + R\text{-}O\text{-}O\bullet \rightarrow R\text{-}O\text{-}O\text{-}R \qquad \text{(XII)}$$

$$R\text{-}O\bullet + R\text{-}O\text{-}O\bullet \rightarrow R\text{-}O\text{-}R + O_2 \qquad \text{(XIII)}$$

The configuration of the double bonds be they conjugated or non-conjugated, influences the preferential cross-linking path. If in the presence of non-conjugated double bonds, the preferential path is shown above(VIII-XIII). In the case of conjugated double bonds, the cross-linking predominantly proceeds via direct addition of radicals to the double bonds.(XIV-XVI)

$$R\bullet + C{=}C \rightarrow R\text{-}C\text{-}C\bullet \qquad \text{(XIV)}$$

$$R\text{-}O\bullet + C{=}C \rightarrow R\text{-}O\text{-}C\text{-}C\bullet \qquad \text{(XV)}$$

$$R\text{-}O\text{-}O\bullet + C{=}C \rightarrow R\text{-}O\text{-}O\text{-}C\text{-}C\bullet \qquad \text{(XVI)}$$

The fatty acids in an alkyd resin are in fact polyunsaturated fatty acids. The most common ones are linolenic acid (α-linolenic acid (9Z, 12Z, 15Z-octadecatrienoic acid) and γ-linolenic acid (6Z,9Z,12Z-octadecatrienoic acid) (Fig. 5.4) which is a major constituent of linseed oil, or linoleic acid (9Z,12Z-octadecadienoic acid) which is a major constituent of sunflower oil and soya oil for example. The high susceptibility of non-conjugated polyunsaturated fatty acids for autoxidation comes from the presence of *bis*-allylic hydrogen atoms, which have a relatively low bond dissociation energy of 314 kJ/mol and can therefore be easily abstracted, resulting in radical chain initiation and thus autoxidation.

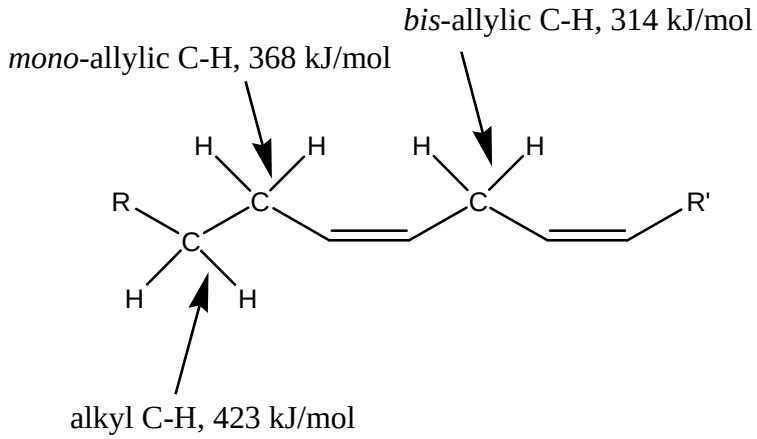

Figure 5.4 Bond dissociation energies of the different C-H bonds in fatty acids

The radical species formed is stabilised by delocalisation due to the local pentanediene structure and molecular oxygen reacts extremely rapidly with this pentanedienyl radical species to form peroxy radicals. These have double bonds that are mainly conjugated, since this is the most stable structure. The following scheme shows the autoxidation reactions for a fatty acid pentanediene structure, forming a hydroperoxide and its decomposition leads to further product

formation, forming cross-linking (non-volatile) species and numerous other oxygen containing products such as alcohol, ketones, aldehydes and carboxylic acids. (Fig. 5.5) [21-25]

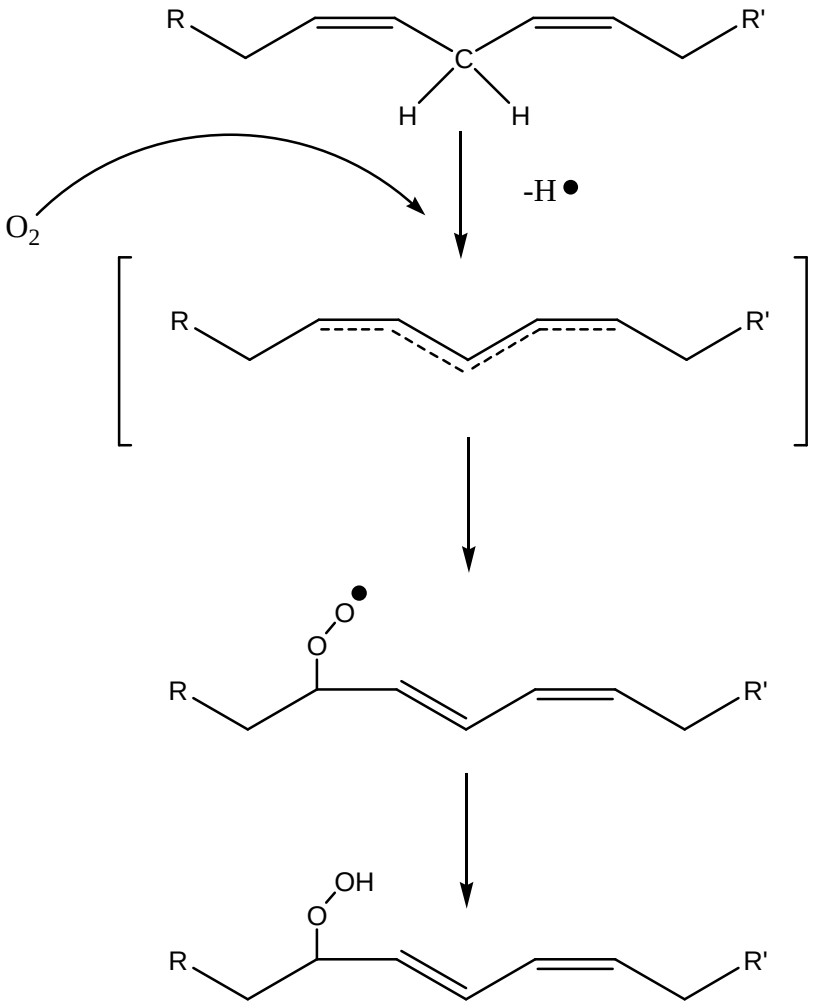

Figure 5.5 Initial Hydroperoxide formation in the autoxidation of the fatty acid chain of an alkyd resin

5.5.6 Side reactions

The typical smell of alkyd paints originates from the formation of volatile by-products. Many side reactions occur during the autoxidation process. One of those side-reactions, β-scission, cleaves the linoleate molecule into aldehydes, such as hexanal, pentanal or propanal [25]. Another kind of degradation is the Norrish reaction, where the action of UV light on carbonyl compounds lead to a photochemical degradation, forming new small organic species such as alcanes, alkenes, alcohols, epoxides or new carbonyl species [26]. (Fig. 5.6)

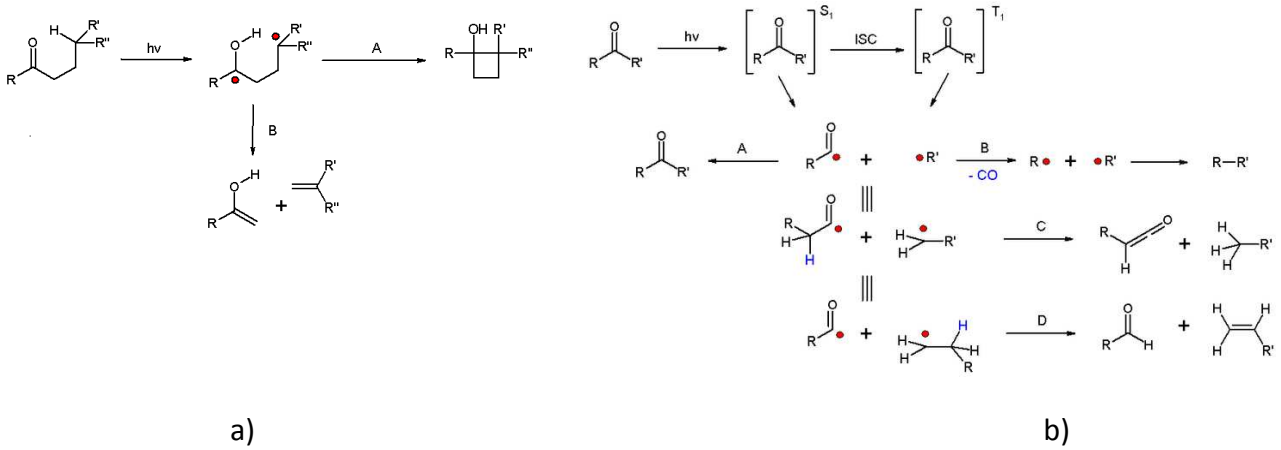

Figure 5.6 The mechanism of the Norrish Reaction a) Type I b) Type II

5.6 Drier of alkyd paints

The additives to speed up the drying of alkyd coatings are called driers. Driers are organometallic compound, which are soluble in organic solvents and binders and chemically belong to the class of soaps.

Driers catalyse the uptake of dioxygen and decomposition of hydroperoxides to free radicals, resulting in hardened cross-linked polymer networks that bind the pigment to the painted surface of the treated object.

The first modern driers were developed in the early 1920's with the preparation of metal naphthenates [22]. The driers that are used today are based upon synthetic acids, like 2-ethyl hexanoic acid and versatic acid, shown in Fig. 5.7. Versatic acids have a tertiary carbon atom adjacent to the carboxylic acid group resulting in a highly branched structure.

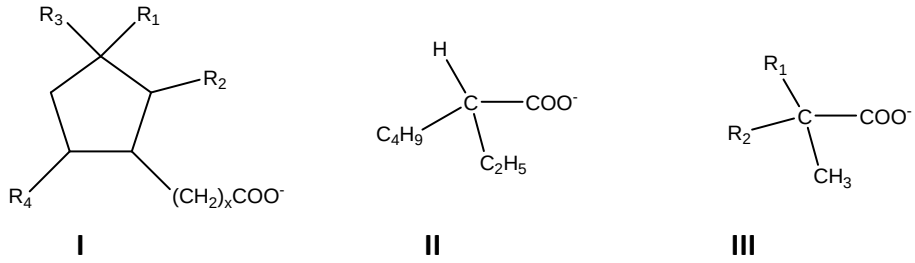

Figure 5.7 Carboxilates used in traditional drier metal soaps. **I:** Naphthenoate derivative, R1-R4 are short alkyl chains or hydrogens. **II**: 2-ethylhexanoate, often referred to as "octoate". **III:** Versetate, typically neodecanoate: R1 and R2 are alkyl groups and the total number of carbon atoms is ten.

The reason for using branched carboxylic acids is to achieve a high solubility in the apolar environment that is the oil paint binder system and to prevent precipitation of the complex.

The metals that have been used in drier compounds can be grouped in three categories: primary driers (also called active or oxidation driers), secondary driers (also called through-driers) and auxiliary driers. The metals used for the driers in each category are listed in Table 5.1.

Primary driers	Secondary driers	Auxiliary driers
Cobalt	Lead	Calcium
Manganese	Zirconium	Zinc
Iron	Bismuth	Lithium
Cerium	Barium	Potassium
Vanadium	Aluminium	
	Strontium	

Table 5.1 The metals used in alkyd paint formulations, in each drier category

Primary driers are autoxidation catalysts, and as such function predominantly as surface driers, where the dioxygen concentration is highest. The most important function for autoxidation catalysts is hydroperoxide decomposition and conseguently all primary drier metals have two accessible valence states that differ by one electron, which allows for catalytic hydroperoxide decomposition. It is most uncommon to use a primary drier in a coating formulation without an additional secondary or auxiliary drier. The most widely used metal in primary drier is cobalt. As a simple metal soap it shows unequalled effectiveness at room temperature, and it can be used in a broad range of coatings and varnishes.[22] The exact structures of the cobalt species present during alkyd paint drying are not precisely known. Based on general autoxidation literature, some structures can be proposed however, in fact Co (III) with carboxylate ligands tends to form polynuclear complexes [27] and Lombard et.al. proposed a dinuclear cobalt (III) species to take part in the catalyzed autoxidation of α-pinene [28] (Fig. 5.8).

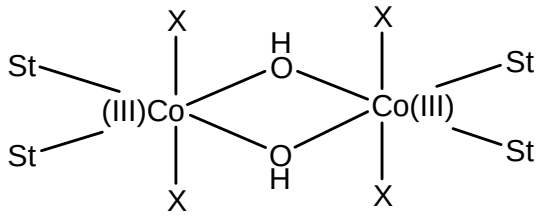

Figure 5.8 Dimeric cobalt complex proposed to be formed in the cobalt stearate catalyzed autoxidation of α-pinene. St= stearate anion, X= water or alcohol

Also, the formation of peroxide and hydroperoxide complexes has been proposed, especially in a media of low polarity like the alkyd color, because the autoxidation takes place in a mixture of pure alkyd resin and pigments, which is very likely a significantly apolar environment.

$$ROOH + M^{n+} \Leftrightarrow [(ROOH)]^{n+}$$
$$[(ROOH)]^{n+} \rightarrow RO\bullet + [(M^{(n+1)+}(OH^{-})]^{n+}$$
$$ROOH + M^{(n+1)+} \Leftrightarrow [(ROOH)M]^{(n+1)+}$$
$$[(ROOH)M]^{(n+1)+} \rightarrow ROO\bullet + M^{n+} + H^{+}$$

Figure 5.9 Metal-hydroperoxide complex formation in media of low polarity

Manganese soaps are also used as primary driers, although they are almost always used in combination with cobalt soaps.[22] The autoxidation activity of manganese soaps can be greatly enhanced by the addition of amine ligands (bipyridine, phenantroline). A disadvantage of the use of manganese is the brown color of its compounds in the trivalent state, and manganese driers are thus not preferred to be used in high concentration in light colored or white paints.

Iron metal soaps are not very good drying catalysts at room temperature. Although iron complexes are very potent redox catalysts in aqueous solutions, in apolar solvents the Fe(III) ion in metal soaps is not easily reduced, which prevents the redox cycle necessary for catalytic hydroperoxides decomposition. [29] Consequently, iron soaps are not used in air-drying alkyd paints, except sometimes in baking enamels. Iron complexes are also very strongly colored, which prevents their use for the same reasons as for manganese complexes. Cerium and vanadium are only used as primary drier metals in specialty coatings.

Secondary driers are active in the cross-linking steps of drying, they are responsible for an overall drying throughout the entire paint layer. [30] Lead has been widely used as a secondary drier metal, but now the use of lead in paints is banned in most western countries, due to its toxicity. Zirconium, bismuth, barium and strontium have all been labeled “lead-replacements”, but zirconium is the most widely accepted replacement for lead [29,30]

Bismuth soaps combined with cobalt driers were found to improve the drying time of alkyd paints especially under adverse conditions of low temperature and high humidity [31].

Aluminium compounds greatly enhance cross-linking. It has been reported that alkyd paint formulations containing cobalt drier and aluminium drier have a significantly increased hardness [32] . Turner et al. have proposed that the increased polymerization drying for aluminium is accomplished by the formation of extra cross-links formed with alumina and polar groups in the oxidized alkyd networks, as schematically shown in Fig 5.10.

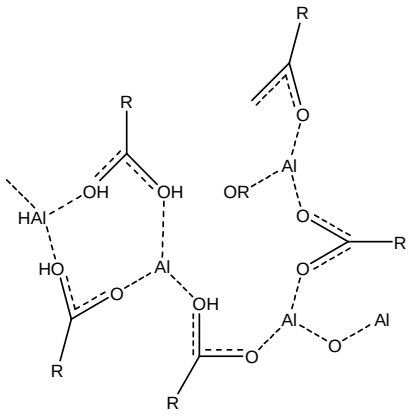

Figure 5.10 Schematic representation of possible alumina cross-links in an oxidised alkyd network

The use of aluminium compounds as additional cross-linkers in high-solids alkyd paints has also been studied [25].

Auxiliary driers are added to enhance or alter the activity of the primary drier, and thereby improve the appearance and quality of the total paint film. The action of these driers at the molecular level is not known. Zinc, lithium and potassium driers are added to paints with a cobalt drier to inhibit wrinkling of the paint film, which is caused by differential hardening of the surface relative to the remainder of the film. Zinc prevents wrinkling by retarding the cobalt drier [30] . Potassium driers combined with cobalt driers were found to be very effective in the through-drying of especially water-borne alkyd systems.[31,33] Calcium driers help improve a multitude of different characteristics , such as hardness and gloss, as well as drying under adverse weather conditions. [22]

Currently, few papers are reported in the literature related to the study of the ageing process of alkyd paints. Stamakatis et.al studied the ageing process of polyester resins by NMR spectroscopy.[34] Phenix studied the increased sensitivity and plasticization of alkyds in water as a result of the formation of hydrophilic groups using an imaging technique.[35] Stava et.al studied the cross-linking reactions occurring during the creation of an alkyd resin film and the catalytic action of cobalt, manganese and their mixed salts as driers.[36] Ouldmetidji et. al and Mallègol et.al described the use of DSC to follow the peroxidation of polymers during ageing.[37] Ploeger et al. described the use of DSC and TGA to investigate the thermal stability of commercial artists' alkyd paints and evaluated the changing occurring with time during natural and artificial ageing of films.[15,26] Colombini et. al. and Wei et.al. characterised the alkyd paints by Py-GC/MS and GC/MS [38-39]. Wei et.al. studied also the effect of ageing and the main oxidization products formed were a mixture of long-chain aldehydes and free phthalic anhydride.[38]

Ye et.al. promoted the formation of single state molecular oxygen as oxidant to accelerate oxypolymerization and chemical drying and proposed a general mechanism for photo-oxidation of alkyds. [40] Cakic analysed the colour change by FTIR as results of UV irradiation correlated it with an increase in the hydroxyl content and broadening of the absorption in the carbonyl region. [41] Chittavanich et.al. demonstrated that different diluents can change the properties of cured paint films, in particular long chain linear structure diluents provide paint films with better impact resistance, flexibility and adhesion over other diluents. [42]Ploeger et.al. determined the rate of surface oxidation by contact angle measurements, and as the films aged, there was a decrease in the contact angle and an increase in the polar components of the paint film surface due to the formation of photo-oxidation products. [43]

Few papers report on the FTIR characterization of alkyd paints and their ageing.[15,20, 41,44-48]

The aim of this work is to investigate the natural and artificial (acid) ageing process of a set of alkyd resins named fast drying oil colour and produced by Winsor & Newton (Griffin series) in the framework of COPAC project concerning the characterization of materials used in modern and contemporary art.

Name colour	Index colour	Chemical composition
Ivory Black	PBK9	Bone black
Titanium White	PW6	Titanium dioxide
Phtalo Blue	PB15	Copper phthalocyanine
French Ultramarine	PB29	Sodium alumino-silicate with sulphur
Phtalo Green	PG7	Chlorinated copper phthalocyanine
Viridian Green	PG18	Hydrated chromium oxide
Winsor Lemon	PY3	Arylamide yellow
Cadmium Yellow Light	PY 35	Cadmium zinc sulphide
Winsor Red	PR170 - PR 188	Naphtol carbamide and naphtol AS
Cadmium Red Medium	PR108	Cadmium sulphoselenide

Table 5.2 Name colour and chemical composition of the paints studied in this work

These paints have a new formulation: the source of fatty acid is a semi-siccative soya oil and a Co-carboxylate drier was added to accelerate the speed of drying. Four colours (red, blue, yellow and green) have been selected in two formulations based on inorganic or organic pigments. Titanium white and black formulated with carbonized bones have been also characterized. Their chemical formulation is summarized in Table 5.2 .

The artificial acid ageing is a common procedure of artificial ageing because acetic acid is one of the atmospheric pollutants that can be found inside museum in concentrations that can produce significant effects in the objects on exhibition. Several materials can suffer fast alteration by exposition to acetic acid vapors, but, probably, it is the lead and the lead alloys that can show more serious consequences [49,50]. Significant problems have been reported with coins [50], document seals [51], weights [52] sculptures [50] or oriental lacquer objects [53] Besides, this pollutant can also attack other materials, such as, for example, copper alloys and copper materials [54,55], paper [56], shell [57] or other calcareous materials [58]. Some recent works demonstrated that acetic acid can attack also polymeric materials, causing depolimerisation by acid hydrolysis. [59-60]

While some of the atmospheric pollutants in museum have its origin outside, the main source of acetic acid is, usually, inside, where it can be released by the building materials or the furniture. The wood, especially wood not aged, wood panels and synthetic polymeric materials used in the museum equipment, namely adhesives, varnishes or other plastics, are among the materials that can release larger amounts of volatile organic compounds, like acetic acid. Even if the amounts of acetic acid released by these materials are low, when they are used in closed spaces, as inside showcases, relatively high concentrations can be reached. In fact, values higher 3000 g m^{-3} were already detected inside museum showcases, when outside the buildings the concentration of the acetic acid in the atmosphere usually is between 0.1 and 100 g m^{-3} , depending on the pollution degree. [61]

The ageing behaviour of this colour set by other chemico-physical techniques (colorimetry, CG-MS, size exclusion chromatography) is in progress in the framework of COPAC project.

My studies also concerned two works of the young Italian painter Patrizia Zara. Zara's works mainly focused on hands, which from a hyper-realistic approach were the object. The hands celebrate the preciousness of a virtuosity that transcends any other content. In fact in her works, hands are often the only or the principal subject of the paintings and recently, a personal exhibition in Milan called "Le mani di Zara" was held.

Patrizia Zara belongs to the hyper-realistic movement. She uses alkyd colours for her works, in particular the Winsor & Newton ones, the same ones studied in this work.

Hyperrealism is a genre of painting and sculpture resembling a high-resolution photograph. Hyperrealism is considered an advancement of Photorealism due to the methods used to create the resulting paintings or sculptures. The term is primarily applied to an independent art movement and art style in the United States and Europe that has been developing since the early 2000's. Hyperrealism, although photographic in essence, often entails a softer, much more complex focus on the subject depicted, presenting it as a living, tangible object. These objects and scenes in Hyperrealism paintings and sculptures are meticulously detailed to create the illusion of a reality not seen in the original photo. That is not to say they're surreal, as the illusion is a convincing depiction of (simulated) reality. Textures, surfaces, lighting effects, and shadows appear clearer and more distinct than the reference photo or even the actual subject itself.

My work focused on two of Zara's paintings: "Salto di qualità" (2003) and "Senza nome " (2007) both alkyd paintings made using the Winsor & Newton - *series Griffin-fast drying oil color*.

Figure 5.11 Patrizia Zara "Salto di Qualità" 2008, alkyd on canvas

Figure 5.12 Patrizia Zara “Senza nome” 2003, alkyd on canvas

All the samples were analysed using ATR-FTIR and DSC techniques. The interpretation of the paint’s spectrum involves separating the spectra into its individual components. This process is often complicated, especially if one component has very strong and broad absorption in the same region as the diagnostic section of another component. For this reason, in many instances it becomes virtually impossible to interpret a paint’s spectrum. Further complications can also arise when more than one of each component is used in the formulation. However, in our case, the spectra becomes relatively straightforward because the filler (dolomite) and the resin formulation is the same as our paint replicas and the only unknown element is the pigment used in the original colour.

These fast drying alkyd paints and Zara’s paintings have been studied in this work using a multi-technique approach, which includes DSC, TGA and FTIR spectroscopy.

5.7 Results and discussion

5.7.1 Thermoanalysis

The physical and chemical drying processes of the alkyd resins were monitored by TG and DSC analyses.

The solvent evaporation, that causes the physical drying, produces a mass loss in TG curves at about 100°C, that disappears in the first 18-24 hours after deposition [15]. In Figure 5.13 The TG curves of yellow cadmium recorded in the first ten hours after paint deposition are reported as an example. Actually a loss of about ninety percent of the total amount of the solvent occurred within the first ten hours (see Fig. 5.13).

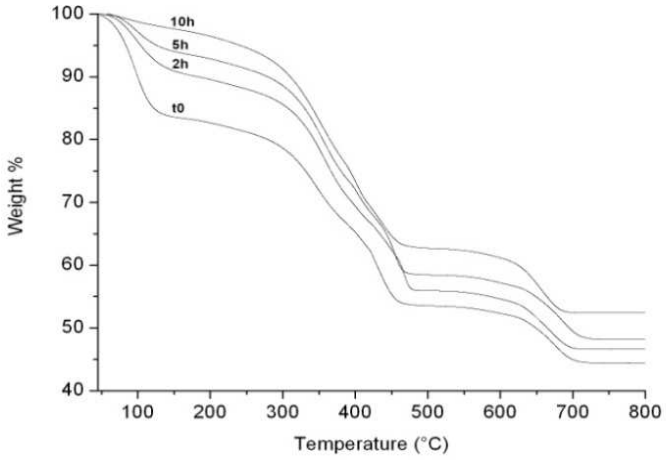

Figure 5.13 TG curves of yellow cadmium (PY35) during the first 10 hours of deposition

Fig. 5.14 (A) shows the comparison between TG curves under air flow of the Titanium White alkyd paints fresh and after different time of ageing. Due to thermal stability of titanium dioxide (rutile) discussed above [62] (see chapter 3), this paint showed the simplest degradation pattern among the different TG experiments.

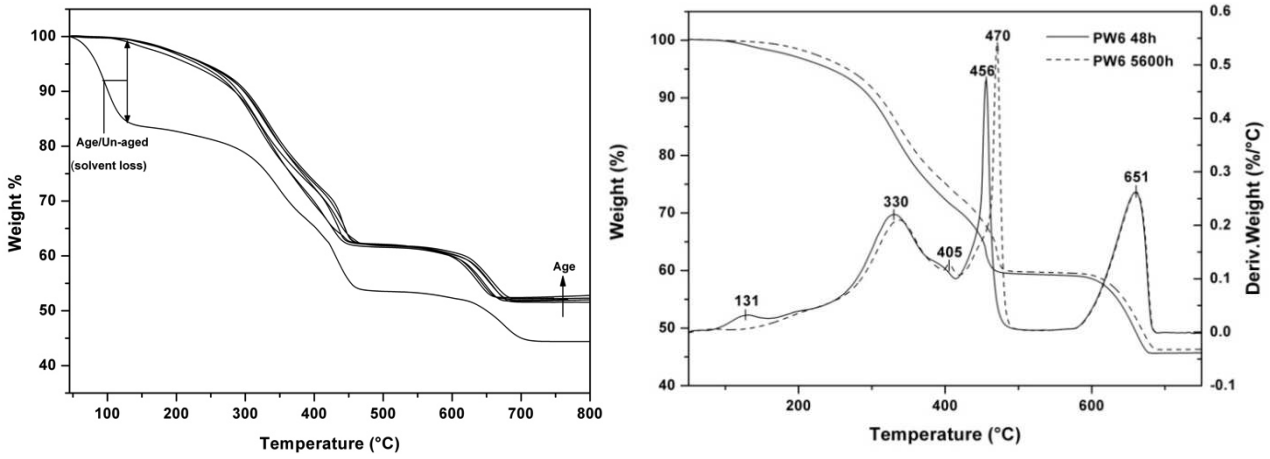

Figure 5.14 Thermogravimetric curves under air flow at 10°C/min of heating rate of Titanium White alkyd paint (a) fresh and after different time of natural ageing; (b) after 48 and 5600 h of natural together with their derivative

In the fresh paint we observed four degradation steps, the first occurring below 150°C and corresponding to a mass loss of about 18-19 % for all the sample studied. This mass loss practically disappeared in the curves of samples aged for 48 h or more allowing us to attribute it to the solvent evaporation (total physical drying). In fact, rescaling the curve of the fresh paint by taking as 100% the value at 150°C, we obtain a new plot practically matching the curve of the 48 h aged sample in the range 150-800°C.

The three remaining degradation steps have been described in the literature [15,26] and were attributed to the first stage of oil oxidative degradation (about 330°C), the main combustion peak (410-480 °C), and the degradation of dolomite present as filler (600-700 °C). (See Fig. 14B)

All other examined paints showed two or three additional mass losses associated to the thermal degradation of the pigments usually occurring in the temperature range between the two main degradation steps of the binder. In aged samples, the mass loss due to the solvent evaporation was absent, as above observed in the case of Titanium White paint. (See Figs. 5.14 and 5.15)

All the TG experiments of samples aged for 48 h, showed in the temperature range 100-200 °C a new mass loss, assigned in literature to the peroxide thermal degradation (See Fig. 5.14 (b)) [15]. With further sample ageing, this signal decreased due to time dependent degradation process involving peroxide decomposition such as cross-linking or oxidation. [15,37] In all the aged films, we observed a corresponding shift toward higher temperature of the degradation step around 400°C in agreement with the presence of cross-linking (see Table 5.3 and Fig. 5.15).

In the Viridian Green sample the mass loss at around 650°C was lacking, indicating that no filler was present in the formulation of this paint. (see Table 5.3 and Fig. 5.15).

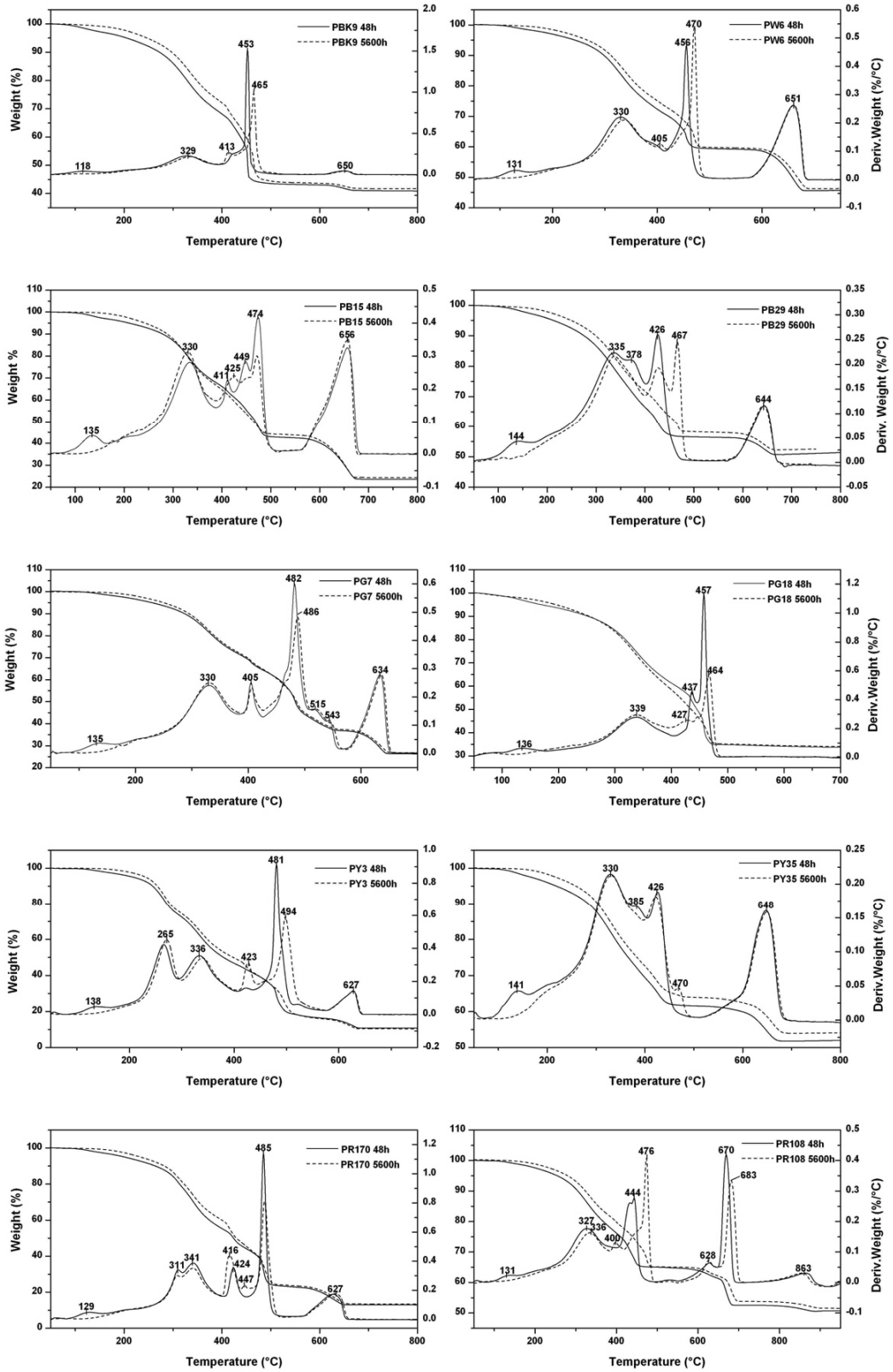

Figure 5.15 Thermogravimetric curves overlap to their derivative (only 48 and 5600 h ageing is reported) under air flow at 10°C/min heating rate, of the alkyd paint replicas studied

Peak	Black Ivory (PBK9)	Titanium White (PW6)	Phtalo Blue (PB15)	French Ultramarine (PB29)	Phtalo Green (PG7)	Viridian Green (PG18)	Winsor Lemon (PY3)	Yellow Cd (PY35)	Winsor Red (PR170-188)	Red Cd (PR108)
1	-	-	-	-	-	-	96.4°C (0.9%)	96.6°C (0.6%)	96.3°C (0.4%)	-
2	118°C (3.1%)	132°C (1.9%)	135.2°C (3.4%)	144°C (3.2%)	136°C (2.7%)	136°C (5.6%)	137.7°C (3.4%)	141°C (2.2%)	129.3°C (2.6%)	131.2°C (1.7%)
3	-	-	-	-	-	-	265°C (22.6%)	-	-	-
4	329°C (28.1%)	330.3°C (27.7%)	330.5°C (28.6%)	335°C (30.2%)[a]	330°C (27%)	339°C (33.3%)	333°C (27.2%)	329°C (28.6%)[a]	310°C (shoulder) 341°C (37.1%)	327°C (21.0%)
5	-	-	-	376°C (30.2%)[a]	-	-	-	385°C (28.6%)[a]	-	-
6	- 437°C[b] (shoulder)	-	411°C (6.9%)	425°C (9.3%)	405°C (6%)	437°C (10.8%)	-	-	424°C (12.5%)	-
7	453°C (25.7%)	455°C (11.1%)	449°C (shoulder) 474°C (18.3%)	-	482°C[c] (27.6%) 515-543°C (shoulder)	457°C (16.6)	480.9°C (24.8%)	426°C (7.5%)	485°C (21.0%)	443°C (12.3%)
8	651°C (2.2%)	652°C (13.6%)	657°C (19%)	644°C (5.6%)	634°C (10.4%)	-	627°C (5.4%)	647°C (9.7%)	627.5 (10.0%)	670°C (11.2%)
Residual mass	40.9%	45.7%	23.6%	51.7%	26.2%	33.8%	10.8%	51.4%	16.4%	53.8%

[a] Mass loss in the range 300-400°C ; [b] Mass loss in the range 400-500 °C; [C] Mass loss in the range 420-560°C

Table 5.3 Experimental temperature, percentage mass loss of thermal degradation steps and residual mass at 800°C of alkyd resin colors under air after 48 h of deposition

TG experiments were performed also in nitrogen flow, (Fig 5.16 and Table 5.4). While being two different degradation pathways, the degradation processes were very similar in air and nitrogen. Fig. 5.16 shows the thermogravimetric derivative profiles obtained under air and nitrogen for Titanium White alkyd paint as an example. The TG curves are very similar, showing a first degradation step at about 330-350 °C with the same mass loss (27 % in air and 26 % in nitrogen), a second degradation step, combustion in air (456°C) (typical sharp peak in DTG) and pyrolisis in nitrogen (523°C) with the same mass loss (11%) and almost the same residual mass losses (45.7 % in air and 45.8 % in nitrogen).

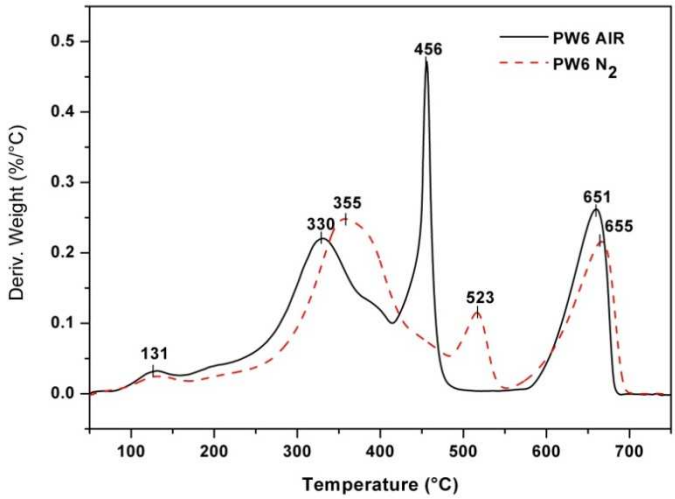

Figure 5.16 Thermogravimetric derivative curves under N_2 (red dash) and air (black line) flow at 10°C/min heating rate of Titanium White alkyd paint after 48 h of ageing.

Peak	Black Ivory (PBK9)	Titanium White (PW6)	Phthalo Blue (PB15)	French Ultramarine (PB29)	Phthalo Green (PG7)	Viridian Green (PG18)	Winsor Lemon (PY3)	Yellow Cd (PY35)	Winsor Red (PR170-188)	Red Cd (PR108)
1	-	-	-	-	-	-	96.4°C (0.9%)	96.6°C (0.6%)	96.3°C (0.4%)	-
2	113°C (3.3%)	125°C (2.2%)	131°C (3.4%)	142°C (3%)	128°C (2.9%)	132°C (5.3%)	131.4°C (3.1%)	130°C (3.2%)	127.3°C (2.7%)	138°C (2.1%)
3	358°C (21.1%)	355.3°C (25.7%)	350.5°C (28.9%)	350°C (30.2 %) 400°C (shoulder)	342°C (25.3%)	359°C (32.3%)	366°C (29.1%)	344°C (24.6%)	300°C (shoulder) 361°C (36.1%)	341°C (28.0%)
4	437°C (24.2%)	-	448°C (4.3%)	-	410°C (21.3%)	450°C (shoulder) 458°C (36.5%)	411.9°C (21%)	451°C (5.8%)	-	455°C (1.9%)
5	-	523°C (11%)	532°C (13.3%)	517°C (6%)	520°C (6.5%)	-	547°C (5.3%)	-	557°C (21.9%)	506°C (16.5%)
6	662°C (3.2%)	671°C (12.6%)	657°C (18.2%)	627°C (6.6%)	634°C (10%)	-	641°C (5.2%)	640°C (9.9%)	643.5 (10%)	651°C (10.4%)
Residual mass 48h	43.9%	45.8%	23.7%	53.0%	26.6%	34.5%	11.8%	54%	15.0%	58.1%

Table 5.4 Experimental temperature, percentage mass loss of thermal degradation steps and residual mass at 800°C of alkyd resin colors under nitrogen flow after 48 h of deposition.

To better understand the degradation pathways of the alkyd resins FTIR spectra of gasses evolved during TG experiments were collected and allowed us to explain each degradation step.

The TG-FTIR experiments showed the formation of water between 150 and 200°C, which supports the theory of peroxide decomposition in this temperature range. Water can be formed through the loss of an OH radical and hydrogen abstraction during the temperature induced decomposition of the peroxides in agreement with Ploeger et al. [15]. The TG-FTIR results showed that the polyester portion of the alkyd resin is volatilized at lower temperature than the fatty acid portion. The IR spectrum of the degradation of Titanium white paint replicas recorded under nitrogen at 350°C and reported in Fig. 5.17, showed the typical absorption peaks associated with polyester (2920, 2854, 1731, 1430 cm^{-1}) and peaks assigned to phthalic anhydride (1867, 1253, 908 and 710 cm^{-1}). [15]

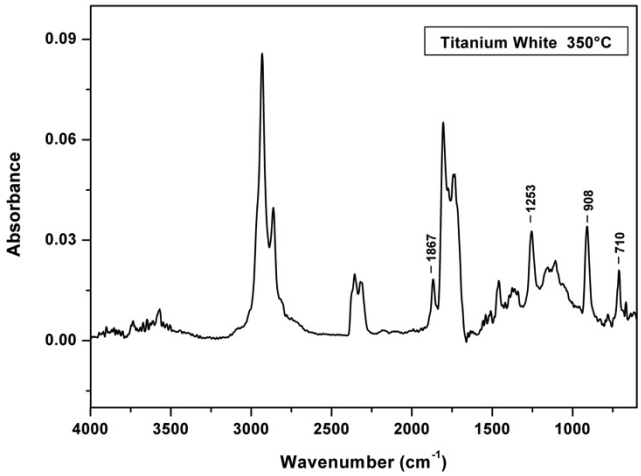

Figure 5.17 FTIR spectrum of the gasses evolved by Titanium white under nitrogen flow at 350°C

The IR spectrum obtained at 520 °C (31 min) is very similar to the spectrum of the degradation of the pure soya oil (1450, 1356, 1150 and 965 cm^{-1}), as reported in Fig. 5.18

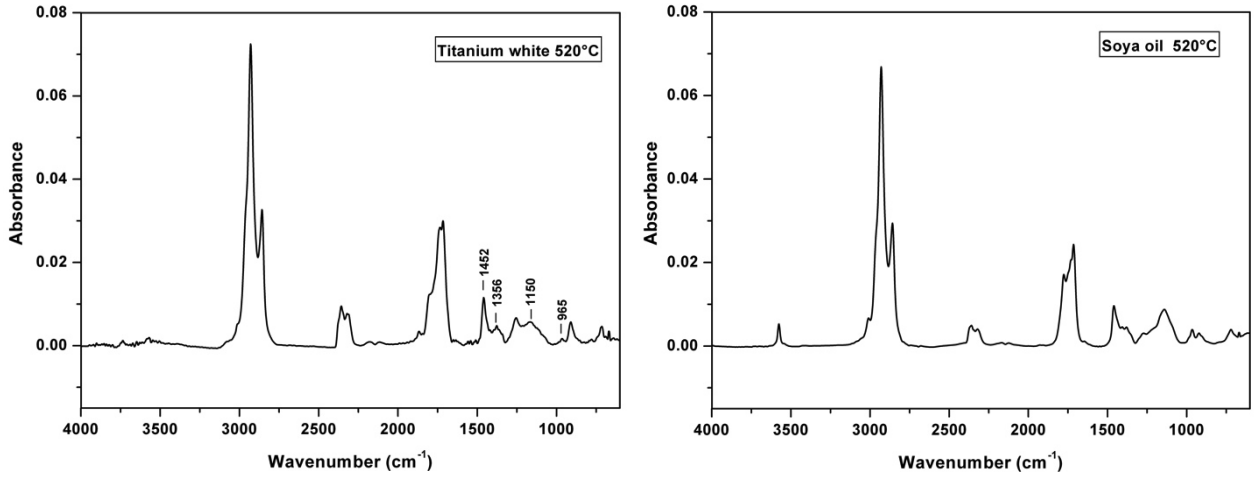

a) b)

Figure 5.18 FTIR spectrum of the gasses evolved by a) Titanium white and b) soya oil under nitrogen flow at 520°C

Naturally aged samples were investigated by DSC. Figure 5.20 shows DSC curves of all the investigated resins in the range 40-180°C at different time of natural ageing (from 48 to 5600h). The typical shape of the DSC curve exhibits a reversible endothermic peak below 90°C, preceded by a shoulder, and an exothermic irreversible broad band in the range from 90 to 180°C. DSC experiments performed at different scan rates allowed us to interpret the shoulder as a glass transition and to determine the corresponding T_g (glass transition temperature) value as the abscissa of the flex point. The values of the T_g for all the alkyd samples are shown in the Table 5.5 .

Alkyd color	T_g 48h (°C)	T_g 5600 h (°C)
Black Ivory (PBK9)	61.5	64.8
Titanium White (PW6)	59.2	64.8
Phthalo Blue (PB15)	59.8	64.2
French Blue (PB29)	56.6	62.9
Phthalo Green (PG7)	59.2	62.7
Viridian Green (PG18)	58.2	62.3
Winsor Lemon (PY3)	58.5	62.4
Yellow Cadmium (PY35)	59.6	65.4
Winsor Red (PR170)	58.9	62.3
Red Cadmium (PR108)	64.2	70.2

Table 5.5 Tg temperature (measured by DSC of the Winsor & Newton, alkyd paint films, after deposition (48h) and after natural ageing of 5600 h.

All the samples had T_g temperatures above room temperature after only 48 h of deposition on glass slides, which means that the paint films are brittle at ambient conditions. With ageing all the samples showed an increasing of T_g values over time within a range of 3-5 degrees in 8 months. This could be due to changes in the network and cross-linking in the films with age, as already seen in TG. There were also the loss of organic materials by the evaporation of low molecular mass degradation products that would otherwise act as plasticizing agents. This process increased the T_g of the paint films. The increasing in T_g temperatures with ageing explains very well the fragile handling properties of the aged paint replicas.

The exothermic signal is time dependent and is due to the peroxide decomposition involving endothermic homolitic scission of the O-O bond and the subsequent exothermic recombinations of the radicals formed which results in a globally exothermic reaction. [15,20,26, 56,57]

The rate of cross-linking of the films was monitored by observing the change in the area of the exothermic peak around 140°C related to peroxide decomposition, including dialkylperoxides (peroxy bridges) and hydroperoxides. Peroxide decomposition is an endothermic process. However, alkoxyl and hydroxyl radicals formed by homolytic scission of the O-O bond can initiate various radical propagation reactions and recombination can lead to an important exothermic effect, which results in a globally exothermic reaction.

Peroxide decomposition increases cross-linking and curing of the resins, and the total heat of reaction calculated by DSC can be considered as proportional to the number of peroxide bonds that have been broken. [15,26, 64] These alkyd paint (added with Co-Carboxilate drier as declared by productor Winsor & Newton) are designed to be dry to the touch within one day, but, as demonstrated in this work, they require more time to be chemically dried (auto-oxidation) and for complete film formation throughout their entire thickness. The thermal degradation of peroxides produced an exothermic band in the DSC curves in the temperature range 90-150°C. This degradation was observed to occur as a single step process, resulting in a single minimum broad band, or as a two steps process giving rise to a more structured band where two (partially resolved) peaks were visible.

Fig. 5.19 shows the change in the peroxide DSC peaks of the Winsor & Newton Titanium White (PW6) and Black Ivory (PBK9) paints, during natural ageing, as representatives of the two limit mentioned behaviors. DSC curves of all others alkyd paints investigated in the presence work during natural ageing are reported in Fig. 5.20.

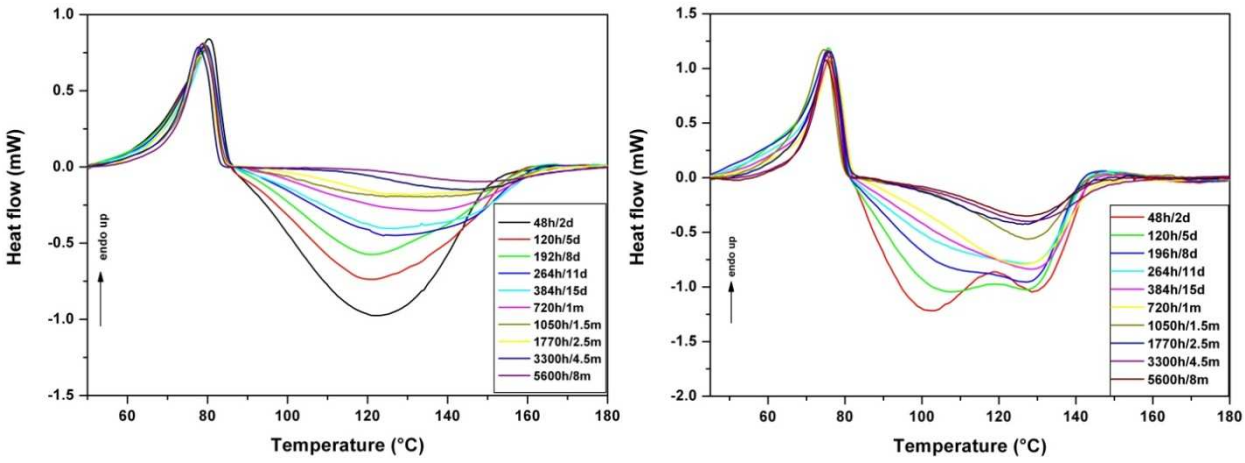

a) b)

Figure 5.19 Peroxide decomposition DSC peak of a) Winsor & Newton Titanium white (PW6) and b) Black Ivory (PBK9t) paint films at different time of natural ageing

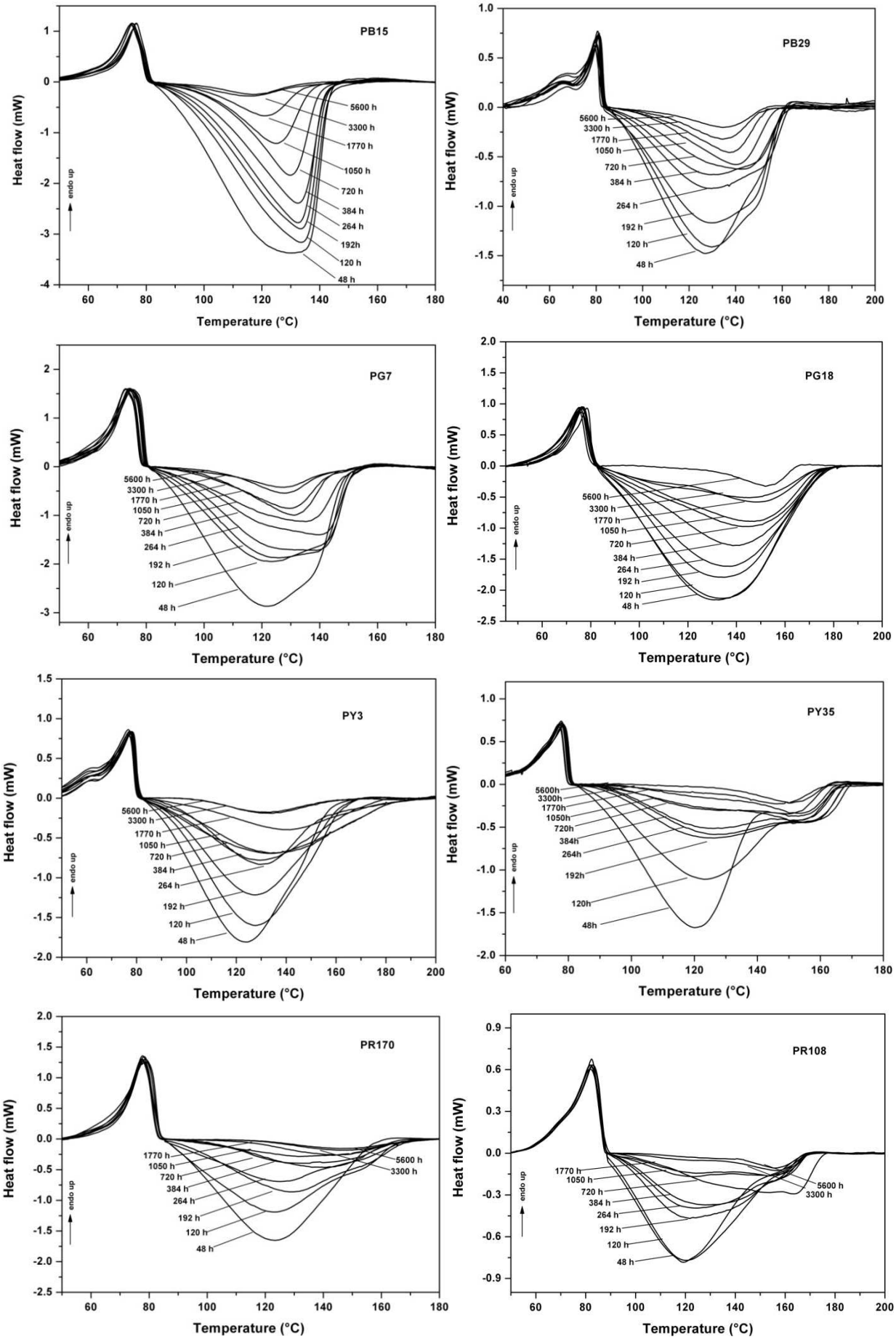

Figure 5.20 DSC peak of Winsor & Newton paint films at different time of natural ageing

Regardless the shape of the peroxides degradation band, the exothermic signal reaches the maximum value after 48 h of natural ageing then slowly decreased up to almost zero after 5600 h, when the chemical drying could be considered as complete. This result confirmed that the small quantity of driers added to the resins to obtain the "fast drying" behavior of Winsor & Newton *series Griffin- fast drying oil colour* guarantees a complete chemical drying after about eight months of natural ageing instead ten years needed by Winsor & Newton alkyd colour (without drier) studied by Chiantore et co workers [15].

Since the peroxide formation is connected to the number of double bonds in the material, the area of the exothermic peak is only related to the lipidic part of the resin. Unfortunately Winsor & Newton Co. did not provide the exact composition of any individual color. Therefore, the content of each component could only be estimated from TG data under air flow. The filler content was determined from the corresponding mass loss considering its stoichiometric decomposition path [65]. The pigment content was then determined from the mass residual at 800°C according to its chemical nature and thermal stability. Finally the lipid fraction was calculated by difference. The composition of the paint containing a completely organic pigments that decomposes in the same temperature range without residual at 800°C was impossible. The compositions of the colors estimated according to this procedure are reported in table 5.6.

Alkyd color	Filler (%)	Pigment (%)	Oil content (%)
Black Ivory (PBK9)	-	49.4	50.6
Titanium White (PW6)	28.6	30.7	40.7
Phthalo Blue (PB15)	39.9	17.5	42.6
French Blue (PB29)	11.7	42.8	45.5
Viridian Green (PG18)	-	33.8	66.2
Winsor Lemon (PY3)	11.4	28.2	60.4
Yellow Cadmium (PY35)	20.3	40.7	39.0
Red Cadmium (PR108)	25.8	39.1	35.1

Table 5.6 Percentage composition of Winsor & Newton alkyd colours determined by TG measurements

Fig. 5.21 reports for each color the areas of the exothermic peak normalized to the resin lipidic content vs. time of natural ageing. The trend of the normalized areas during ageing from 48 to 5600 h were practically the same for all the colours, thus demonstrating that the number of peroxides formed, broken and radicals recombined were independent on the nature of the pigment's colour (organic or inorganic) and only dependent on the number of double bonds in the starting material. At 5600 h of natural ageing the area of the peroxidic peak goes to zero for all the samples studied, indicating the end of the auto-oxidation process.

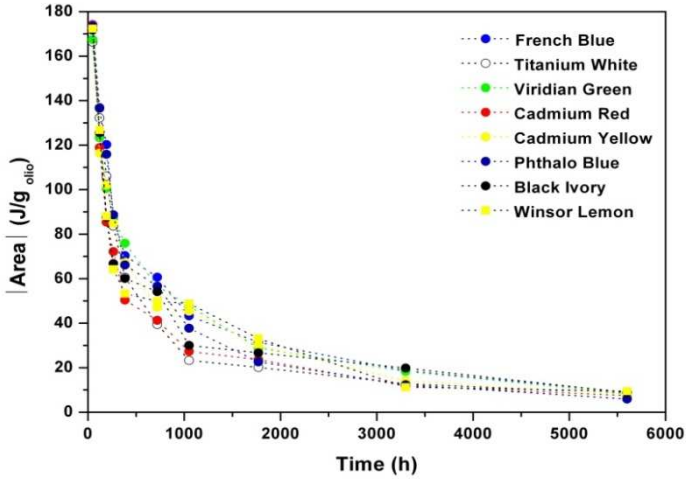

Figure 5.21 DSC degradation of peroxides in function of time for alkyd samples studied normalized for oil mass

As above mentioned, by considering in detail the form of the DSC exothermic peak during ageing, two phenomena at different temperatures were identified. In some resins, like Black Ivory (PBK9), the two phenomena are well set apart and both present since the first stage of ageing. In other resins, like Titanium White (PW6), the phenomenon at lower temperature overlays and overcomes the one at higher temperature, that becomes evident at longer time of ageing, when the first one is disappearing.

The two phenomena have been attributed in the literature to two different processes of peroxide decomposition; the first maximum was assigned in the literature to the hydroperoxide bimolecular decomposition [64] .

During the drying process the bimolecular decomposition becomes rapidly less effective due to the decreasing of peroxide concentration and to the decreasing mobility of chains for cross-linking reaction and, therefore, the monomolecular decomposition at higher temperature is the only process observed. The Phtalo Blue (PB15) has a different behaviour, the phenomenon at higher temperature is strongly predominant since the first step of ageing.

These experimental observation suggest that while the quantity of peroxides formed is only dependent on the oil quantity in the starting materials, their decomposition pathways are pigment dependent. If we consider the Titanium White alkyd resin as the system where the pigment and the resin are not interacting, we can assume its DSC profile as DSC profile of the resin alone (not interacting with pigment). Giving that and looking at the DSC profiles, we can assume low pigment-resin interactions in French Ultramarine (PB29) and Viridian Green (PG18). It must be noted that these resins contain inert inorganic pigments. These results matches with those obtained with TG analysis, where the number and position of the mass losses and their shift during ageing was very similar in the three resins.

According to the hypothesis formulated by Mallegol et. [64], a kinetic model based on two parallel competitive mechanisms, mono- and bi-molecular respectively, was considered, though still giving unsatisfactory results. For this reason we chose the fitting equation according to a *trial and error* approach. The best results were obtained with a double exponential decay and a constant term (equation 1).

$$-\Delta H\left(\mathrm{J\ g_{oil}^{-1}}\right) = 148.8 \cdot e^{-0.073 \cdot t} + 62.7 \cdot e^{-0.00061 \cdot t} + 6.1 \qquad (1)$$

Though a complete kinetic study needs a much larger set of experimental data, and despite equation 1 is basically empirical, its form suggests that at least two decomposition pathways are effective. The small constant term in equation 1 probably accounts for a thermal effect present in the examined DSC region independent of peroxide decomposition. In Figure 8 is also reported the cumulative fitting curve. The insert of figure 7 shows the plot of residuals, which appear fairly well distributed.

It is worth to note that equation 1 can also be employed to estimate the oil content of a *Winsor & Newton series Griffin- fast drying* alkyd paint of unknown composition from the area of the peroxide decomposition peak and the ageing time, provided that the latter is less than 5600h.

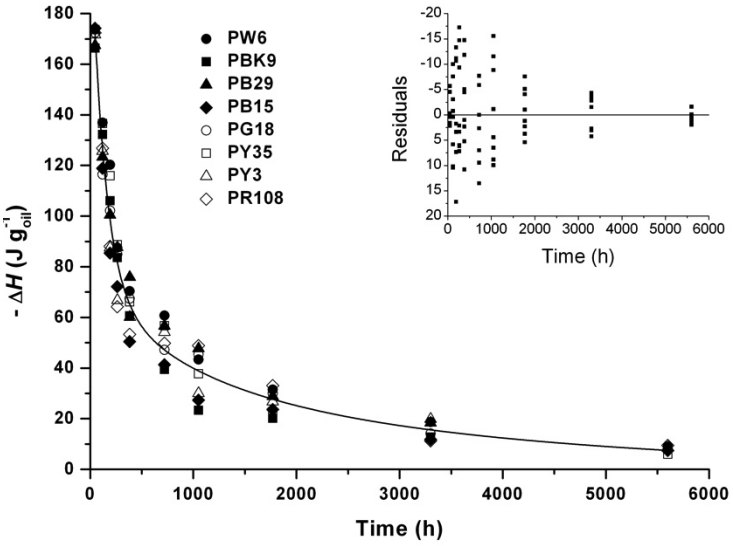

Figure 5.22 Exotermic peak areas at different times of natural ageing normalized to the resin lipidic content versus the time of ageing for each resin.

Looking at the endothermic peak, after 48 h of natural ageing, all the alkyd samples showed a maximum in the range 75-80°C. During ageing this maximum moved to higher temperatures, reaching a maximum shift of about 4°C after 5600 h of natural ageing. This results matches with an increase of resin cross-linking.

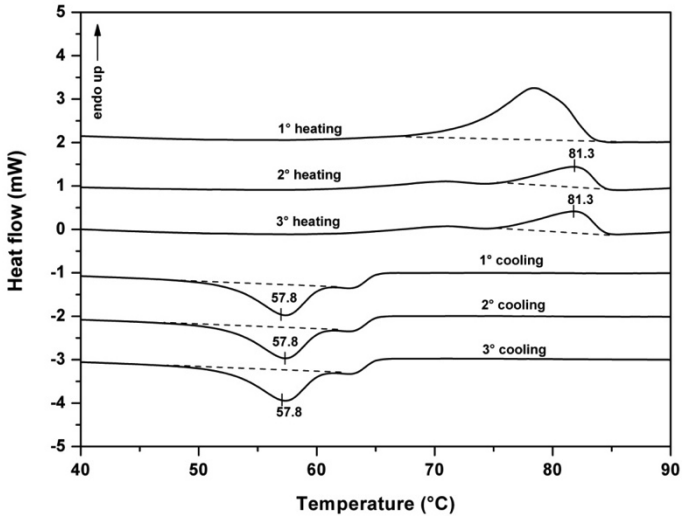

Figure 5.23(a) DSC multiple heating-cooling cycle in the temperature range 40-90°C performed on a Titanium white (PW6) sample 5600 h naturally aged

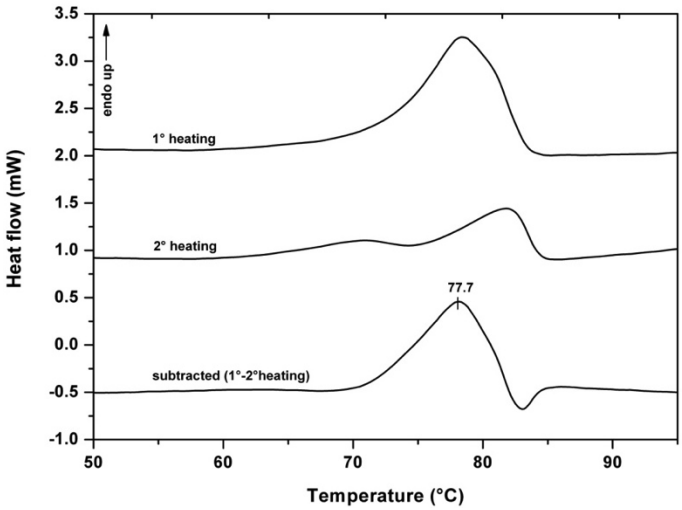

Figure 5.23(b) DSC heating curve and substracted heating curve in the temperature range 50-90°C performed on a Titanium white (PW6) sample 5600 h naturally aged

As previously claimed this endo effect is only partially reversible. Fig. 5.23a shows a multiple heating-cooling cycle in the temperature range 40-90°C performed on a PW6 sample 5600 h naturally aged. The first heating scan significantly differed from the following ones that were practically identical. In the curves of the second and third heating the glass transition at about 65°C was followed by a reversible endo effect with a maximum at 81.3 °C ascribable to the melting of the resin. The reversibility of the thermal effect could be argued by comparing heating and cooling curves. The latter still showed the glass transition at 65°C whereas the crystallization peak moved to 58°C due to hysteresis. The melting and crystallization peaks showed practically the same area, though the integration was somewhat difficult due to the presence of the glass transition. Accounting for the polymer content in the samples, the enthalpy of fusion of the resin could be roughly estimated obtaining 5.5 J g^{-1}. Heating-cooling cycles in the temperature range 30-100°C repeated on the same sample after one week gave identical DSC curves.

In view of the above considerations, the first heating curve should embed the glass transition, the reversible melting of the resin and a further contribution due to an irreversible process. To highlight the latter effect, we subtracted the second heating curve from the first one (see Fig. 5.23b). The curve obtained by subtraction clearly showed a prevailing endo effect with a maximum at 77.7°C. A possible hypothesis to explain this effect involves the evaporation of small quantities (less than 1 % not detectable by TG measurements) of volatile components trapped in the resin occurring after the softening of the resin itself.

It is worth to note that the area of the endo peak during the first heating was practically independent of the sample ageing (see Fig. 5.20), thus indicating that the cross-linked fraction was a small portion of the material.

5.7.2 FTIR

The efficiency of drying and the rate of auto-oxidation has been also studied by infrared spectroscopy, following the change occurring in IR spectra of fresh and aged paint samples [45-48]. This information is complementary to thermal data and, if correlated, may present a faster, non-invasive approach to the study of alkyd paint ageing.

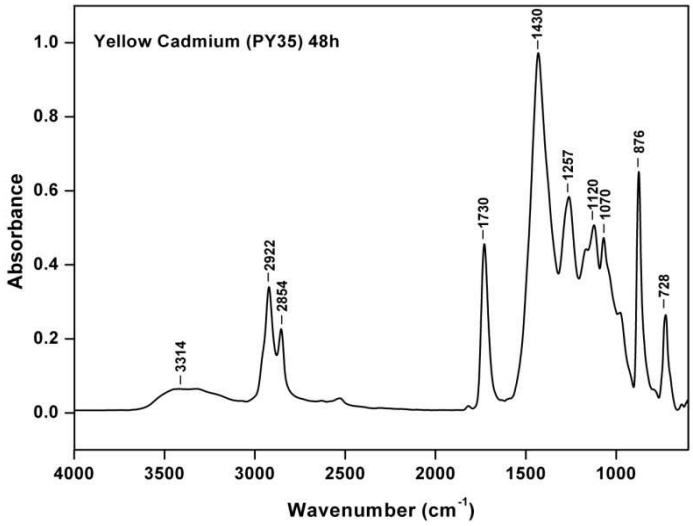

Figure 5.24 ATR-FTIR of Winsor & Newton alkyd colour Yellow cadmium (PY35) unaged (48 h of deposition)

Frequency (cm^{-1})	Assignment	Ref.
728	δ C-H (aromatic)	[14]
876	ν C-O (CO_3^{2-})	[14]
1070	ν C-O	[14]
1120	ν C-O	[14]
1257	ν C-C	[14]
1430	δ CH_2 overlap ν C-O (CO_3^{2-})	[14]
1730	ν C=O	[14]
2854	ν_{as}C-H	[14]
2922	ν_s C-H	[14]
3314	ν O-H	[14]

Table 5.7 FTIR absorption Winsor & Newton alkyd paint color Yellow cadmium (PY35) and vibrational assignment

Fig 5.24 shows, as example, the spectrum of unaged (48h) Yellow cadmium (PY35) sample. The spectrum showed the typical peaks of alkyd resin. The FTIR absorption and relative assignment for the sample Yellow cadmium are showed in Table 5.7.

The signal relative to CO_3^{2-} of filler ($CaMg(CO_3)_2$) was present in all paint samples (except in Viridian green colour). Fig. 5.25 shows the comparison of FTIR spectra of all the alkyd colour sample unaged (after 48 h of deposition) and aged (5600h).

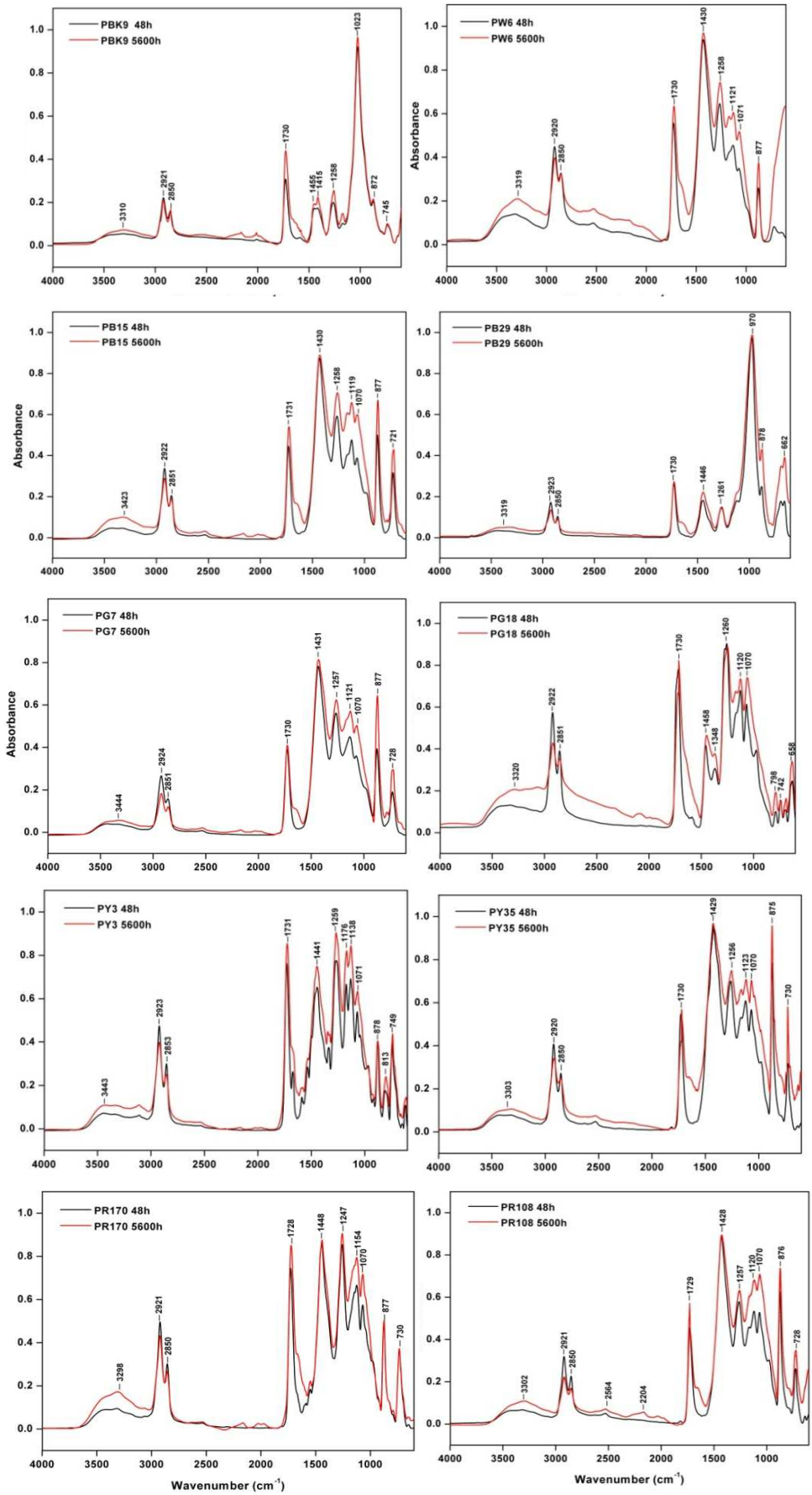

Figure 5.25 ATR-FTIR of Winsor & Newton alkyd colour studied unaged (black line) and aged (red line)

The FTIR difference spectrum (Fig. 5.26) evidences the effects of ageing. With ageing we observed the increase and broadening of the OH groups peak around 3300 cm^{-1} and the increase of the C=O carbonyl stretching peak at 1730 (shoulder, esters), 1707 (carboxylic acids) and 1649 (C=C olefinic stretching band) cm^{-1}. These are due to oxidation reactions taking place during natural ageing with the formation of alcohols and carbonyl species. [15,26] Similar changes are also observed during the ageing of oil paints. [66]

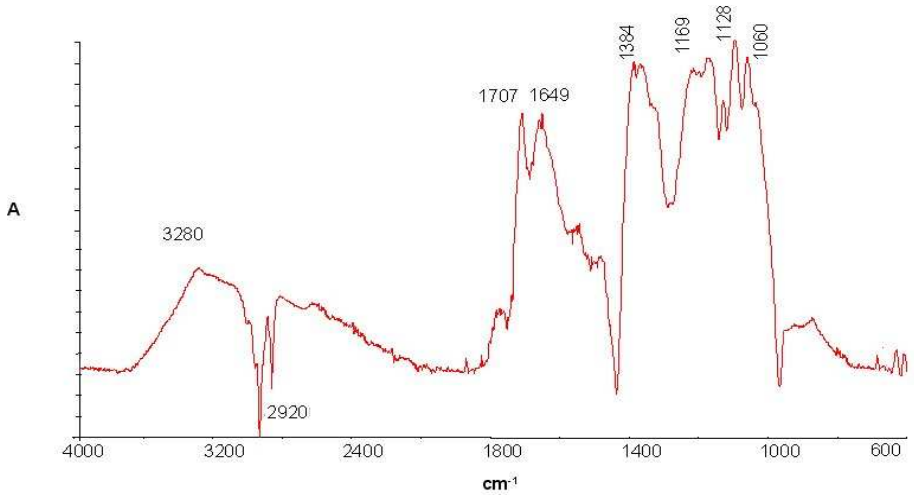

Figure 5.26 Difference spectrum between aged/unaged FTIR spectra of paint replicas Yellow cadmium

An increment of absorbance in the fingerprint region is due to the formation of new C-O and C-C bonds induced by cross-linking occurring during ageing.

A decrease of aliphatic C-H groups (absorptions at 2920, 2855 and 1460 cm^{-1}) were also observed, in agreement with Muizebelt et al. [25] and Perrin et al. [46], due to the termination of the drying process. A low fraction of methylene groups are also susceptible to disappearance through Norrish type I and Norrish type II reactions. [26] .

The Norrish reaction Type I is homolytic cleavage of aldehyde or ketone by photoexcitation to singlet and triplet state leading to the formation of acyl radical and allyl radical. These reactions start with absorption of UV light (230-330 nm) leads the molecule to singlet excited state which is converted to triplet excited state by intersystem crossing. After this step the fragmentation of C-C bond adjacent to C=O group to acyl radical or allyl radical occur. The two different radicals further react to give different products i.e. hydrocarbon (a), ketone (b) and alkene (c). (Fig. 5.27)

The Norrish reaction Type II involves aldehydes and ketones in $n \rightarrow \pi^*$ excited state, followed by an intramolecular *γ*-hydrogen abstraction and fragmentation resulting into diradical which is converted in cyclobutane by ring closure or in enol and alkene by C-C fragmentation. The enol molecules give a carbonyl compound (ketone) by tautomerism. (Fig. 5.28)

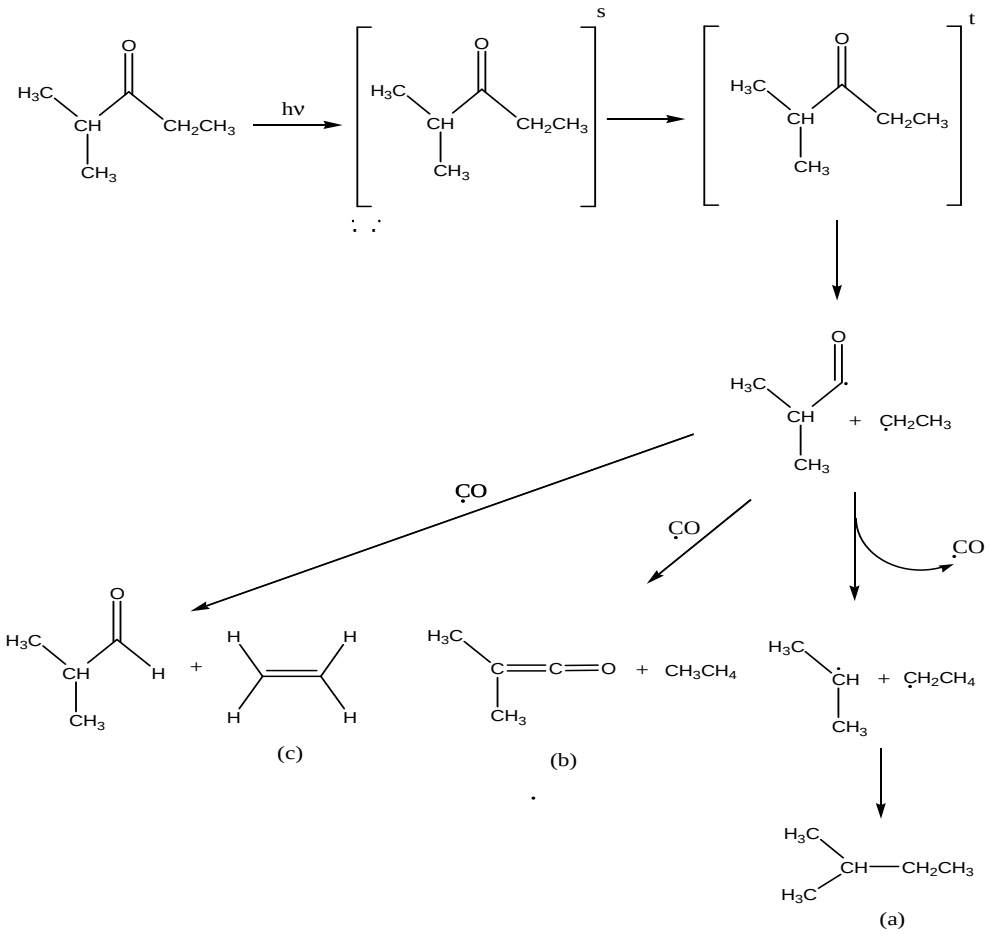

Figure 5.27 Mechanism of the Norrish Reaction Type I, that lead the formation of alkanes, alkenes and carbonyl compounds

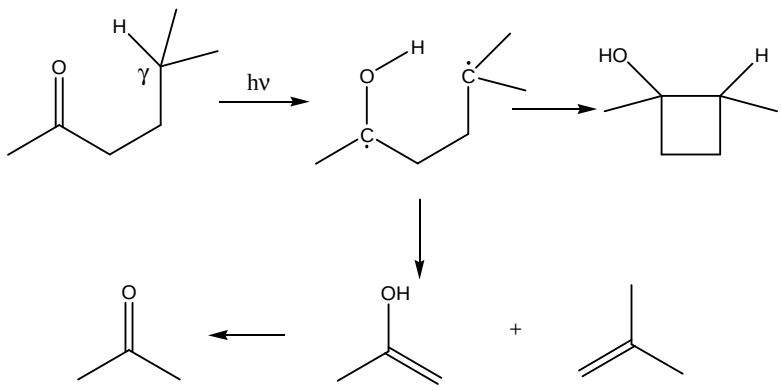

Figure 5.28 Mechanism of the Norrish Reaction Type II, that lead the formation of alkanes and ketones

5.7.3 Ageing with CH_3COOH

After 6 months of ageing all the paint replicas showed white efflorescence on the surface, particularly visible in the Black ivory samples (Fig 5.30). The two phthalocyanine alkyd colors (PB15 and PG7) lost completely pigmentation giving a white residue. This decoloration can be explained by the reaction of acetate with Cu(II) of phthalocyanine pigments that lead the formation of stable copper (II) acetate salts and free phthalocyanine, which are colorless species. [54,55](Fig. 5.29)

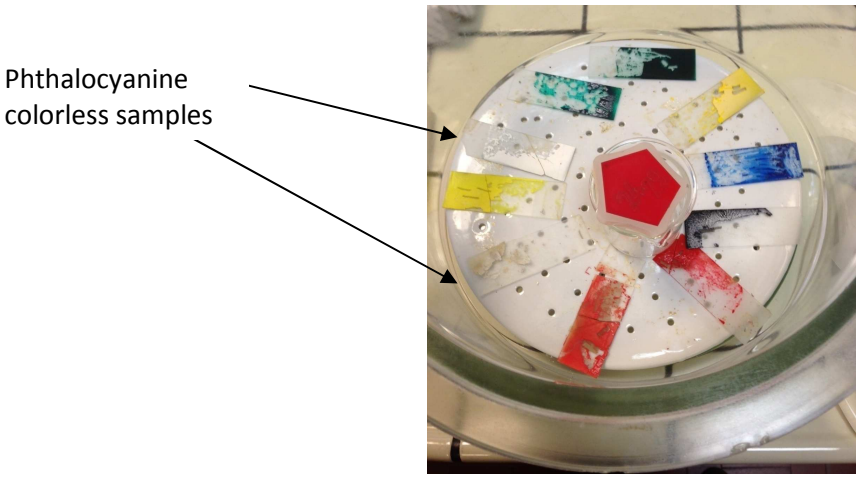

Figure 5.29 Winsor & Newton alkyd samples after acid ageing of six months

Figure 5.30 Winsor & Newton Black Ivory (PBK9) alkyd samples after acid ageing (6 months)

Table 5.8 shows the T_g of unaged, 5600 h naturally aged and artificial acetic acid aged alkyd paint replicas.

Alkyd color	T_g 48h (°C)	T_g 5600 h (°C)	T_g CH_3COOH 6 months(°C)
Black Ivory (PBK9)	61.5	64.8	-
Titanium White (PW6)	59.2	64.8	65.0
Phthalo Blue (PB15)	59.8	64.2	63.6
French Blue (PB29)	56.6	62.9	61.7
Phthalo Green (PG7)	59.2	62.7	62.6
Viridian Green (PG18)	58.2	62.3	62.4
Winsor Lemon(PY3)	58.5	62.4	62.3
Yellow Cadmium (PY35)	59.6	65.4	64.6
Winsor Red (PR170)	58.9	62.3	60.8
Red Cadmium (PR108)	64.2	70.2	69.4

Table 5.8 T_g of the Winsor & Newton alkyd paint films, after deposition (48h), natural ageing of 5600 h and artificial acid ageing (6 months in acetic acid atmosphere)

After 6 months of acid ageing there were little variations in T_g temperatures respect to the values recorded after 5600 h of natural ageing. Black Ivory only does not show any T_g temperature any more.

To better understand the modification occurred in the resin backbone during acid ageing FTIR spectra were collected. Fig. 5.31 shows as an example the FTIR spectrum of phthalocyanine blue color (PB15) after 6 months of ageing with acetic acid.

Changes in the spectrum includes for all the samples studied:

- A broadening and an increase in absorption in the region between 1600-1690 cm^{-1};
- A decrease in absorption in the peaks of phthalate esters (1732 and 1250-1260 cm^{-1});
- A decrease in absorption in C-H stretching (2850-2960 cm^{-1});
- An increase in absorption in the region of O-H stretching (3300-3400 cm^{-1})

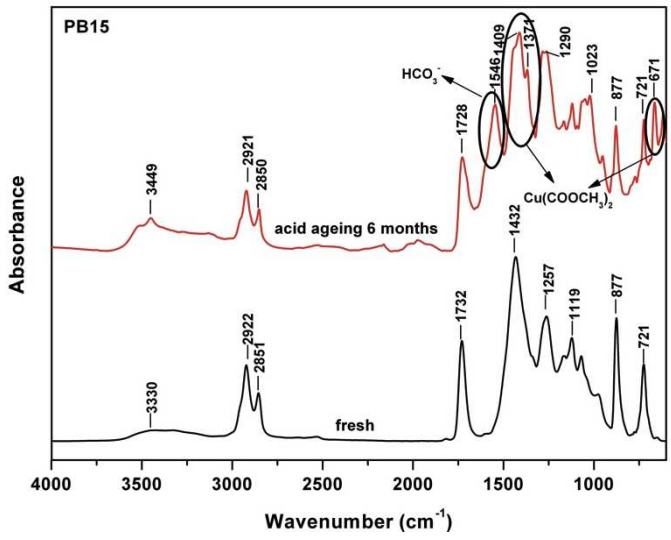

Figure 5.31 ATR-FTIR spectrum of Winsor & Newton alkyd colour Phthalocyanine blue (PB15) after 6 months of acid ageing (red line) overlap with spectrum of un aged sample (48h) (black line)

The spectrum of aged samples showed a decrease in absorption of peaks due to carbonate (peaks at 877 and 1432 cm^{-1}) which corresponding with an increase in absorption of peak due to HCO_3^- (940, 1370 and 1545 cm^{-1}) formed by reaction of dolomite with H^+ ions of acetic acid. The increase in absorption in the range 1600 -1700 cm^{-1} (carbonyl stretching) and in the range 3300-3400 cm^{-1} (OH stretching) can be attributed to the formation of different species like mono-carboxylic acids (hexanoic, heptanoic, nonanoic, dodecanoic or octadecanoic) or di-carboxylic acids (heptanedioic, nonanedioic (Azelaic)). Alkyd resin are polyesters and many works studied acid hydrolysis of polyesters polymer and demonstrated the formation of these species by Py-GC-MS spectrometry and FTIR spectroscopy [59]. The decrease of absorption in C-H stretching (2850-2960 cm^{-1}) and at 1732 cm^{-1} confirmed that a partial depolymerization and hydrolysis of resin occurred with loss of organic volatile species. The ageing with acetic acid promoted the formation of white efflorescences which were due to crystallization of organic salts, such as phthalate, carboxilyc and di-carboxylic acids and inorganic salts (carbonate and bicarbonate) with Mg^{2+} and Ca^{2+} ions from filler.

The spectra of phthalocyanine alky color showed also characteristic absorption due to $Cu(COOCH_3)_2$ (small peak at 661 cm^{-1} and double broad peak at 1371 and 1409 cm^{-1}) due to reaction of Cu(II) ions present in pigments with acetate ions.

5.7.4 Patrizia Zara's paints

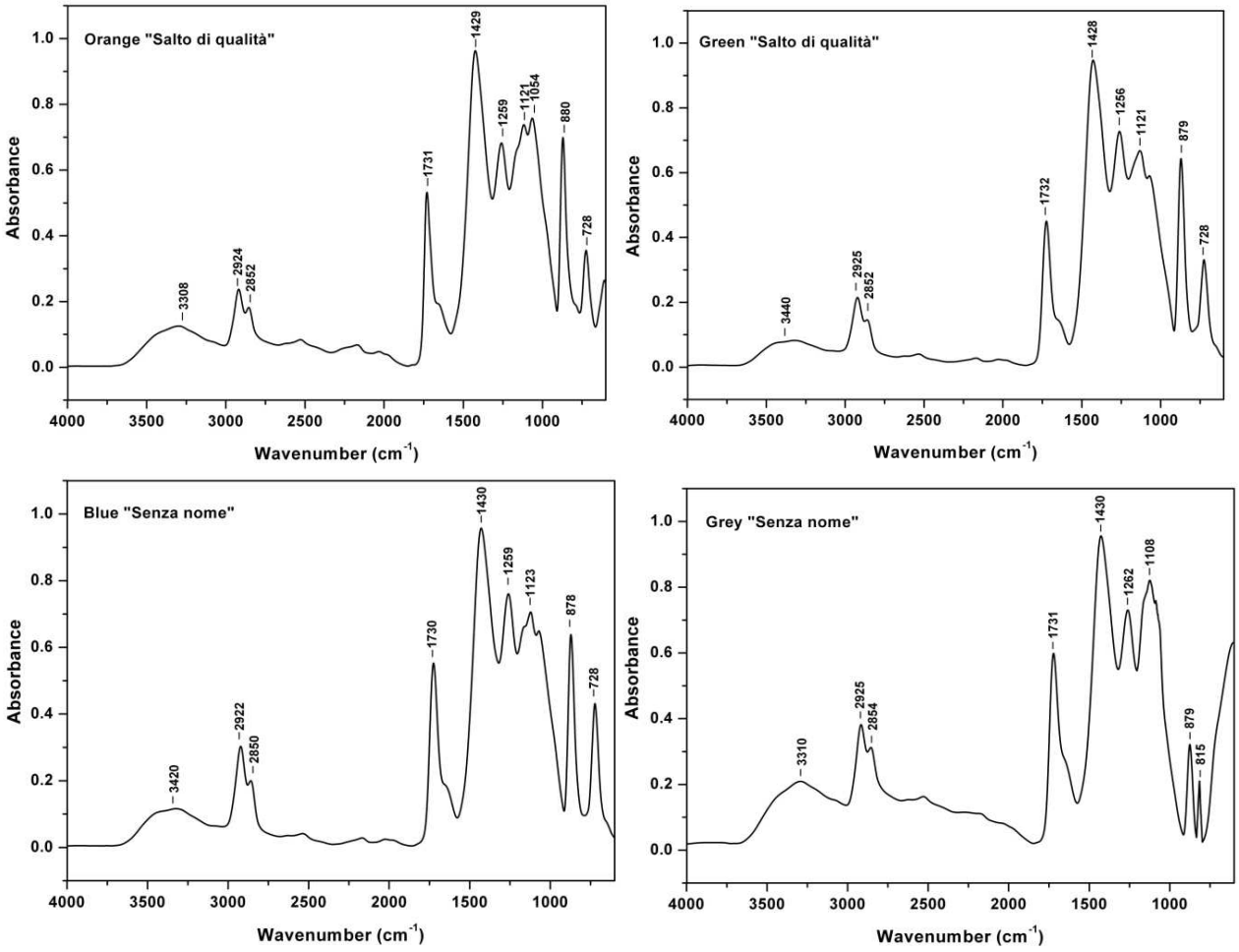

Figure 5.32 FTIR spectra in the range 4000-600 cm^{-1} of four colour used by Patrizia Zara: Orange and Green from *Salto di qualità* (2003), Blue and Grey from *Senza nome* (2007)

The spectra shows typical signal due to alkyd resin: the broad band at 3300-3400 cm^{-1} attributed to OH groups and the two peaks relative to C-H stretching at about 2925 and 2854 cm^{-1} are characteristic of an alkyd or pure drying oil. The carbonyl absorption at 1731 cm^{-1} suggests an alkyd resin (drying oils absorb nearer to 1740 cm^{-1} in this region), an this is confirmed by the strong and characteristically rounded peaks at 1260 and 1120 cm^{-1} due to esters and C-C , C-O stretching .In addition , the alkyd peaks due to C-H aromatic banding is present at 728 cm^{-1}. The band at 876 cm^{-1} is due to stretching C-O of CO_3^{2-} of filler. The small peaks at 2520 cm^{-1} confirm the presence of dolomite.

All the sample shows a typical shoulder and broad absorption in the range 1600 -1700 cm^{-1} (carbonyl stretching) relative to an aged alkyd resin like showed for the alkyd colour paint replicas. (see chapter 3.3.2).

The spectra of samples green and blue are relatively straightforward, in fact are like the same of the paint replicas blue and green phthalocyanine pigments (PB15 and PG7) (see Fig. 5.25)

The spectrum of orange sample is quite similar to the two alkyd paint replicas with inorganic sulphide pigments, PY35 yellow cadmium and PR108 red cadmium (see Fig. 5.24 and 5.25), so the final colour can be obtained by a mixture of both or pure PO20 , Cadmium orange sulphoselenide.

The colour grey of "senza nome" is slightly different from the spectra analyzed before, in fact it shows a strong and broad band with maximum at about 1108 cm^{-1} and a peak at 815 cm^{-1}, which can attributed to a Si-O bond and high absorption band below 700 cm^{-1} which is relative to TiO_2 pigment (see PW6 spectrum in Fig. 5.25). This suggest that the colour is present an inorganic pigment, in particular powdered slate, a grey pigment composed by a mixture of oxides (SiO_2 and TiO_2 and traces of Al_2O_3, MgO and CaO) which often is added to a Carbon Black (PBK19) to get the desired shade of gray . The identification of pure Carbon Black is difficult whit a single FTIR analysis because its absorption is overlap to the absorption of alkyd polymer.

The T_g of the samples were measured by DSC, and the results are showed in table 5.8 .

Paint sample colour	**T_g (°C)**
Orange "*Salto di qualità*"	64.2
Green "*Salto di qualità*"	65.4
Blue "*Senza nome*"	64.8
Grey "*senza nome*"	65.5

Table 5.8 T_g temperatures measured by DSC of the colour studied from the Patrizia Zara works

The T_g temperatures are very similar to the T_g values of the paint replicas naturally aged 5600 h (8 months). (see Table 5.6)

After the end of chemical drying (auto-oxidation) no significant modifications occur in older samples aged respectively 6 (*Salto di qualità*) and 10 years (*Senza nome*) like shown in the ATR-FTIR spectra and DSC values of T_g temperatures.

5.8 Conclusions

The study of alkyd paint colours combined thermal and spectroscopic techniques for the characterisation of changes occuring during the natural ageing of alkyd resins. TGA showed an increase of film network density due to ageing, which was likely caused by (I) reactions of cross-linking occurring during auto-oxidation processes, (II) a lower content of the organic component in the film due to the loss of volatile low molecular mass degradation products such as carboxylic acids, alcohol, aldehydes or ketones.

Auto-oxidation and cross-linking of the aged samples were followed using DSC by monitoring the exothermic peak associated with the degradation of the peroxides in the film. It was shown that after 5600 h of natural ageing, the auto-oxidative cross-linking reactions via peroxide decomposition were mostly finished. Although dry to the touch within one day, the alkyd paints studied still required some time before the oxidation processes occurred and before developing and completing a stable film network.

The trends of the normalized areas during ageing from 48 to 5600 h were practically the same for all the paints, thus demonstrating that the number of peroxides formed, broken and radicals recombined were independent on the nature of the pigment's colour (organic or inorganic) and only dependent on the number of double bonds in the starting material. The equation (1) nicely fit the normalized areas of all the paints during ageing from 48 to 5600 h. It can also be employed to estimate the oil content of a *Winsor & Newton series Griffin- fast drying* alkyd paint of unknown composition from the area of the peroxide decomposition peak and the ageing time, provided that the latter is less than 5600h.

Winsor & Newton, *series Griffin- Fast drying oil colour* showed ageing after 8 months, similar to the 10-years old Winsor & Newton alkyd colour (without drier) studied in a previous work by Chiantore et.al . If the presence of the drier increases the speed of drying and curing of the resins, it also accelerates their speed of degradation and ageing.

FTIR data confirmed the formation of new bonds during chemical drying, such as methylene ether and ester linkages and the formation of new carboxylic species.

This is the first study which has been carried out on these "new", fast-drying paint formulations employed in contemporary art.

Ageing with acetic acid promoted the formation of white efflorescences, which were due to the crystallisation of organic species, such as phthalate, carboxilyc (hexanoic, heptanoic, nonanoic, dodecanoic or octadecanoic) or di-carboxylic acids (heptanedioic, nonanedioic (Azelaic)). These results, with the support of FTIR analysis, confirmed that a partial hydrolysis of resins occurred.

The two phthalocyanine pigments seem to be more susceptible to acid ageing due to the abstraction of Cu(II) metal centre of pigments which results in the loss of dye properties.

Studies on Patrizia Zara's painting allow us to better understand the resin modifications occurring in authentic art works many years after being carried out. We can assert that this kind of new alkyd colours are stable over a period of ten years.

References

[1] Blegen JR, Fuller WR. *Alkyd resins: unit five.* Book, Federation series of organic coatings,(1967) Philadelphia , PA;

[2] Ploeger R, Scalarone D, Chiantore O . *The characterization of commercial artists' alkyd paints.* J of Cult Herit (2008) 9, 412-419;

[3] Oldring P. *Resins for surface coatings.* Book, SITA Technology,(1987) London;

[4] Patton TC. *Alkyd resin technology: formulating techniques and allied calculations.* Interscience Publishers,(1962) New York-London;

[5] Kask T, Leset F. *Processes and equipment for alkyd and unsaturated polyester resin manufacture.* Prog Org Coatings (1991) 19, 283-331;

[6] Von Fisher W. *Paint and varnish technology.* Book, chapter 9,(1988) Reinhold Publishing Co., New York;

[7] Holmberg K. *High solids alkyd resins.* Marcel Dekker Inc,(1987) New York;

[8] Daniel JH, Jonh C. *Modified alkyd resins with styrene and acrylonitrile.*(1952) US Patent 2600623;

[9] Clark MD, Helmer BJ. *Acrylic modified waterborne alkyd dispersion.*(2001) US Patent 6242528B1;

[10] Noble KL. *Waterborne polyurethanes.* Prog Org Coatings (1997) 32, 131-136;

[11] Bussell GW. *Epoxy modified water soluble.* (1962) US Patent 3027341;

[12] Gauthier LA, Legrow GE. *Silicone-alkyd resins and methods for their preparation.* (1983) European Patent EP0075326A1;

[13] Foley MJ, Graham T. *Solvent-based alkyd paints.* European Patent (1994) EP0341916 B1;

[14] Clark M, Boon J.*Molart, a multidisciplinary priority project on molecular aspects af ageing in painted works of art.* Report;(2002)

[15] Ploeger R, Chiantore O, Scalarone D. *Thermal analytical study of the oxidative stability of artists' alkyd paints.* Pol degrad and Stab (2009) 94, 2036-2041;

[16] Lundberg WO, Scofield F, Greenwald FM . *Panel discussion on mechanism of drier action.* Industr and Engin Chem (1954) 46, 570-572;

[17] Basu SK, Scriven LE, Francis LF. *Mechanism of wrinckle formation in curing coatings.* Prog Org Coat (2005) 53, 1-16;

[18] Laven J, Uravind UK . *The chemical drying process in alkyd emulsion paint films.* Athens conference on coatings science and technology;(2003)

[19] Marton B . *A depth-resolved look at the film formation and properties of alkyd-based coatings.*(2004) PhD thesis, University of Twente;

[20] Wise JK. *Introduction. Mechanism of drier action.* Ind and Eng Chem(1954) 46, 562;

[21] Mueller ER. *Proposal mechanism of drier action. Ind and Eng Chem* (1954) *46, 562-569;*

[22] Bieleman JH. *Additives for coatings.* Wiley-VCH. Weinheim(2000)

[23] Porter NA. *Mechanism for the autoxidation of polyunsaturated lipids.* Acc Chem Research (1986) 19, 262-268;

[24] Oyman ZO, Ming W. *Oxidation of drying oils containing non-conjugated and conjugated double bonds catalyzed by a cobalt catalyst.* Prog in Org Coat (2005) 54, 198-204;

[25] Muizebelt WJ, Nielen WF, Hussem JB, Zabel KH. *Oxidative cross-linking of alkyd resin studied with mass spectrometry and NMR using model compounds.* J of Coat and Tech(1998) 70, 83-93;

[26] Ploeger R, Scalarone D, Chiantore O. *The characterization of commercial artists' alkyd paints.* J of Cult Herit (2008) 9, 412-419;

[27] Denisov ET, Emanuel NM. *Polynuclear complexes of carboxylate ligands.* Russ Chem Rev (1960) 29, 645-653;

[28] Lombard L, Rommert L. Bull Soc Chim France 36(1956) ;

[29] Schaich KM. *Metals and lipid oxidation . contemporary issue.* Lipids (1992) 27, 209-214;

[30] Middlemiss RG, Olszanski DJ. *New catalysts for high-solids coatings.* Am Paint Coat J (1993) 78, 35-46;

[31] Bellettiere SJ, Mahoney DM. *Multi-metallic complexes: the next generation of driers.* J Coat Tech (1987) 59, 101-110;

[32] Ali M, McWhinnie WR. *Organobismuth (III) and (V) carboxylates and their evaluation as paint driers.* App Organomet Chem (1993) 7, 137-145;

[33] Landau M, Bellettiere SJ. *Accelerator system for the peroxide-catalized curing of unsaturated polyester resin*. (1979) US Patent 4175064;

[34] Stamakatis G, Knuutinen U. *Analysis and aging of unsaturated polyester resins in contemporary art installations by NMR spectroscopy.* Anal Bioanal Chem (2010) 398, 3203-3214;

[35] Phenix A. *The swelling of artists' paints in organic solvents.* J Am Inst Conserv(2002) 41, 61-90;

[36] Stava V, Vesely D, Kalenda P. *Catalytic effects of transitoon metals in the form of the salts of arganic acids in the crosslinking of alkyds.* Pigm Resin Tech (2008) 37, 67-72;

[37] Ouldmetidji Y, Gonon L, Commereuc S. *A differential scanning calorimetry method to study polymer photoperoxidation.* Polym Test (2001) 20, 765768;

[38]Wei S, Pintus V, Schreiner M. *A comparison study of alkyd resin used in art works by Py-GC/MS and GC/MS: the influence of aging.* J Anal Appl Py (2013) 104, 441-447;

[39] Colombini MP, Modugno F, La Nasa J. *Alkyd paints in art: characterization using integrated mass spectrometry.* Anal Chim Acta (2013) 797, 64-80;

[40] Ye G, Courtecuisse F, Allonas X, Ley C. *Photoassisted oxypolimerization of alkyd resins: kinetics and mechanism.* Prog Org Coat (2012) 73, 366-373;

[41] Cakic SM, Ristic IS, Vladislav JM, Stamenkovic JV. *IR-change and colour change of long-oil air drying alkyd paints as a results of UV irradiation*. Prog Org Coat (2012) 73, 401-408;

[42] Chittavanach P, Miller K, Soucek MD. *A photo-curing study of a pigmented UV-curable alkyd.* Prog Org Coat (2012) 73, 390-400;

[43] Ploeger R, Musso S, Chiantore O. *Contact angle measurements to determine the rate of surface oxidation of artists' alkyd paints during accelerated photo-ageing.* Prog Org Coat (2009) 65, 77-83;

[44] Bartolozzi G, Marchiafava V, Mirabello V, Picollo M. *Chemical curing in alkyd paints: an evaluation via FTIR and NMR spectroscopies.* Spectrochim Acta (2014) 118, 520-525;

[45] Cakic SM, Ristic IS, Vladislav JM. *IR-change and colour changes of long-oil air drying alkyd paints as a results of UV irradiation* . Prog Org Coat (2012) 73, 401-408;

[46]Perrin FX, Irigoyen M. *Artificial aging of alkyd paints: a micro-ATR spectroscopic study.* Pol Degrad and Stab (2000) 70, 469-475;

[47] Domenech-Carbò T, Bitossi G, silva MF. *Study of ageing of ketone resins used as picture varnishes by FTIR spectroscopy, UV-Vis spectrometry, ATM and scanning electron microscopy X-Ray microanalysis.* Anal Bioanal Chem (2008) 391, 1351-1359;

[48] Marengo E, Liparota MC, Robotti E. *Monitorin of paintings under exposure to UV light by ATR-FTIR spectroscopy and multivatiate control charts.* Vibrat Spectr (2006) 40, 225-234;

[49] Cruz AJ, Pires J, Brotas M. *Comparison of adsorbent materials for acetic acid removsl in showcases.* J of Cult Herit (2008) 9, 244-252;

[50] Sharma VC, Lal US, Singh T. *Method for stabilization of leaded bronzes affected by corrosion of lead.* Stud Conserv (2003) 48, 203-209;

[51] Dubus M, Aucouturier M, Colinart S. *Evaluation de la corrosion du plomb aux archives nationales de France.* 13th meeting Rio de Janeiro(2002) 22-27 Sept 2012;

[52] Degrigny C, Le Gall R. *Facies de corrosion developpes sur des poids en plomb du musee du CNAM du Paris.*(1996) J Brigland Ed;

[53] Healt D, Martin G. *The corrosion of leads an tin alloys occurring on Japanese lacquer objects.*(1988) Kyoto Congress, 19-23 sept 1988;

[54] Thickett D, Lee L. *Assessment of the risks to metal artifacts posed by volatile carbonyl pollutants.* Science Publ ltd . (1998) London 260-264;

[55] Tetreault J, Vano E, Scott DA. *Corrosion of copper and lead by formaldehyde, formic abd acetic acid vapours.* Stud Conserv (2003) 48, 237-250;

[56] Dupont AL. *Cellulose degradation in an acetic acid environment.* Stud Conserv (2000) 45, 201-210;

[57] Tennent NH, Baird T. *The deterioration of Mollusca collections: identification of shell efflorescence.* Stud Conserv (1985) 30, 73-85

[58] Brokherof AW. *Deterioration of calcareous materials by acetic acid vapour.* J Brigland Ed. (1996) 769-775;

[59] Rethy ES, Szmercsanyi IV. *Investigations on acid hydrolysis of polyesters.* Chem Zvesti (1971) 26, 390-396;

[60] Campanelli JR, Kamal MR. *A kinetic study of the hydrolitic degradation of polyethylene terephthalate at high temperatures.* J Appl Pol Sc(2003) 48, 443-451;

[61] Kontozova V, Godoi R. *Characterization of air pollutants in museum showcases.* G Mermann Ed. (2002) Proceedings of art 2002;

[62] Nolan NT, Seery MK, Pillai SC. *Spectroscopic investigation of the anatase-to-rutile transformation of sol-gel synthesized TiO_2 photocatalysts.* J Phys Chem (2009) 20, 65-73;

[63] Ye G, Courtecuisse F, Allonas X, Raja P. *Photoassisted oxypolimerization of alkyd resin: Kinetics and mechanism.* Prog in Org Coat (2012) 73, 366-373;

[64] Mallegol J, Gonon L, Verney V. *Thermal (DSC) and chemical (iodometric titration) methods for peroxides measurements in order to monitoring drying of alkyd resin.* Prog Org Coat (2001) 41, 171-176;

[65] Learner TJS. *Exthenders in modern paints, analysis by FTIR and pyrolysis GC-MS spectrometry.* (2004) Research in conservation, Getty publications.

[66] Lazzari M, Chiantore O. *Drying and oxidative degradation of linseed oil.* Pol Degrad and Stab (1999) 65, 303-313;

6 Analysis of silane and siloxanes as coatings

6.1 Introduction

As water penetration is the most destructive agent to walls, the decrease in the water uptake is a very important feature. Effective masonry paints reduce water absorption by more than 70% without noticeably lowering the water vapor permeability of the impregnated substrate. [1] The water repellency of a surface is obtained by adding powdered or aqueous silicone to the mixture of paint and building materials [1] or by treating the painted surface with solvent containing silicones, silanes or silicoxanes. [2] Silicon occupies a hybrid position between inorganic and organic polymers corresponding to a quartz structure modified with organic groups.

Possessing both organic and inorganic properties, silicones react with the polymeric and mineral components of the surface, forming durable covalent bonds across the interface. [1,2] It has been demonstrated that these bonds are hydrolysable, but they can reform easily resulting in improved coating adhesion and surface durability [1-3] Organosilicon compounds have found many applications as restoring and conserving agents of buildings and monuments [1-5] The most commonly used products are monomers, oligomers and preformed polymers. Their handling and penetration properties are largely determined by the solvent and the different condensation degrees. Some organosilicon compounds exhibit their protecting and dirt repelling effects after crosslinking *in situ*. [2,3]

This thesis concerns the characterization of two alkoxy-silanes/siloxanes named Disboxan 450 (purchased by Caparol) and Hydrophase (purchased by Phase Restauro) used as protective coatings.

Hydrophase is a ready to use monomeric coating agent, with no film-forming properties and a molecular size comparable with water molecules (5-10 Å). Hydrophase penetrates deep down in the wall precluding the absorption of water, the damage of ice formation and the corrosion due to pollutants and acid rain. Differently, Disboxan 450 is composed by micro-emulsion of oligomeric alkyl alkoxysilane. Giving that its higher molecular size, Disboxan 450 does not penetrate deep down in the support and its interaction with the substrate is mainly on the surface.

Hydrophase and Disboxan 450 are both alkyl silicon compounds but their chemical formulas are unknown because they are protected by patents. The general formula of an alkoxy siloxane (or silane) is $R_nSiX_{(4-n)}$, where R is a non hydrolysable organic moiety that can be either an alkyl, aromatic, organofunctional, or a combination of any of these groups, while X represents alkoxy moieties, most tipically methoxy or ethoxy, which react with hydroxyl groups and liberate methanol or ethanol. The alkoxy groups of siloxanes provide the linkage with inorganic substrates to improve coatings integrity and adhesion. They react with hydroxyl functionalized surfaces with a four steps reaction as reported in literature [3] and schematized in Fig. 6.1.

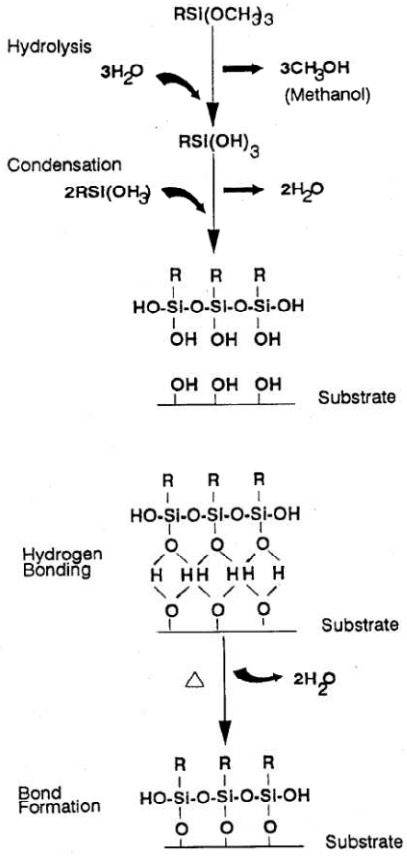

Figure 6.1 Reaction process of alkoxy siloxanes

First, the hydrolysis of two methoxy groups leads to the siloxane oligomerisation. Then the hydrolysis of last methoxy group leads to the formation of a silanolic group that finally reacts with the substrate during drying or curing thus forming a covalent bond with the substrate toghether with water release. At the interface, only one bond for each silicon of the organosilane is formed. The most straightforward method of silylating a surface with a silane is from an alcohol solution (methanol , ethanol or like in Hydrophase isopropanol) and the solution can be wiped, dipped or sprayed onto the surface. After the surface dries, excess material can be gently wiped, or briefly (alcohol) rinsed off. [2-4]

Although polysiloxanes are used as protective coatings for a variety of specialized applications [3-5], degradation processes appear when they are used for long time in outdoor conditions. Israeli and co-workers focused on the photoreactivity of the main substituent groups used in the silicone field. Photo-oxidation of PDMS (poly-dimethyl-siloxanes) oils with various content of hydride SiH, vinyl, dimethylene, methane, MePh and MePh2 groups have been studied. [6,7]T. H. Thomas et.al. studied the molecular weight and molecular weight distribution changes taking place during isothermal depolymerization of PDMS. [8] Grassie and co-workers reported on the thermal stability of siloxanes to 300°C under vacuum. [9] Deshpande and Rezac showed that the cyclic oligomers hexamethyltrisilozane and octamethyltetrasiloxane are the main decomposition products of vinyl siloxanes after thermal degradation under inert atmosphere .[10] Camino et.al studied the thermal degradations of PDMS by using TG-FTIR. [11,12]. The products of

the thermal degradation are essentially determined by the temperature and the heating rate [12]. As the heating rate increases, the PDMS thermal volatilization becomes dominated by the rate of diffusion and evaporation of oligomers produced on its decomposition [11]. Tomer et.al characterized the thermal degradation profile and the volatile products evolved during thermal degradation of different polysiloxanes by using TG-FTIR [13]. In the same work the photo-ageing of the different polysiloxanes is investigated by means of photo-DSC. This tecnique measure the changes in thermal transitions of a material, taking place upon photo-ageing directly in DSC furnace.

In this work, Hydrophase and Disboxan 450 were studied both unaged and after two years of natural outdoor ageing. This study was carried out in the framework of COPAC project, concerning the characterisation of materials used in modern and contemporary art. COPAC project also provided the cleaning and restoring of the acrylic wall painting "Tuttomondo" painted in 1989 by Keith Haring on the Church wall of St. Antonio in Pisa (Fig. 6.2). The aim of this study was to find out the best preservative agent. The interaction of Disboxan 450 and Hydrophase with Caparol acrylic colour was investigated together with their stability over time. In particular, Hydrophase was used as a coating for Caparol acrylic Yellow and Disboxan 450 as one for Caparol acrylic Blue in paint replicas. The paint films were systematically examined after drying using DSC, TGA and FTIR spectroscopy before and after two years of outdoor natural ageing.

Figure 6.2 Keith Haring "*Tuttomondo"*, 1989 St. Antonio Church, Pisa

6.2 Results and discussion

6.2.1 Thermoanalysis of alkyl silanes and siloxanes

The thermal degradation of Hydrophase and Disboxan 450 pure and applied on the surface of acrylic paint replicas was studied by TG and DSC. The TG curves and the corresponding derivative curves recorded under nitrogen and air flow of Hydrophase and Disboxan 450 are reported in Fig. 6.3 (nitrogen) and 6.4 (air) respectively, whereas the corresponding DSC curves under air flow are shown in figure 6.5. The temperatures of their mass losses under air and nitrogen flow and the mass loss percent are reported in Table 6.1 .

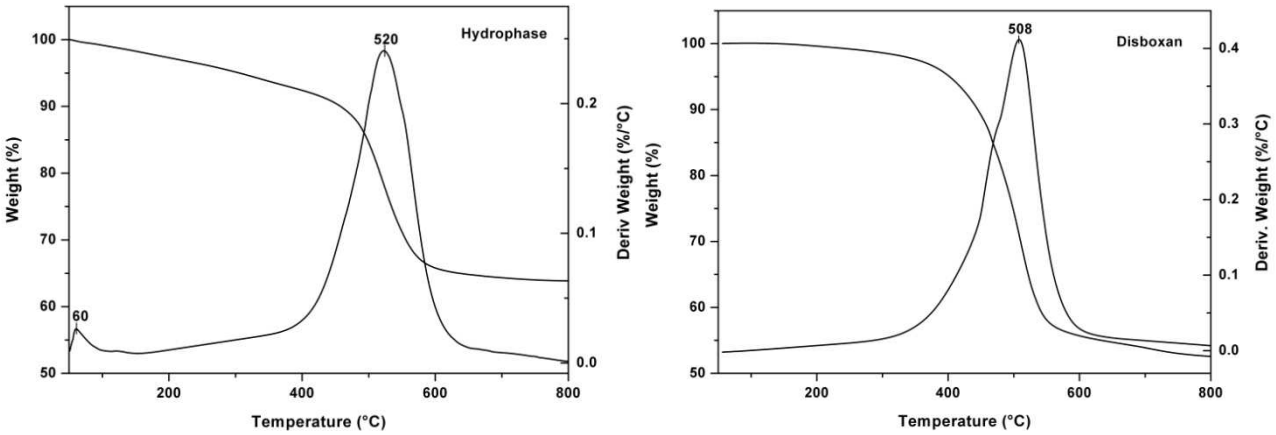

Figure 6.3 TG curve and its derivative of Hydrophase (left) and Disboxan 450 (right), performed under nitrogen flow at 10°C/min heating rate.

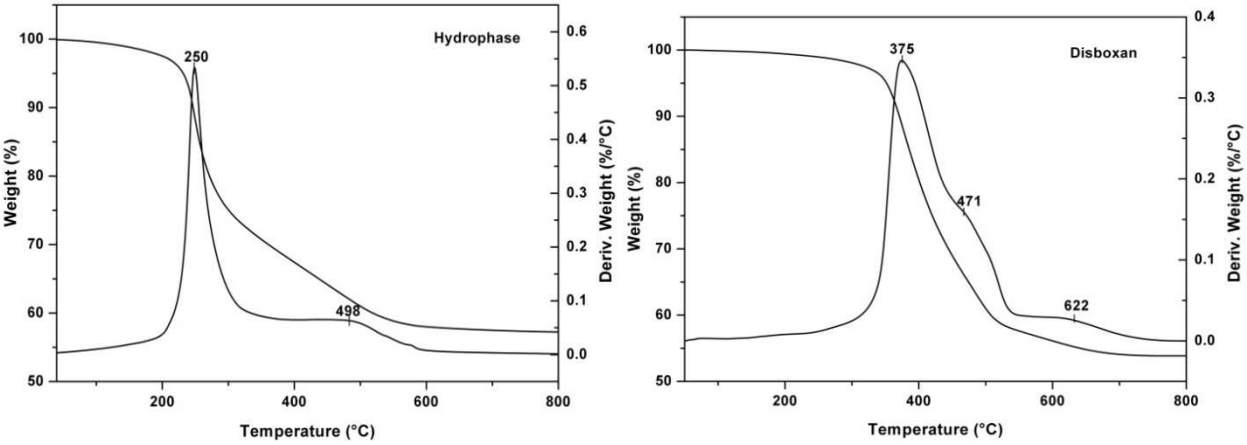

Figure 6.4 TG curve and its derivative of Hydrophase (left) and Disboxan 450 (right), performed under air flow at 10°C/min heating rate.

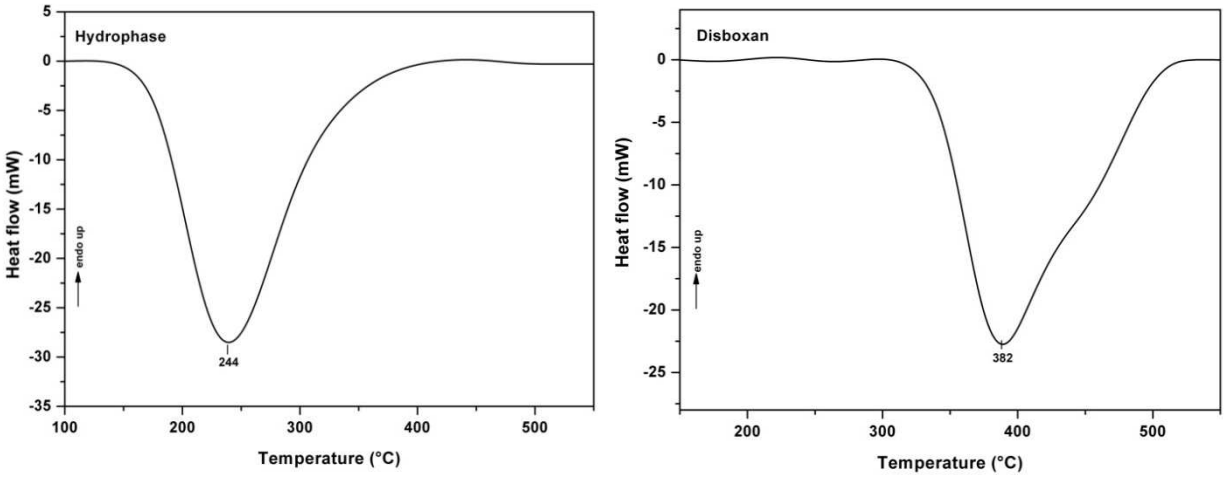

Figure 6.5 DSC curve under air flow of alkoxysiloxanes studied, Hydrophase (left) and Disboxan 450 (right) at 10°C/min heating rate

The thermo-oxidative stability of Hydrophase and Disboxan 450 is different according to their monomeric and oligomeric nature. Hydrophase is less thermo stable than Disboxan and it shows a main mass loss at 225°C corresponding to an exotermic peak in DSC. Differently, Disboxan 450 degradates with a main broad mass loss with a maximum at 375°C and a shoulder at 470°C to whom corresponds an exothermic effect. The TG curves in nitrogen show that Hydrophase and Disboxan 450 pyrolise with a single mass loss at 508 °C and 520°C , respectively. (Fig. 6.3)

N° step	Hydrophase air	Hydrophase nitrogen	Disboxan 450 air	Disboxan 450 nitrogen
1	-	60°C (1%)	-	-
2	250°C (33%)	-	-	-
3	-	-	375°C (38.8%)	-
4	498°C (10%)	-	471°C (shoulder)	-
5	-	520°C (35.4)	-	509°C (46.5%)
6	-	-	622°C (7.6%)	-
Residual mass	57%	63.6 %	53.6 %	53.5 %

Table 6.1 Experimental temperature and mass loss percent of thermal degradation steps in air and nitrogen of siloxanes coatings

Note that the residual masses of Hydrophase and Disboxan 450 at 900°C obtained both under air and nitrogen flow are very high and similar to each other. Whatever the molecular formula of the siloxanes in the starting material, the product recovered after heating up to 900°C under air is SiO_2. Nevertheless, SiO_2 can also be the residual product al 900°C of the pyrolysis of

siloxanes. The IR spectra of the volatile products evolved during both pyrolysis and sample oxidation of Hydrophase and Disboxan 450 by means of TG-FTIR are reported in Fig 6.6-6-8.

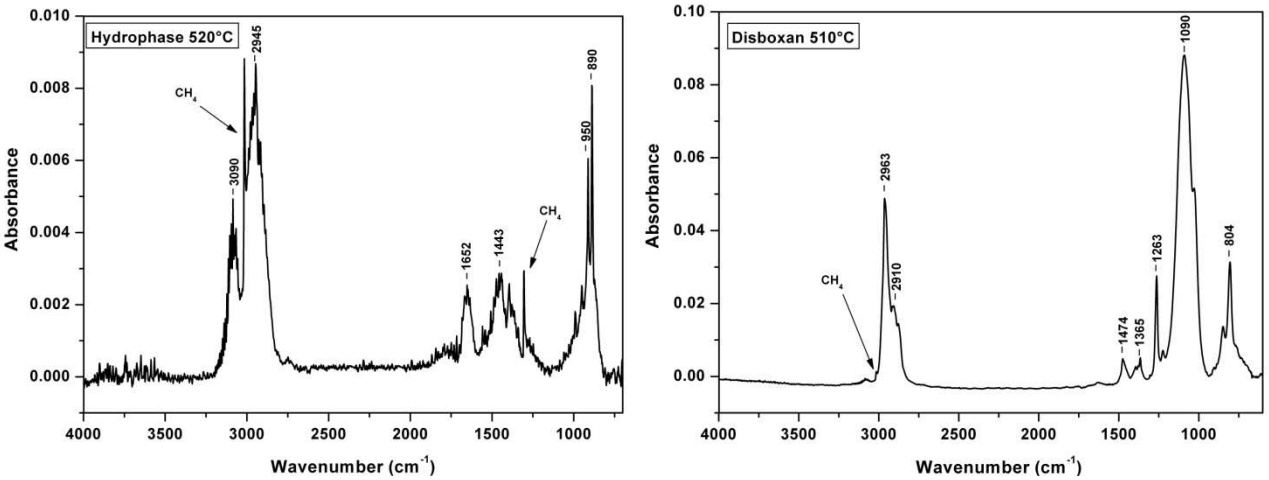

Figure 6.6 FTIR spectrum of volatile products during TGA of Hydrophase (left) (520°C) Disboxan 450 (right)(510°C) in nitrogen flow at 20°C/min heating rate

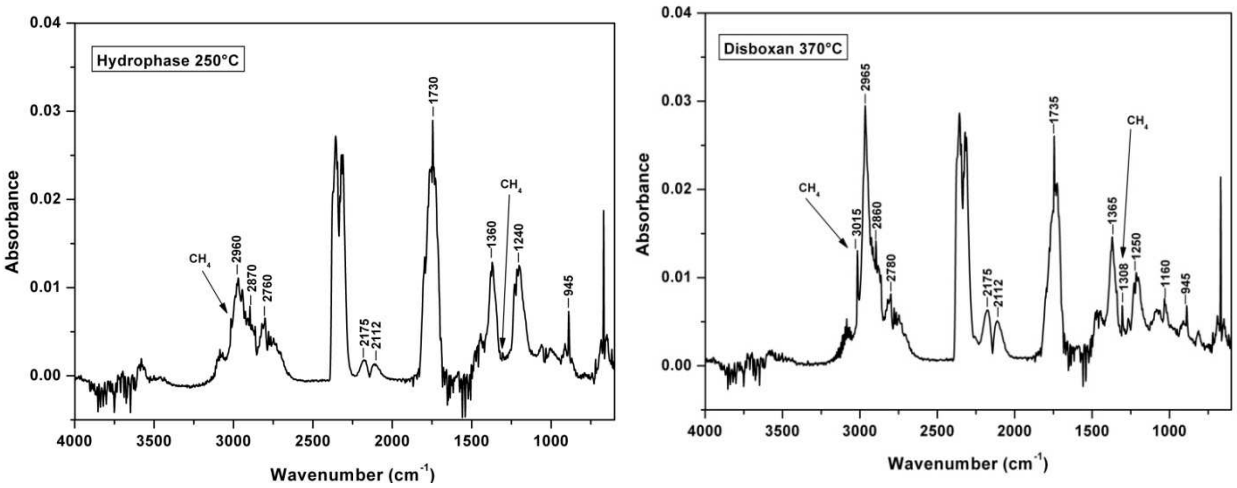

Figure 6.7 FTIR spectra of volatile products during TGA of Hydrophase at 250°C (left) and Disboxan 450 at 370°C (right) under air flow at 20°C/min heating rate

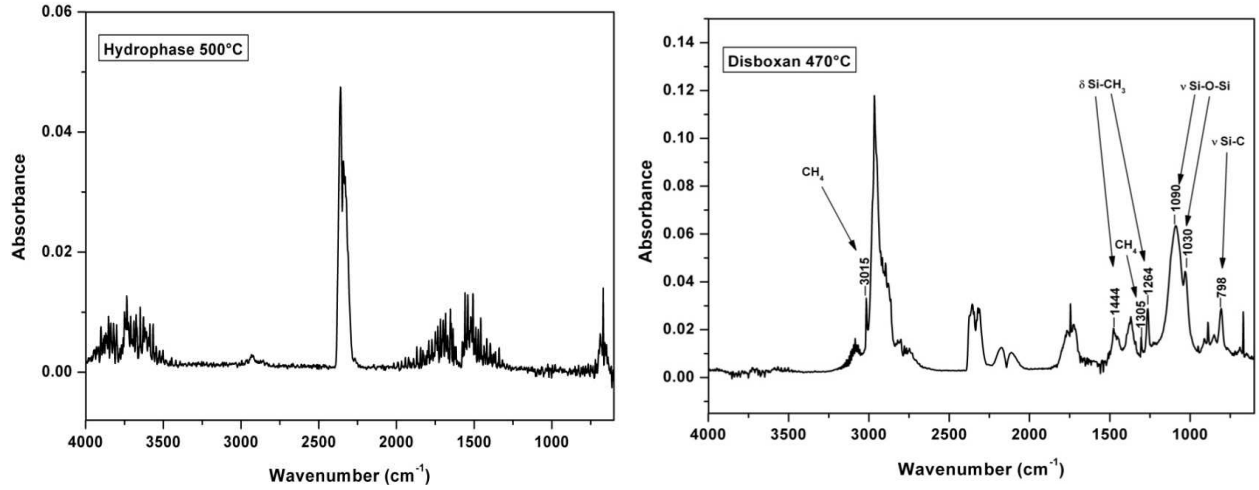

Figure 6.8 FTIR spectrum of volatile products during TGA of Hydrophase at 500°C (left) and Disboxan 450 at 470°C (right) in air flow at 20°C/heating rate

The spectrum of the volatiles evolved under nitrogen flow of Hydrophase at 520°C (Fig 6.6 (left)) shows the presence of CH_4, indicative of homolitic Si-CH_3 bonds scission followed by H abstraction [12], and of hydrocarburic compounds only. The corresponding spectrum for Disboxan 450 at 510°C (Fig. 6.6 (right)) shows IR peaks ascribable to oligomers of silanes (four bands between 810 and 1260 cm^{-1}), according to [13], together with CH_4.

The spectrum of the volatiles evolved under air flow during the mass loss at about 250°C for Hydrophase and at 370°C for Disboxan 450 (Fig. 6.7) indicates for each sample the formation of CH_4 (3015 and 1304 cm^{-1}), formaldehyde (1730, 2785, 2870, 1250 and 1160 cm^{-1}), acetaldehyde (614, 945, 1360, 1730, 2760 and 2850 cm^{-1}) (assigned with the Varian Library), carbon dioxide (2330-2360 and 684 cm^{-1}), carbon monoxide (2112 and 2175 cm^{-1}). Above 300°C, the thermo oxidative degradation of Hydrophase produces carbon dioxide and water only, while Disboxan 450 (see Fig. 6.8 (right)) shows also FTIR peaks ascribable to oligomers of silanes (four bands between 810 and 1260 cm^{-1}).

To sum up, both Hydrophase and Disboxan 450 thermal decompositions under nitrogen and under air produce methane, short chain aliphatic compounds and compounds obtained by oxidation of methane or reaction between CH_3 and CO. Oligomers of silanes are present only in the decomposition pathway of Disboxan that is very similar to that of PDMS [12,13].

On this basis we can hypothesize that the most probable components of Disboxan 450 are oligomers of dimethilsiloxane. A monomeric compound such as R_3SiOH, with R short alky chain, can be hypothesized for Hydrophase.

Taking into consideration Trimethylsilanol as the simplest constituent monomer, stoichiometry considerations lead to calculate a SiO_2 residual of 55.5% with respect to the initial quantity, very close to the observed residual under air flow and close enough also to the residual under nitrogen. The residual of Disboxan 450 under nitrogen is slightly lower than that of Hydrophase, due to the partial degradation of the silicones into volatile organo-silicon compounds.

The study of these two products is important to evaluate which one is the best product to be applied as coating agent on the acrylic wall painting “Tuttomondo” painted by Keith Haring on an external wall of the S. Antonio Church in Pisa. Paint replicas were prepared by applying on the wall surface miming material Capatec Putz, a layer of Caparol acrylic colour and on the top a layer of silicone coating. In particular Hydrophase was applied on a layer of Caparol Yellow and Disboxan 450 on Caparol Blue. It must be noted that the Disboxan 450 coating changed the appearance of blue paint replicas, that became more shiny and smooth to the touch. The paint replicas were analyzed before and after two years on natural outdoor ageing.

Fig. 6.9 and Fig 6.10 compares the TG curves and the corresponding derivative curves recorded under air flow and the DSC curves under air flow, of Caparol Yellow and Blue paint reconstructions with and without siloxane coatings. The experimental temperatures and the percentage mass loss of the corresponding thermal degradation steps are reported in Table 6.2.

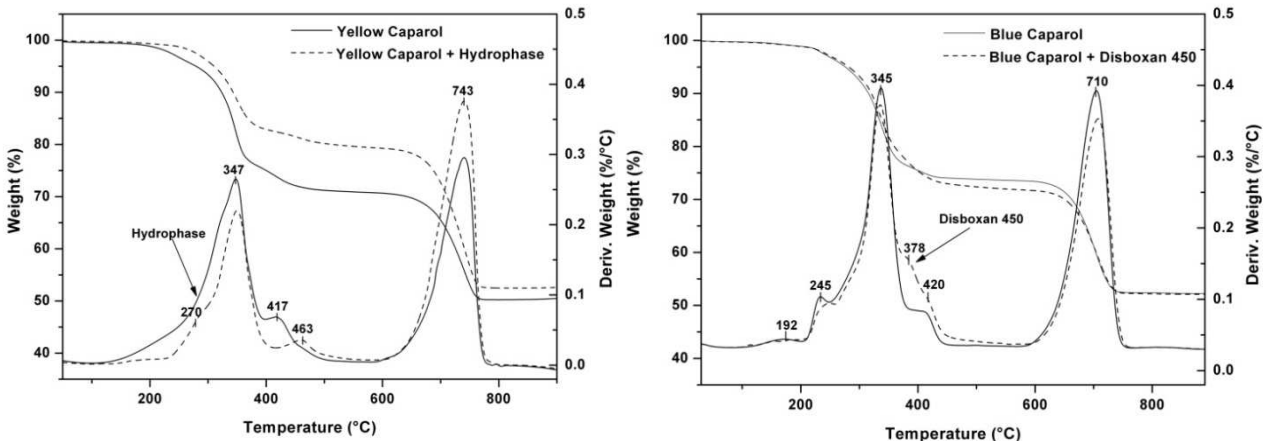

Figure 6.9 TG curve and its derivative of the acrylic samples studied, alone and with siloxane coatings, performed under air flow at 10°C/min heating rate.

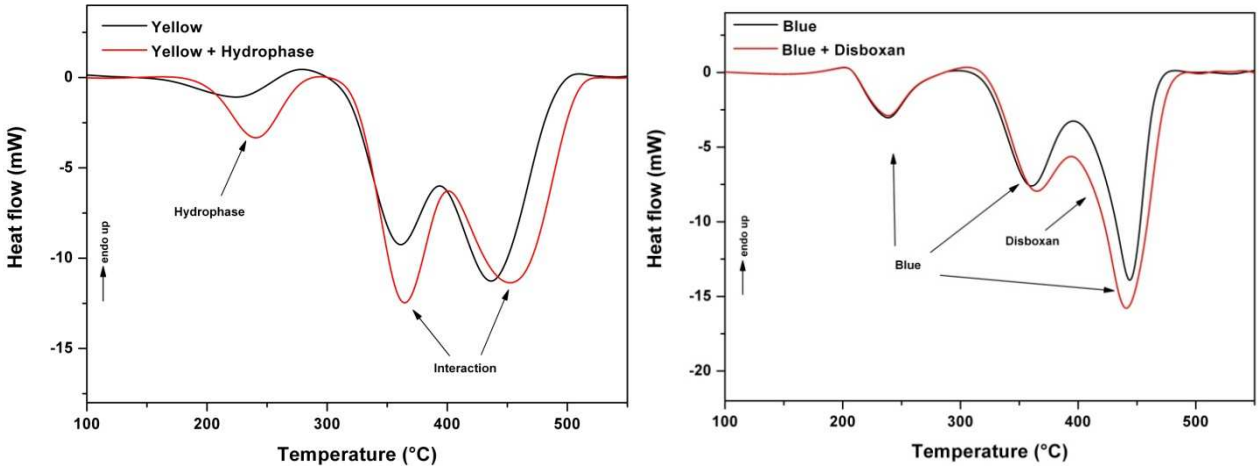

Figure 6.10 DSC curve of acrylic colour (black) and with alkoxysiloxanes coatings (red) under air flow at 10°C/min heating rate.

N° step	Yellow	Yellow + Hydrop.	Blue	Blue + Disboxan 450
1	-	-	192°C (0.3%)	192°C (0.3%)
2	-	250°C (shoulder)	245°C (8.1%)	245°C (7.7%)
3	347°C (23.6%)	347°C (17.8%)	345°C (15%)	345°C (15.6%)
4	-	-	-	390°C (shoulder)*
5	417°C (4.4%)	463°C (2.3%)	420°C (4.3%)	420°C (6.4%)* (shoulder)
6	743°C (22%)	743°C (27.4%)	710°C (20.5%)	710°C (18.6%)

*Total mass loss of the peak at 390 and 420°C

Table 6.2 Experimental temperature and mass loss percent of thermal degradation steps in air of the sample colour with and without siloxanes coatings

The thermogram of Caparol yellow paint replicas show three steps, due to the degradation of acrylic copolymer (347 and 417 °C) and the decarboxilation of $CaCO_3$ (743°C) [15], used as extender in the wall surface miming material Capatec Putz. The DSC curve of the pure Caparol yellow shows three exothermic processes in the temperature range 25-550°C, which correlate with the first three main TG decomposition steps. When Hydrophase is added one additional shoulder is present (270°C) in the TG curve due to the coating itself and a shift of about 50°C of the peak at 417 °C occurs. The same behavior can be observed in DSC curve when the exothermic thermo-oxidation of Hydrophase appears and the exothermic effect at about 450°C is shifted to higher temperatures.

The Caparol blue shows a small mass loss at 190°C and a broad mass loss centered at 345°C, with a shoulder in the DTG curve at 250°C and another at 420°C, ascribable to the thermo-oxidative degradation of the acrylic copolymer (192, 345 and 420 °C) and of the blue pigment (245 °C) and a mass loss at 710°C due to the $CaCO_3$ decarboxilation. The only modification in the DTG curve due to the Disboxan 450 coating is the appearance of a shoulder at 378°C due to the degradation of Disboxan 450 itself. The DSC of Caparol blue is practically unaffected by the Disboxan 450 coating.(Fig 6.9-6.10)

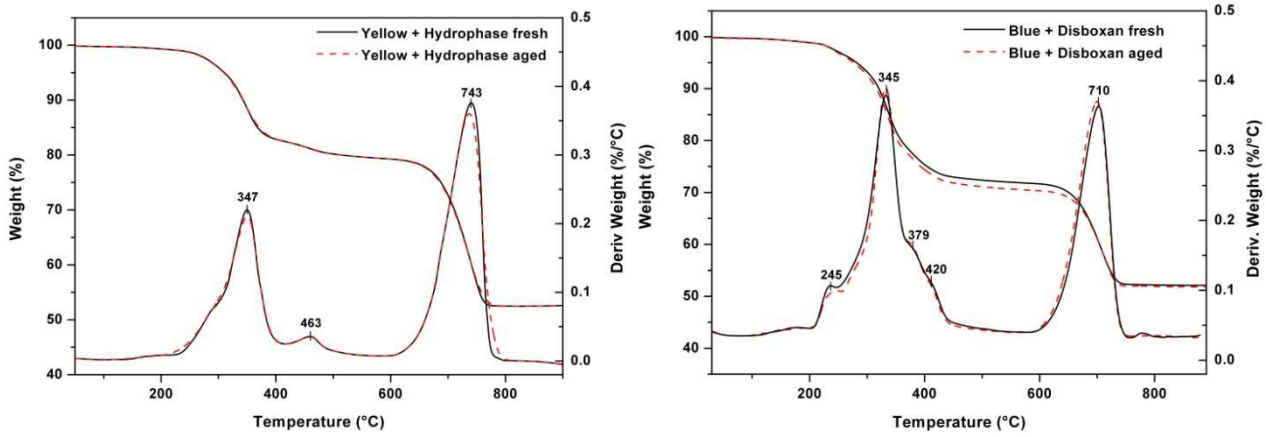

Figure 6.11 TG curve and its derivative of the acrylic samples studied with siloxane coatings fresh (black) and aged (red dash), performed under air flow at 10°C/min heating rate.

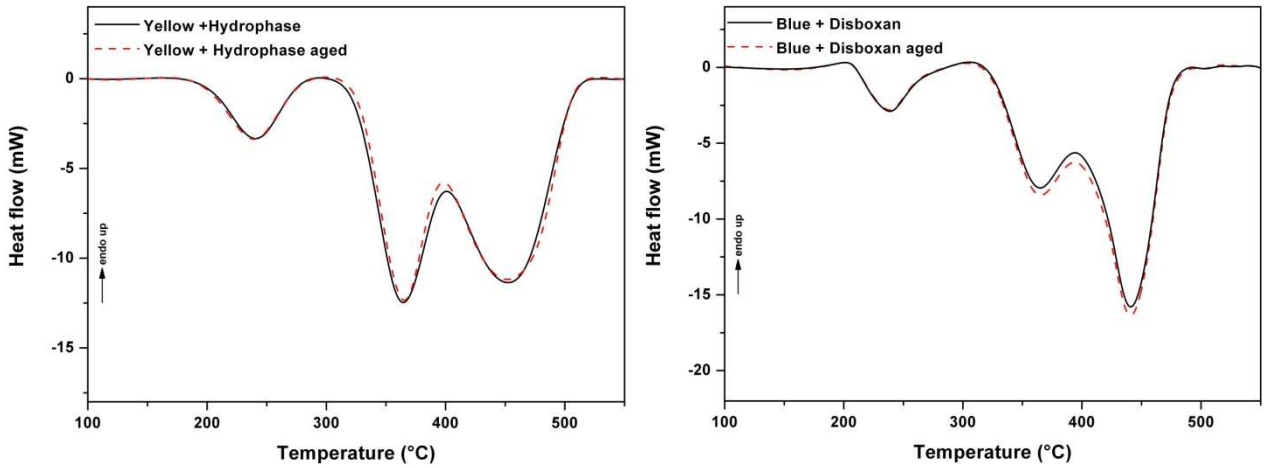

Figure 6.12 DSC curve of acrylic sample studied with siloxane coatings fresh, (black line) and aged (red dash line) under air flow at 10°C/min heating rate.

These results allow us to reveal an effective interaction only between Caparol yellow and Hydrophase

The TG and DSC analyses on the two years outdoor naturally aged samples do not show any appreciable modification on the TG and DSC profiles, as can be observed in Fig. 6.11 and Fig. 6.12.

6.2.2 FTIR of alkyl silanes and siloxanes

Hydrophase and Disboxan 450 were also characterized by FTIR-ATR spectroscopy. Their FTIR spectra are reported in Figure 6.13 and Table 6.3 summarizes their FTIR absorption and the corresponding vibrational assignment.

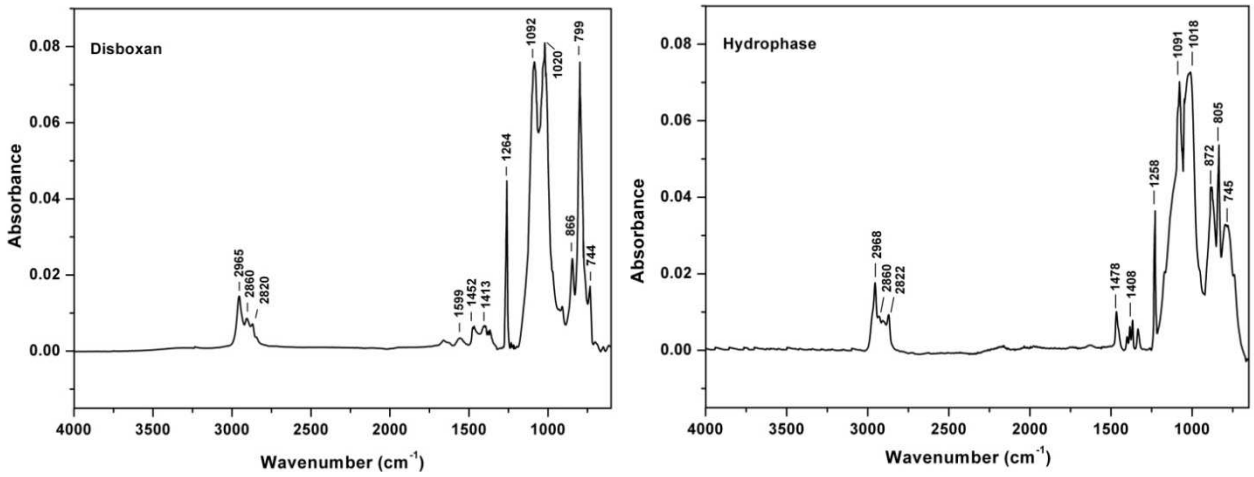

Figure 6.13 FTIR spectra in the range 4000-600 cm^{-1} of two siloxanes studied

Frequency (cm^{-1}) Disboxan 450	Frequency (cm^{-1}) Hydrophase	Assignment	Ref.
744	745	δ Si-O	[14]
799	805	ν O-Si-C	[14]
866	872	CH_3 rocking (Si-CH_3)	[14]
1020	1018	ν_{as} Si-O	[14]
1092	1091	ν_s Si-O	[14]
1264	1258	$\delta_s CH_3$ (Si-C) (umbrella)	[14]
1380	1375	δ_s C-H	[14]
1413	1408	δ_{as} C-H	[14]
1452	1478	δ_s C-H	[14]
2820-2965	2822-2968	ν C-H of CH_2 and CH_3	[14]

Table 6.3 FTIR absorption of both siloxanes studied and vibrational assignment

Figure 6.14 shows FTIR spectra of the acrylic Caparol yellow and blue applied on the wall surface miming material Capatec Putz and Table 6.4 summarizes the most important FTIR absorption and the corresponding vibrational assignment.

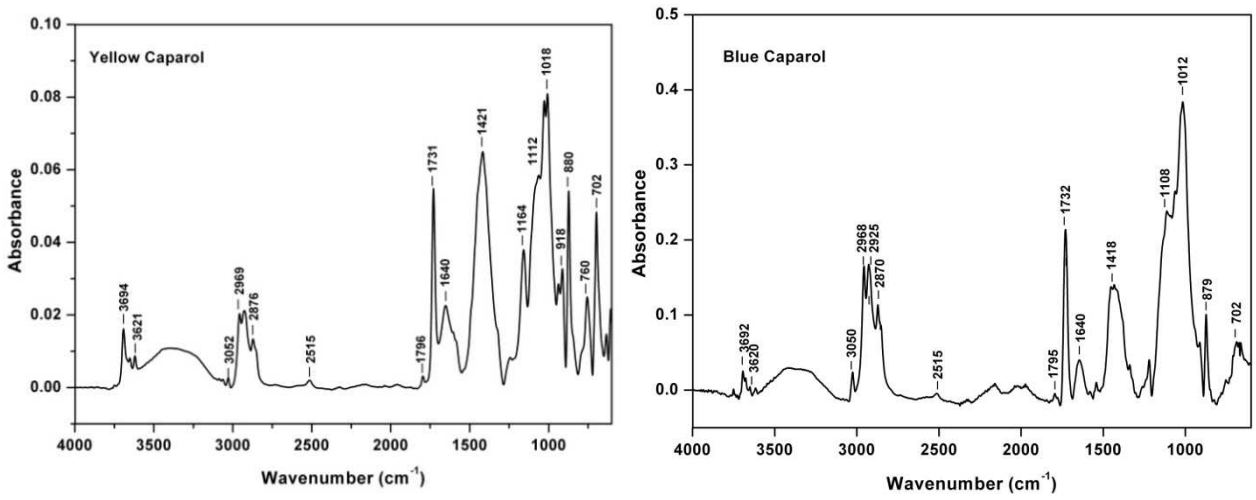

Figure 6.14 FTIR spectrum in the range 4000-600 cm^{-1} of pure Yellow Caparol (left) and Blue Caparol (right)

Frequency (cm^{-1}) Yellow paint replicas	Frequency (cm^{-1}) Blue paint replicas	Assignment
Yellow Caparol	Blue Caparol	
702, 760	702, 762	ρ =C-H
1164, 940	1180, 945	ν C-O and ν C-C
1640	1640	Aromatic breathing and δ C-H
1731	1732	ν C=O
2876, 2969	2870-2968	ν C-H of CH_2 and CH_3
3081	3080	ν C-H of C=C
3470	3456	ν O-H
Extenders ($CaCO_3$)	Extenders ($CaCO_3$)	
880	879	δ C-O of CO_3^{2-}
1421	1418	ν C-O of CO_3^{2-}
Extenders (china clay)	Extenders (china clay)	
3621, 3694	3620, 3692	ν O-H
1112, 1018	1108, 1013, 918	ν Si-O

Table 6.4 FTIR absorption of Yellow and Blue paint replicas and vibrational assignment

In the spectra the typical bands of acrylate and styrene due to the acrylic colours are present together with the bands of China clay (hydrated aluminum silicate) and $CaCO_3$ present as extenders. China clay absorbs strongly between 900 and 1150 cm^{-1} (1112, 1018 and 918 cm^{-1}) and between 3620 and 3700 cm^{-1}, where O-H stretching frequency occurs (3621 and 3694 cm^{-1}). Calcium carbonate is characterized by a very strong absorption between 1360 and 1550 cm^{-1} (at 1421 cm^{-1}), by a strong and sharp absorption at 880 cm^{-1} and less strong but still sharp peaks at 1796 and 2515 cm^{-1}. These latter two peaks prove extremely useful for the identification of $CaCO_3$ in actual paint formulations.[16]

The comparison of FTIR spectra of the siloxane coated and uncoated acrylic paint replicas are reported in Fig. 6.15. The main effect of both Hydrophase and Disboxan 450 coatings on the spectra of acrylic paint replicas is the decrease of the OH stretching absorbance at about 3300 cm^{-1} and the increase of the Si-O stretching absorbance in the range 1000-1120 cm^{-1}. These results shows the reduction of the free OH content and the correspondent bond between siloxanes and

acrylic paint. The Hydrophase coating shows an increase of the C-H stretching absorbance (2870-2965 cm-^{1}) on the spectra of acrylic paint replicas due to the alkyl groups bonded to Si atom of the coating. It has to be noted that Hydrophase coating gives the major effect compared to Disboxan 450, in accordance with its monomeric nature.

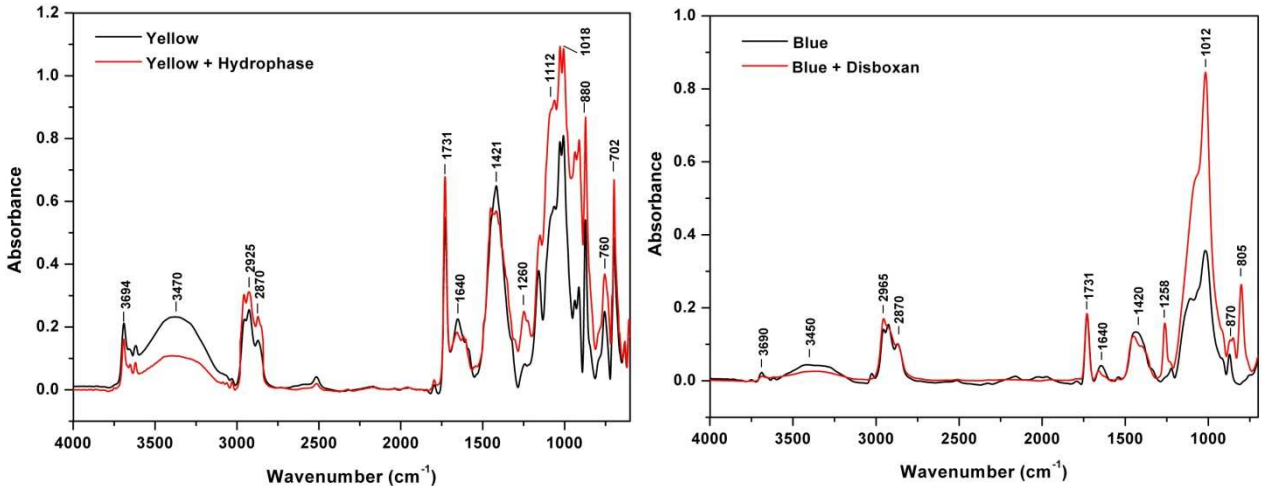

Figure 6.15 (Left) FTIR spectra of Caparol Yellow (black) and Hydrophase coated Caparol Yellow (red) paint replica ; (right) FTIR spectra of Caparol Blue (black) and Disboxan 450 coated Caparol Blue (red) paint replica.

The FTIR of siloxane coated acrylic paint replicas (Fig. 6.16) after two years of natural outdoor ageing showed , a decrease of signal due to the coatings (1090-1120 cm^{-1} and 2870-2965 cm^{-1}) in the Hydrophase coated samples while no changes were observed in the Disboxan ones.

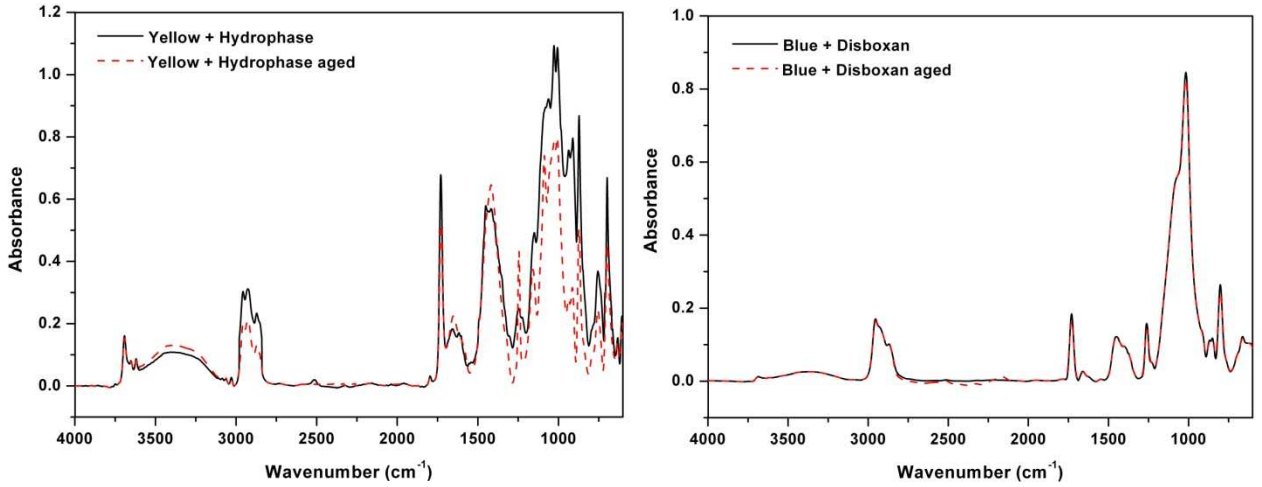

Figure 6.16 (Left) FTIR spectra of Hydrophase coated Caparol Yellow paint replica fresh (black) and 2 years naturally outdoor aged (red dash); (Right) Disboxan 450 coated Caparol Blue paint replica (black) and 2 years naturally outdoor aged (red dash).

This suggest that the monomeric dispersion (Hydrophase) is less stable with time respect to oligomeric (Disboxan 450). Its decomposition can lead to breakage of Si-C bonds and formation of

CH_4 and SiO_2 by radicalic reactions that can occur under the effect of light, heat etc. during the outdoor exposure.

6.3 Conclusions

In this chapter the thermal degradation of two commercial siloxane coating products named Hydrophase and Disboxan 450 were investigated by means of TG, TG-FTIR and DSC. The study of alkyl alkoxy-siloxanes aimed at evaluating a possible application for one of these products as a coating for the acrylic wall painting "Tuttomondo" painted by Keith Haring on an external wall of St. Antonio Church in Pisa. Paint replicas were prepared by applying a layer of Caparol acrylic colour on to the wall surface miming material Capatec Putz and then a layer of silicone coating on top. In particular, Hydrophase was applied on a layer of Caparol Yellow and Disboxan 450 on Caparol Blue. The paint replicas were analysed before and after two years of natural outdoor ageing.

The experimental results show that:

- Disboxan 450 coating changes the appearance of blue paint replicas, that became more shiny and smooth to the touch.
- The thermo-oxidative stability of Hydrophase and Disboxan 450 is different with respect to their monomeric and oligomeric nature. Hydrophase is less thermo stable than Disboxan 450.
- Both Hydrophase and Disboxan 450 thermal decompositions under nitrogen and under air produce methane, short chain aliphatic compounds and compounds obtained by oxidation of methane or reactions between CH_3 and CO. Oligomers of silanes are only present in the decomposition pathway of Disboxan 450, which is very similar to that of PDMS.
- The monomeric dispersion (Hydrophase®) shows a stronger interaction with the acrylic colour , inducing an increase in the resin's thermal stability.
- The oligomeric dispersion (Disboxan 450 ®) does not show any modifications in thermal stability of acrylic support .
- Both Hydrophase and Disboxan 450 coatings decrease the OH stretching absorbance at about 3300 cm^{-1} of the spectra of acrylic paint replicas thus confirming the bond between siloxanes and acrylic paint and the reduction of the free OH content.
- Hydrophase gives a higher effect than Disboxan 450. These result can be considered as further proof of the smaller size of Hydrophase compared to Disboxan 450, and of its major penetration power.
- The natural outdoor ageing of Disboxan 450 coated paint replicas does not produce any modification of their thermal and spectroscopic behaviour, thus indicating that the coating is stable over time. On the other hand, the IR spectrum of aged Hydrophase coated paint replicas highlight a partial decomposition of the coating.

Hydrophase coating seems to be a better coating agent than Disboxan 450 for the acrylic wall painting "Tuttomondo" because it does not change the visual appearance of the paint and it is less stable during time, forming a easily removable coating layer.

References

[1] Witucki GL. *A silane primer: chemistry and applications of alkoxy silanes.* 57th annual meeting of the federation of societies for coatings technology on October 21, 1992, Chicago, IL;

[2] Simpson TR, Tabatabaian Z, Keddie JL. *Influence of interfaces on the rates of crosslinking in PDMS coatings.* J Pol Sc (2003). 42, 1421-1432;

[3] Tsakalof A, Manodis P, Karapanagiotis I. *Assessment of synthetic polymeric coatings for the protection and preservation of stone monuments.* J of Cult Herit(2007). 8, 69-72;

[4] Balaba WM, Mozelevski F. *Siloxane coatings for aluminium deflectors.* (1994)US patent 5527562;

[5] Tedeschi G, Laurel WL. *Thromboresistant coating using silanes and siloxanes.*(2000) European Patent EP0982041;

[6] Kaharaman MV, Kugu M, Gungor A, Menceloglu Y. *The novel use of organo alkoxy silane for the synthesis of organic-inorganic hybrid coatings.* J of Non-Cryst Sol (2006) 352, 2143-2151;

[7] Radhakrishnan TS. *Thermal degradation of Poly(dimethylsilylene) and Poly(tetramethyldisilylene-co-styrene).* J Appl Pol Sc (2005) 99, 2679-2686;

[8] Thomas TH, Kendrick TC. *Isothermal depolymerization of PDMS.* J Pol SC (1969) 7, 537-549;

[9] Grassie N, Francey KF. *The thermal degradation of polysiloxanes.* Pol Degr and Stab (1980) 2, 67-83;

[10] Deshpande G, Rezac ME. *The effects of phenyl content on the degradation of poly dimethyl diphenyl siloxane polymers.* Pol Degr and Stab(2001) 2, 363-370;

[11] Camino G, Lomakin SM, Lazzari M. *PDMS thermal degradation Part 1. Kinetic aspect.* Polymer (2001) 6, 2395-2402;

[12] Camino G, Lomakin SM, Lazzari M. *PDMS thermal degradation Part 2. The degradation mechanism.* Polymer (2002) 7, 2011-2015;

[13] Tomer SN, Jestin FD, Frezet L. *Oxidation, chain scission and cross-linking studies of polysiloxanes upon ageing.* J of Org Pol Mater (2012) 2, 13-22;

[14] Danilov V, Wagner HE, Meichsner J. *Modification of PDMS thin films in H_2 radio-frequency plasma investigated by Infrared Reflection Absorption spectroscopy.* Plasma Process Polym (2011) 8, 1059-1067;

[15] Pavese A, Catti M, Parker SC. *Modelling of the thermal dependance of structural and elastic properties of calcite, $CaCO_3$.* Phys Chem Minerals (1996) 23, 89-93.

[16] Learner TJS. *Exthenders in modern paints, analysis by FTIR and pyrolysis GC-MS spectrometry.* (2004) Research in conservation, Getty publications.

CONCLUSIONS

This thesis present some cases where techniques based on the thermal analysis and calorimetry are applied within the context of the characterization of art objects and materials, providing an example of the interdisciplinary character of these techniques in relation to the chemistry applied to cultural heritage.

Thermogravimetry (TG), Derivative Thermogravimetry (DTG) and Differential Scanning Calorimetry (DSC) are examples of the analytical methods that find application in the field of art and archaeology. The results obtained in this work by TG and DSC have been related with Fourier Transform Infrared Spectroscopy (FTIR), a well-established technique, confirming the relevant complementary nature of thermal analysis. Thermal analysis and calorimetry in fact give information on the macroscopic scale, while FTIR spectroscopy gives information on the molecular scale.

One important aspect of thermoanalytical techniques is that, although being in general destructive, only few milligrams of sample are usually needed, a fact that is very important in the study of objects with historical or cultural value.

Among the most important contributions that chemistry can offer to cultural heritage conservation there are not only the understanding of the original execution techniques but also the identification of the problems affecting artworks, allowing the choice of the most effective and durable intervention.

With thermal analysis is possible to characterize a large range of materials and compounds with different chemical-physical properties, such as inorganic salts or oxides used as pigments, natural proteinaceous materials or synthetic resin used as binders, synthetic product used in restoration as protective or coatings for stone monuments, painting or metal surfaces.

The TG/DSC analysis of proteinaceous binders revealed that the presence of inorganic pigments in tempera paints reconstructions in most cases induces a decrease in thermal stability, and a labilization of protein network. On the other hand, the studies clearly show that ageing can induce aggregation, oxidation of some amino acid side chains and hydrolysis of the polypeptide chain in both pure and pigmented proteins. Pigments may act directly on the stability of the protein structure because of their interaction with amino acid functional groups or indirectly, promoting oxidative stress, which may induce global unfolding rearrangements of the proteins, which decrease their thermal stability. Spectral deconvolution of Amide I FTIR bands confirm and support the TG/DSC results, highlighting the disruption of the protein-protein intermolecular interaction due to the pigment and hydrolysis of side chain with the formation of aggregates in aged paint replicas.

Through thermal analysis it was possible the characterization of changes occurring during the natural and artificial acid ageing of a new series of artists' alkyd paints produced by the Winsor & Newton. These paints have a new formulation and very little is known about their features and consequently, about their curing and ageing. TG allowed us to understand their composition through the study of the thermogravimetric curves of both pure pigments and paint replicas. TGA of naturally aged films showed that with age there is an increase in film network density, which is likely caused by an increased amount of cross-linking, and revealed the formation of peroxide

bonds during the auto-oxidation. Chemical drying and cross-linking of naturally aged paint replicas was followed with DSC, monitoring the exothermic peak associated with the degradation of peroxides in the film. We observed that after 5600 h of natural ageing the auto-oxidative reactions via peroxide decomposition can be considered complete. DSC showed that the presence of pigments do not influence the rate of auto-oxidation which is only related to the amount of oil content in the final formulation of paint color. FTIR data confirmed the formation of new bonds during chemical drying, such as methylene ether and ester linkages, and the formation of new carboxylic species.

The study and characterization of any materials or product used in restoration (consolidating, coating) is critical, not only for the effective success of intervention, but especially for establishing restoration procedures that do not damage or alter the visual appearance of the artwork itself. TG/DSC techniques allowed us to study the chemical-physical properties, the chemical structures and thermal stability of two commercially available polysiloxane coatings. One of these two products had to be chosen as a protective coating for the Keith Haring's wall painting "Tuttomondo" in Pisa. The monomeric dispersion (Hydrophase) resulted less thermostable than the oligomeric one (Disboxan 450) but it showed a stronger interaction with the acrylic color, inducing an increase in the acrylic resin's thermal stability. If TG/DSC results highlighted that both coatings are stable over time of two years, FTIR showed that natural outdoor ageing promotes a partial decomposition of the Hydrophase which seems to be a better coating agent than Disboxan, because it is less stable during time, thus resulting a easily removable coating layer.